

**Technetium environmental chemistry:
Mechanisms for the surface-mediated reduction of
Tc(VII)**

D I S S E R T A T I O N

zur Erlangung des akademischen Grades

**Doctor rerum naturalium
(Dr. rer. nat.)**

vorgelegt

dem Bereich Mathematik und Naturwissenschaften
der Technischen Universität Dresden

von

MSc. Diana Marcela Rodríguez Hernandez
Geboren am 10.06.1992 in Bogota, Kolumbien

Eingereicht am 16.03.2021
Verteidigt am 01.06.2021

Gutachter:
Prof. Dr. Thorsten Stumpf
Prof. Dr. Gero Frisch

Die Dissertation wurde in der Zeit von November 2017 bis Januar 2021 im Institut für
Ressourcenökologie des Helmholtz-Zentrums Dresden-Rossendorf e.V. angefertigt

Dejo en el rio un canto para que
vuelva a rodar...

Acknowledgements

One of the nicest things of living abroad is the possibility of live your life in different languages. Therefore, I have decided to write these acknowledgments in a mixture of Spanish and English, just as my life has been in the last three years (hopefully one day I'll include German too!).

Por supuesto, y como siempre, empezaré agradeciéndole a mi Familia. Sin su amor y apoyo yo jamás habría podido cumplir este sueño. Sin importar los 9000 km de distancia, ellos siempre han sabido estar aquí para mí.

This thesis was developed in the frame of the VESPA II project supported by the German Federal Ministry of Economic Affairs and Energy. I am very grateful with Helmholtz-Zentrum Dresden-Rossendorf for the amazing working conditions I enjoyed and specially with the Institute of Resource Ecology, where I developed most of the experiments presented in this work. A huge acknowledgement goes to my supervisors Vinzenz Brendler and Katharina Müller who have been great scientific advisors and also fundamental part of my personal development. And I also specially thank my Doktorvater, Thorsten Stumpf for all his helpful advice.

I would like to thank the Karlsruhe Institute of Technology where we performed the XAS measurements and that would not go without thanking a lot Andreas Scheinost and Andre Roßberg for their help with all the data analysis. I am also very grateful with Dieter Schild for our fruitful collaboration through XPS, Jérôme Kretzschmar for all his help with NMR and Salim Shams who always found time for my last minute XRDs. Y por supuesto le agradezco montones a Andrés Parra por todo su apoyo en la electroquímica.

Thanks a lot to Stephan Weiß for all his help in the lab. Y también muchísimas gracias a Susana Jiménez por su genial compañía en el 14.2 y por siempre poner mis muestras de primeras jajaja

A nadie debo tanto agradecimiento como a mi queridísima Natalia. No sólo porque fuiste una mentora excepcional, sino también por tu invaluable amistad. Estoy completamente segura de que mi vida en Alemania no habría sido ni la mitad de lo divertida que fue si tú no hubieras estado presente. ¡Gracias, mil gracias!

También estoy inmensamente agradecida con Félix, mi compañero de aventuras, cuyo apoyo y compañía han sido fundamentales personal y académicamente.

I feel really thankful for my beloved Inner Core. I loved every single party, every single game and every single small meeting throughout these years. Thanks for everything! And of course another huge “thank you” goes to the Happy Thursday crowd as well as to my dear friends Edu (¡mamerto! jaja), Isi, Franzy and to all my other fellow PhD students for the evenings of drinking and complaining, the nice times in Scheffau, Stephan’s wine seminar and in general for the super nice working environment we had.

Por último, pero ciertamente no menos importante, le quiero agradecer de todo corazón a mi segunda familia: mis amigos UN. A Juan porque aunque la causa siga perdida lo seguiremos intentando; a Lau con quien empecé este viaje y a quien agradezco infinitamente todo su apoyo

en el proceso; a los borrachos de Andresito, Tata y Farja que siempre me hacen feliz sin importar la situación y a Cami y a Wii en la horrible, horrible distancia.

It is quite probable that I am missing someone in these acknowledgements since a lot of people have been of huge help during the last three years. Therefore, I just want to say: To each and every person who has been part of this process, thank you, thank you with all my heart!

Abstract

Technetium is the lightest element whose isotopes are all radioactive. Among them, ^{99}Tc (hereafter simply referred as technetium or Tc) is the most abundant and raises great environmental concern due to its relatively long half-life of 2.14×10^5 years and the high mobility of pertechnetate, Tc(VII)O_4^- , its most stable form under aerobic conditions. The reduction from Tc(VII) to Tc(IV) is one of the most successful strategies for Tc immobilization; however, the mechanism of this redox reaction is not yet fully understood. This presents a large gap in the general knowledge of technetium chemistry and a significant obstacle for the modeling of its reactivity in contexts like a nuclear waste repository. This thesis was developed in the frame of the BMWi funded VESPA II project, and it studies the surface-mediated reduction of $^{99}\text{Tc(VII)}$ using a combination of fundamental chemistry and its application for remediation and nuclear waste management.

First, spectro-electrochemical methods (cyclic voltammetry, rotating disk electrode, chronoamperometry coupled with UV-vis, Raman microscopy and nuclear magnetic resonance) were employed to study the reduction mechanism of 0.5 mM KTcO_4 in non-complexing media (2 M NaClO_4) in the pH range from 2.0 to 10.0. It was found that the mechanism depends on the pH. At pH 2.0 it splits into two steps: Tc(VII) gains 2.1 ± 0.3 electrons and becomes Tc(V) that rapidly reduces to Tc(IV) with the transfer of further 1.3 ± 0.3 electrons. In contrast, at $\text{pH} \geq 4.0$ there is a direct transfer of 3.2 ± 0.3 electrons. The complete reduction of Tc(VII) yielded a black solid that was successfully characterized by NMR and Raman microscopy as Tc(IV) regardless of the initial pH at which the reaction occurred. Unfortunately, it was not possible to observe the Tc(V) species at pH 2.0 by the spectroscopic tools used.

Second, the reductive immobilization of Tc(VII) by pure pyrite and a synthetic mixture marcasite-pyrite 60:40 (synthetic FeS_2 , with both minerals being polymorphs) was studied by a combination of batch sorption experiments (Tc-removal was studied varying pH, contact time, ionic strength and Tc concentration) and several spectroscopies and microscopies such as Raman microscopy, scanning electron microscopy, X-ray photoelectron spectroscopy and

X-ray absorption spectroscopy. It was found that both pyrite and the synthetic FeS_2 promote the reduction of Tc(VII) to Tc(IV) . In the case of pure pyrite, the Tc-removal is complete after one day in contact at $\text{pH} \geq 5.5$. The spectroscopic analysis showed at $\text{pH } 6.0$ an inner-sphere complex between Tc(IV) dimers and hematite formed as secondary mineral on the pyrite surface. In contrast, at $\text{pH } 10.0$ Tc(IV) gets incorporated into surficial magnetite by replacing Fe^{3+} in octahedral position, with Fe^{2+} providing reasonable charge compensation for Tc^{4+} .

The presence of marcasite made the process slower and less efficient since the synthetic FeS_2 was capable to remove 100% Tc from solution only after seven days in contact at $6.0 < \text{pH} \leq 9.0$ while the Tc-removal at $\text{pH } 10.0$ was only around 80%. At $\text{pH } 6.0$ the formation of hematite was also observed, suggesting that the formed Tc(IV) species at the surface is the same as with pure pyrite. However, at $\text{pH } 10.0$ the formation of sulfate minerals evidences a change of redox active species: S^{2-} instead of Fe^{2+} . This, combined with the fact that in both solids the formation of TcS_x species was detected by XPS at $\text{pH } 10.0$, shows the potential of sulfur as another reducing agent for Tc(VII) . The effect of polymorphism on the Tc removal is remarkable and this work shows the relevance of more studies on the interaction of radionuclei with other mineral polymorphs.

Regardless of the kinetics of the Tc removal, both pyrite and synthetic FeS_2 hindered the re-oxidation of Tc(IV) when exposed to ambient atmosphere for two months. This feature makes them good candidates for the remediation of technetium from contaminated waters. Moreover, natural attenuation effects can be expected for technetium in the near and far field of nuclear waste repositories wherever iron sulfide is present.

The results presented in this work contribute to a better understanding of the fundamental aqueous chemistry of technetium and confirm pyrite, a ubiquitous mineral, as a very good candidate for technetium scavenging even in the presence of marcasite. These results close important gaps in thermodynamic databases that are needed for the safety assessment, i.e. modeling of fission products.

Contents

Abstract.....	VII
Symbols and abbreviations	X
Introduction.....	1
Chapter 1. Spectro-electrochemical studies of the reduction Tc(VII)/Tc(IV).....	7
1.1. Theoretical background	9
1.1.1. Technetium redox chemistry	9
1.1.2. Electrochemical methods	12
1.2. Reduction of Tc(VII) in NaClO ₄	22
1.2.1. Cyclic voltammetry.....	22
1.2.2. Rotating disk electrode.....	23
1.2.3. Spectro-electrochemical measurements	26
1.2.4. Solid analysis	27
1.3. Summary	30
Chapter 2. Reductive immobilization of technetium by iron sulfide (FeS₂)	31
2.1. Theoretical background	33
2.1.1. Geochemical barriers.....	33
2.1.2. Technetium geochemistry.....	34
2.1.3. Technetium detection and quantification in this work	41
2.2. Technetium immobilization by pure pyrite.....	45
2.2.1. Pyrite characterization.....	45
2.2.2. Technetium removal from solution: Batch experiments.....	46
2.2.3. Morphology of pyrite studied by SEM and Raman microscopy.....	49
2.2.4. Spectroscopic determination of the Tc-removal mechanism.....	51
2.3. Tc immobilization by a mixture marcasite-pyrite.....	57
2.3.1. Solid characterization	57
2.3.2. Tc-removal by the synthetic FeS ₂ : Batch experiments	58
2.3.3. Spectroscopic analysis of the Tc-loaded solids.....	59
2.3.4. Re-oxidation essays	64
2.4. Summary	66
Concluding remarks, environmental significance and perspectives	69
Experimental methods.....	73
I. Spectro-electrochemical experiments	73
II. Tc scavenging experiments	75
Scientific output	81
References.....	85

Symbols and abbreviations

Symbols

Symbol	Meaning	Unit	Definition
c	concentration		Group of four quantities characterizing the composition of a mixture with respect to the volume of the mixture
$E^{\circ'}$	Formal potential	V	Potential of a redox reaction at a certain temperature T
E	Electric potential	V	Energy / Charge
E_h	Redox potential	V	Tendency of a chemical species to be reduced or oxidized
E_i	Initial potential	V	Initial potential of the cyclic voltammetry
E_f	Final potential	V	Final potential of the cyclic voltammetry
E_{\max}	Maximum potential	V	Maximum potential value reached during the voltammetry
E_{\min}	Minimum potential	V	Minimum potential value reached during the voltammetry
E_p	Peak potential	V	Potential at which the current reaches a maximum (or minimum) during a redox reaction
$E_{1/2}$	Half-wave potential	V	Potential at which polarographic wave current is one half of diffusion current
I	Current	A	Voltage / resistance = Charge / time
I_{ap}	Anodic peak current	A	Height of the anodic peak
I_{cp}	Cathodic peak current	A	Height of the cathodic peak
I_p	Peak current	A	Maximum current of a peak
M	Molar concentration	mol L ⁻¹	Mole of solute per liter of solvent
R	Universal gas constant	J mol ⁻¹ K ⁻¹	--
T	Temperature	K	--
$t_{1/2}$	Half-life		Time after which the concentration of the species drops to half the initial value
ν	Scan rate	V s ⁻¹	dE/dt

Abbreviations

Abbreviation	Concept
Au-SERS	Gold surface-enhanced Raman scattering
CA	Chronoamperometry
CA/UV-vis	Chronoamperometry coupled with UV-vis
CP	Cathodic peak
cpm	Counts per minute
CV	Cyclic voltammetry
DL	Diffusion layer
DLS	Dynamic light scattering
DMSO	Dimethyl sulfoxide
DPV	Differential pulse voltammetry
DRG	Deep geological repository
EDX	Energy dispersive X-ray spectroscopy
EXAFS	Extended X-ray absorption fine structure
FP	Fission products
FTM	Fourier transform magnitude
ICP-MS	Inductively coupled plasma mass spectrometry
ITFA	Iterative transformation factor analysis
LSC	Liquid scintillation counting
NA	Avogadro's number
NEA	Nuclear Energy Agency
NEA-TDB	NEA Thermochemical Database
NMR	Nuclear magnetic resonance
pHIEP	Isoelectric point
OM	Organic Matter
Ox	Oxidated species
RDE	Rotating disk electrode
Red	Reduced species
SEM	Scanning electron microscopy
Tcsol	Technetium in solution
UV-vis	Ultraviolet-visible spectroscopy
XANES	X-ray absorption near edge structure
XAS	X-ray absorption spectroscopy
XPS	X-ray photoelectron spectroscopy
Z	Atomic number
z-potential	Zeta potential

Introduction

Technetium (Tc, $z = 43$) was discovered in 1937 in Italy by Carlo Perrier and Emilio Segrè.^{1,2} It was produced synthetically by deuteron activation of a piece of metallic molybdenum that had undergone bombardment in the cyclotron in Berkeley, California. With this discovery, the gap between molybdenum ($z = 42$) and ruthenium ($z = 44$) predicted by Mendeleev during the 1860s was finally closed. Thus, technetium is located in the seventh group of the periodic table between manganese and rhenium (Figure 1). These transition metals have high melting and boiling points and they exhibit several oxidation states that, in the case of technetium, range from -1 to +7, as it will be discussed later.

24 Cr Chromium 51.996	25 Mn Manganese 54.938	26 Fe Iron 55.845
42 Mo Molybdenum 95.95	43 Tc Technetium 98.907	44 Ru Ruthenium 101.07
74 W Tungsten 183.84	75 Re Rhenium 186.207	76 Os Osmium 190.23

Figure 1. Technetium in the periodic table.

Technetium is the lightest element whose isotopes are all radioactive. Among them, the longest-lived ones are ^{97}Tc ($t_{1/2} = 4.21 \times 10^6$ years), ^{98}Tc ($t_{1/2} = 4.20 \times 10^6$ years) and ^{99}Tc ($t_{1/2} = 2.14 \times 10^5$ years), the last being the most abundant. Initial fission products (FP) of uranium and plutonium typically have a high neutron/proton ratio that makes them decay to reach stabilization. The radioactive decay of the FP of mass 95 – 98 stops at molybdenum, while for FP with mass > 100, it continues until ruthenium. Therefore, ^{99}Tc (hereafter, simply referred as technetium or Tc) is practically the only technetium isotope produced by nuclear fission. It is worth mentioning that

while ^{99}Tc is a pure β^- emitter, its meta stable isotope, $^{99\text{m}}\text{Tc}$, emits gamma rays (140 keV) which, in combination with its short half-life (6.01 hours), makes it very useful for medical diagnosis. This application was first published in the early 60s³ and, since then, $^{99\text{m}}\text{Tc}$ has been used for imaging of the brain, myocardium, thyroid, lungs, liver, gallbladder, kidneys, skeleton, blood, and tumors.

Even though Tc may occur naturally at ultra-tracer levels through the spontaneous fission of ^{238}U , neutron-induced fission of ^{235}U or cosmic ray reactions with molybdenum, ruthenium and niobium present in the Earth's crust, it is mainly found in the environment due to anthropogenic sources.⁴ During the thermal neutron fission of ^{235}U and ^{239}Pu , technetium is produced with a yield of approx. 6.1% in nuclear power plants^{5,6} and the use and testing of nuclear weapons, during the past century.^{4,6} Other techniques, like $^{99}\text{Mo}/^{99\text{m}}\text{Tc}$ generators (Figure 2), are employed to produce the metastable isotope for medical applications by separating the soluble $^{99\text{m}}\text{TcO}_4^-$ from its parent isotope $^{99}\text{MoO}_4^{2-}$ in a chromatographic column,^{7,8} leading to the production of low to intermediate-level nuclear waste.

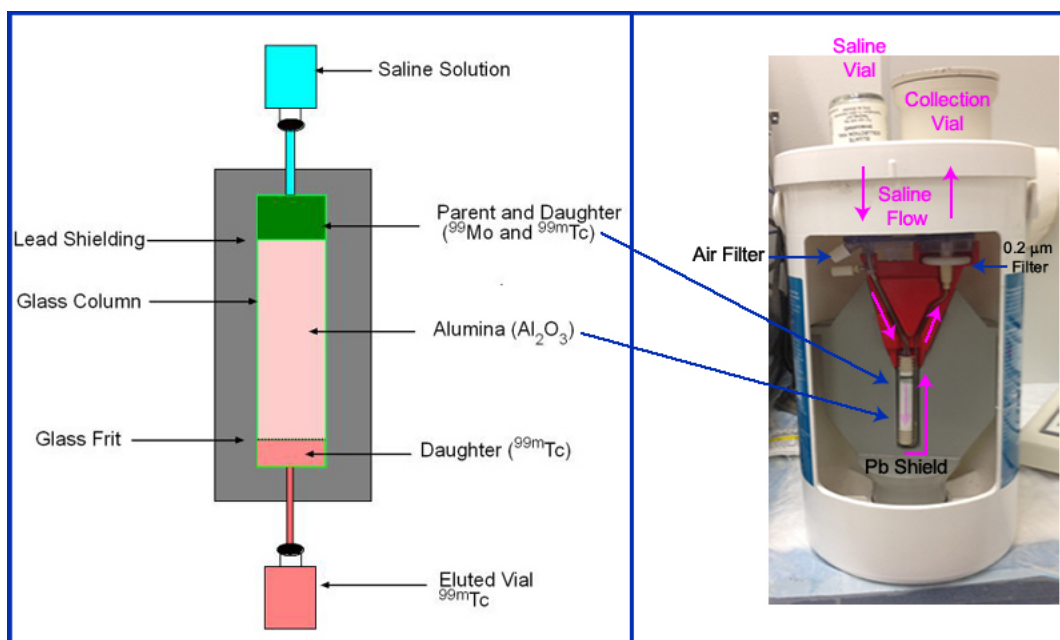


Figure 2. $^{99}\text{Mo}/^{99\text{m}}\text{Tc}$ generator. Taken from reference ⁹.

It is estimated that from 1943 to 1987, 100 to 140 TBq of technetium have been released due to atmospheric nuclear weapon testing, from which a large fraction has been deposited or incorporated into sediments.¹⁰ However, the largest amount of technetium has been produced during active nuclear power generation. According to Kloosterman¹¹ 21 kg of technetium,

equivalent to 13.2 TBq, are produced annually in a large 1 GW generator. Its estimated global inventory gives account of 78×10^3 kg of technetium produced until 1994 and projected 15.1×10^3 kg generated only in 2007. Assuming the Tc production of 2007 as a roughly average, there are approximately 470.6×10^3 kg of technetium (296.3×10^{15} Bq) expected on Earth in 2020, the majority of which is still waiting for proper disposal.¹¹

In order to ensure a safe storage of radioactive pollutants, deep geological disposal has been suggested by the International Atomic Energy Agency in 2003¹² and, nowadays, it is widely accepted by the international community for the long-term storage of high-level radioactive waste.^{13,14} Such disposal relies on a multi-barrier approach that combines engineered barriers (containers and geotechnical buffers) and the natural geological barrier provided by the repository host rock.¹³ In the worst-case scenario water enters the repository, promoting canister corrosion and mobilizing with it soluble radionuclides. Therefore, it is crucial to understand the interaction of technetium with the materials used for the engineered barrier construction and the minerals that form the geological barrier.

Technetium migration behavior and bioavailability strongly depend on its speciation in aqueous solution and on its oxidation state. Under aerobic conditions, it mainly exists as pertechnetate, Tc(VII)O_4^- , a highly water-soluble anion that does not significantly sorb on minerals or sediments^{4,15}, i.e. it is considered inert and therefore, its migration with groundwater is favored. Under reducing conditions, Tc(VII) becomes Tc(IV), whose main species, TcO_2 , is a solid with a low solubility product ($\text{Log } K_s = 8.17 \pm 0.05$ ¹⁶) and, thus, its mobility decreases. Due to its high mobility, pertechnetate can easily enter the food chain. In humans, it is mainly localized in the thyroid gland (75%), gastrointestinal tract (20%), and the liver (5%), and the biological half-lives for Tc in these organs are 1.6 days, 3.7 days, and 22 days, respectively.¹⁷ The US Environmental Protection Agency has established its permitted contamination limit at 0.04 mSv per year, because exceeding this dose increases the risk of cancer and other health problems.¹⁸

The clear importance of technetium speciation on environmental processes contrasts with the lack of knowledge of technetium redox chemistry. Despite several years of studies, it is still not clear whether the reduction mechanism from Tc(VII) to Tc(IV) in water involves the direct transfer of three electrons or if there is an intermediary oxidation state formed during the reaction.^{19,20} Hence, a mechanism for the aqueous reduction from Tc(VII) to Tc(IV) has not been formulated yet. Additionally, the effects of the pH and the ionic strength on the reaction have not been systematically studied. Therefore, the redox potentials reported for the reduction reaction significantly differ from each other depending on the conditions used. This is a

substantial problem for the modeling of the behavior of technetium for example, in the near and far field of a nuclear waste repository.

As mentioned above, the mobility of technetium can be drastically decreased by reducing Tc(VII) to Tc(IV). Thus, several works approached Tc removal from water by using Fe(II) minerals, as they trigger the Tc reduction and lower its mobility by incorporating, sorbing or precipitating Tc(IV).^{21–24} Among them, pyrite (cubic FeS₂), the most common redox sensitive sulfur mineral, has shown to scavenge Tc from solution in presence²⁵ and absence of humic substances.^{26,27} However, several issues like the pH effect and the marcasite (orthorhombic FeS₂) effect have not been determined yet. Furthermore, the molecular mechanisms involved in the Tc removal by pyrite are not understood at all. This constitutes a lack of understanding required to design and optimize a sustainable and efficient retardation strategy for Tc contamination. Moreover, it is important to bear in mind that usually the re-oxidation from Tc(IV) to Tc(VII) is very fast. Therefore, a proper material for technetium immobilization must inhibit such re-oxidation for as long as possible and this has not been investigated yet with technetium immobilized by pyrite.

This thesis deals with two approaches aimed at filling several gaps in the knowledge of technetium chemistry. In the first chapter, spectro-electrochemical methods (cyclic voltammetry, Randles-Sevcik and Levich analysis and chronoamperometry coupled with UV-vis) were used to study the reduction from Tc(VII) to Tc(IV) in the presence of sodium perchlorate (NaClO₄). This background electrolyte was chosen because it is not supposed to form complexes with technetium,^{28–31} being, therefore, a good approximation to the behavior of Tc interacting solely within pure water. A wide range of pH (2.0 to 10.0) was applied to determine its effect on the reaction pathway. The solid produced after the complete reduction of Tc(VII) was analyzed by Raman microscopy and nuclear magnetic resonance (NMR) to verify its chemical identity and confirm the findings of the spectro-electrochemical methods.

In the second chapter, the reductive immobilization of Tc(VII) by pure pyrite and a synthetic FeS₂ (mixture marcasite-pyrite 60:40) was studied with the aims of i) understanding the effects of pH, Tc loading and ionic strength on Tc removal and ii) identifying the molecular mechanisms involved. Batch experiments were performed in a pH range from 3.5 to 10.5 in deionized water and in 0.1 M NaCl under N₂ atmosphere. In addition, re-oxidation studies were carried out under ambient atmosphere. Scanning electron microscopy (SEM) was used to analyze the morphology of the minerals before and after Tc interaction. X-ray absorption spectroscopy (XAS), X-ray photoelectron spectroscopy (XPS) and Raman microscopy were

applied to identify the Tc retention mechanisms and the molecular environments after its interaction with the minerals.

Since the two approaches used in this work employ very different experimental methods, it is expected that each chapter can be independently read from each other. To this propose, the theoretical background of the experimental methods employed is presented in each corresponding chapter and at the end of the thesis, an experimental section with all the technical details can be found.

Together, the spectro-electrochemical and the reductive Tc immobilization approach generate an enormous contribution to the knowledge about technetium fundamental aqueous chemistry and the understanding of the reactive behavior of transition metals. This, in turn, will be very helpful for the modeling of technetium migration through natural and anthropogenic environments. Moreover, this work provides sorption data required for the safety analysis of a nuclear waste repository placed in crystalline or argillaceous host rocks where iron sulfide will most likely be present.^{32,33}

Chapter 1.

Spectro-electrochemical studies of the reduction Tc(VII)/Tc(IV)

The reduction from Tc(VII) to Tc(IV) is of great importance from the radioecological point of view because it is the main strategy for its immobilization and/or further remediation.^{4,5,34} However, more than 80 years after the discovery of technetium, it is still not clear how does this reduction proceed in water due to the irreversibility of the process, the formation of colloid or solid phases that render the determination of thermodynamic data impossible, or the lack of systematic studies on this matter. As it will be shown in the next section, even though many authors have studied Tc(VII) reduction, the conflicting and contradictory results prevent the construction of an accurate Latimer diagram at alkaline pH.

The lack of thermodynamic data is not only an enormous gap in the basic understanding of technetium and the transition metals chemistry, but is also represents a large problem for the modeling of the behavior of Tc in legacies or contaminated sites and, maybe more important, for the nuclear waste management. The latest update of the Nuclear Energy Agency Thermochemical Database (NEA-TDB) of technetium³⁵ presents a standard potential value for the Tc(VII)/Tc(IV) reduction under acidic conditions that actually varies from 0.746 ± 0.012 V to 0.757 ± 0.006 V depending on how fresh is the amorphous hydrated TcO₂ produced. It might be related to the formation of intermediary oxidation states combined with kinetic effects. This shows the importance of understanding the reduction mechanism in water, since that would make the derivation of thermodynamic data not only easier but also more reliable.

In this work a combination of electrochemical methods (cyclic voltammetry, rotating disk electrode, chronoamperometry) and several spectroscopies (UV-vis, Raman microscopy and nuclear magnetic resonance) were used to determine the reduction mechanism of Tc(VII) in non-complexing media, i.e. NaClO₄. This approach aims to come closer to the molecular reactions of Tc in pure water to expand the general understanding on technetium aqueous chemistry.

1.1. Theoretical background

1.1.1. Technetium redox chemistry

Technetium oxidation states range from -1 to +7, with -1, +1 and +2 being the least stable, while the most common valences are +4 and +7 due to the $[\text{Kr}]4d^5 5s^2$ configuration that promotes the stability of the higher oxidation states.³⁶

In his paper of 1978, Grassi³⁷ summarized the general knowledge about technetium redox chemistry available at that time. Most of the studies were done in chloride, sulfate and perchlorate media but the interpretation of the polarographic data was complicated and most of the time contradictory due to the uncertainty on the oxidation states involved. Thus, Salaria et al.^{38,39} proposed the reduction of pertechnetate in acidic media in two steps, as described in Eq. [1] and [2]:



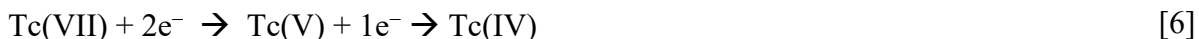
However, these results contradicted those of Zhdanov et al.⁴⁰, who reported that the first step should be as shown in Eq. [3], where Tc(IV) would be present as TcO_2 .



Similar differences were found in alkaline media: while Salaria et al.³⁸ proposed Eq. [4] and [5] to describe Tc(VII) reduction:



Other authors^{36,41,42} reported a mechanism like the one presented in Eq. [6]:



More than 30 years after the publication of Grassi's paper, the reduction mechanism of Tc(VII) in aqueous media is still not well understood.^{20,29,43,44} The scarcity of thermodynamic data describing the process is noticeable when analyzing the Latimer diagrams of technetium; even though all of its oxidation states have been observed at low pH values, only four of them are represented in the diagram (Figure 3).²⁰ Even worse is the case at alkaline pH values where the contradictory reports of technetium thermodynamic behavior at such conditions have made the construction of the diagram impossible.

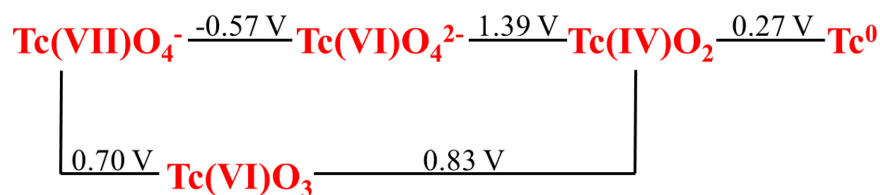
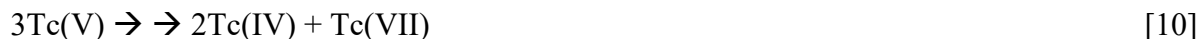


Figure 3. Latimer diagram of technetium under acidic conditions.²⁰

Despite the lack of thermodynamic data, it is possible to establish a stability scale of technetium oxidation states in non-complexing media by using the literature reports on the Tc(VII) reduction, as shown in Eq.[7]. As Eq. [7] establishes that Tc(VI) is the most unstable, it can be deduced that any species of Tc(VI) will immediately disproportionate to Tc(V) and/or Tc(VII), thereafter forming Tc(IV), like shown in Eq. [8] – [10].⁴³



Studies in acidic media^{45,46} seem to agree with such processes, as they have found that dimeric structures of Tc(IV) are formed in non-complexing environments. The Tc(IV) dimers have been characterized by UV-vis where they show bands at 250 nm, 320 nm and 495 nm that are well distinguished from the band at 400 nm presented by TcO_2^+ . However, as already mentioned, no further spectroscopies (NMR, XAS, etc) have been used to support such a reaction mechanism. Moreover, no thermodynamic constants describing the disproportionation have ever been provided.

Alkaline matrices seem to favor the formation of Tc(VI) during the reduction of Tc(VII).^{47,48} It has been found that the mechanism of disproportionation of Tc(VI) depends strongly on the ionic strength: high values lead to lower availability of free water for hydration/hydrolysis and lower amount of dissolved oxygen, enhancing the stability of Tc(VI) species.^{47,48} Using this fact, Chatterjee et al.²⁰ managed to stabilize Tc(VI) species in a matrix of 5 M NaNO₃ at 0 – 2 M NaOH during almost 2 days for their characterization.

Chotkowski et al.⁴⁴ reports the formation of two types of Tc(V) species as the intermediaries in the reduction of Tc(VII) when dissolving KTcO₄ in solutions from 0 – 10.6 M NaOH with no other electrolyte. Soluble Tc(V) compounds disproportionate rapidly to Tc(IV) and Tc(VII), while another Tc(V) species is deposited on the electrode surface. Even though they reported UV-vis and gold surface-enhanced Raman scattering (Au-SERS) data for such compounds, these techniques were not capable to reveal their structure. Moreover, just like in acidic media, the experimental evidence is still not conclusive, and, therefore, it is not possible to provide a reliable reduction mechanism for Tc(VII), which also makes it extremely difficult to determine thermodynamic data of the process.

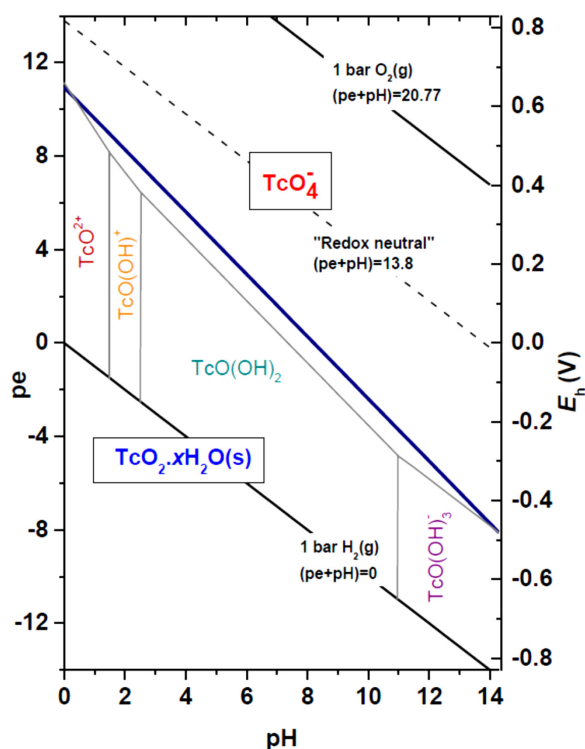


Figure 4. Pourbaix diagram of Tc calculated for ionic strength = 0 with thermodynamic data selected in the NEA–TDB. Bold blue line corresponds to Tc(VII)/Tc(IV) equilibrium. Taken from reference ⁴⁹.

Figure 4 shows the calculated Pourbaix diagram of technetium in water.⁴⁹ The diagram is based on Eq. [11], which is considered the main redox reaction between Tc(VII) and Tc(IV) in the NEA-TDB.^{28,35,50}

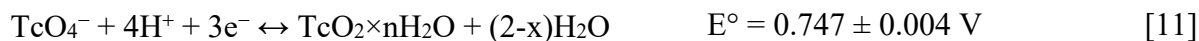


Figure 4 shows no information concerning the intermediary oxidation states of technetium such as aqueous Tc(III) species that have been reported under reducing conditions and high concentrations of acid.^{43,51} The irreversibility of almost all the redox processes between unusual technetium oxidation states in water makes the calculation of thermodynamic data almost impossible.⁵² On the other hand, reports of unusual oxidation states, mostly Tc(III), Tc(V) and Tc(VI), have been given for different media (various pH values, electrolytes and ionic strengths) and there is no reproducible pattern that allows conclusions about the reduction mechanism to be drawn when combining such studies.

It is noteworthy to mention that Eq. [11] is an overall reaction that does not account for the number of elementary reactions that are most likely to happen together in order to produce it. If such elementary reactions occur in parallel, the mechanism behind the Tc reduction would be very difficult to understand. However, the kinetic pathways by which technetium oxidation states evolve could be studied by a combination of electrochemical and spectroscopic techniques. If, otherwise, those elementary reactions are sequential, not only the reduction mechanism would be very well established, but also the reaction rate could be limited by the use of additives that disrupt or increase the production of Tc(IV). A better understanding on the individual elementary reactions that are involved in the reduction will increase the knowledge on the basic chemistry on technetium, which is key for the design of safe strategies for nuclear waste management.

1.1.2. Electrochemical methods

Electrochemical methods are divided in three types: conductometry, potentiometry and amperometry/voltammetry. Conductometric methods are used to determine the charge concentration by measuring the solution resistance and, in consequence, they are not species-selective.⁵³ Potentiometry is performed in equilibrium, it measures the potential of an indicator electrode vs. a reference electrode by using a high impedance voltmeter, meaning that the measurement is done effectively at zero current.⁵³ The selectivity of the technique depends

on the material of the electrodes and, once optimized, potentiometry is very useful to determine the concentration of a species in solution, as well as to obtain relevant thermodynamic data of a redox reaction, like the reaction potential or the reaction constant.⁵³

Amperometry and voltammetry are both performed by using a potentiostat that maintains a constant potential in the working electrode by adjusting the current with an auxiliary electrode.⁵⁴ These two techniques have a high sensitivity (they can detect analytes in picomolar concentrations when optimized) and can be used to determine redox reaction mechanisms as well as their thermodynamic constants. In amperometry, a chosen potential is applied to the working electrode causing a chemical reaction and a current flow. The analysis of the behavior of the current in a certain period (chronoamperometry) yields the amount of electrons involved during the redox process, which can be used for the mechanism determination. Voltammetry measures the current as a function of the applied potential, allowing the simultaneous determination of several species that react at different potentials within the same experiments with no further need for separation techniques.

As the aim of this work is to understand the redox behavior of technetium and produce reliable thermodynamic constants to describe it, cyclic voltammetry (CV), rotating disk electrode (RDE) and chronoamperometry (CA) coupled with UV-vis have been selected to study the reduction of Tc(VII).

a) Cyclic voltammetry (CV)

Cyclic voltammetry is one of the most popular methods of electroanalysis; it is widely used for the study of redox processes because it gives information about the stability of the reaction products, the presence of intermediates and the reversibility of the reaction. When the reaction is reversible, CV can also be used to determine the amount of electrons involved in the redox process, the reduction potential of an analyte and the reaction constant. In addition, CV is often applied for the determination of the concentration of redox active analytes, exploiting the proportionality between current and concentration.⁵⁵

During a cyclic voltammetry, the potentiostat applies a linear potential sweep to the working electrode in cyclical phases, as shown in Figure 5a. The potentials depicted as maximum and minimum (E_{\max} and E_{\min}) in Figure 5a constitute the working potential window that depends on the redox behavior of the analyte. It is critical for the selection of the background electrolyte,

which must be inert throughout the potential window, and the working electrode, on which hydrogen or oxygen evolution must not occur during the CV.

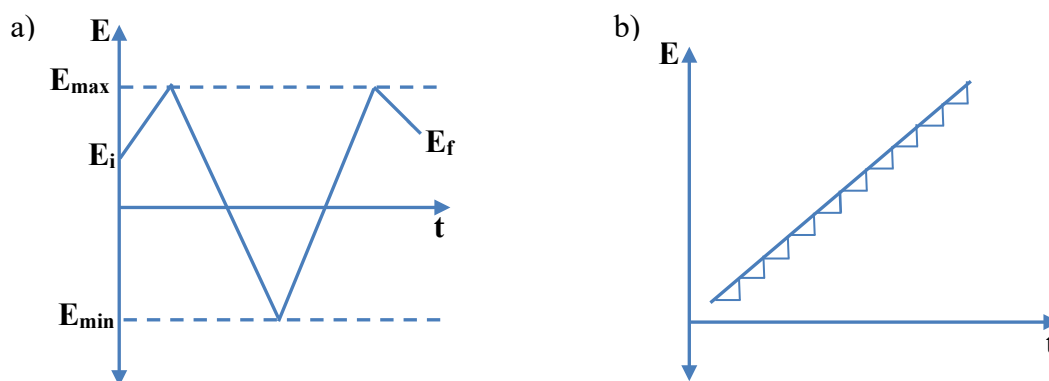


Figure 5. a) Potential waveform of a cyclic voltammetry. E_i is the initial potential, E_f the final potential. E_{\max} and E_{\min} are the maximum and the minimum potentials, respectively. b) Staircase used by modern devices for the potential sweep.

In addition to the potential window, there are two parameters of importance for the CV result: the scan rate and the step potential. The scan rate (v) is defined as $v = |dE/dt|$ and it determines the speed at which the sweep is executed. Both too low and too high scan rates can lead to loss of information during the process. In the case of the step potential, it is necessary to bear in mind that most of the modern electrochemical devices do not perform a linear sweep like the one shown in Figure 5a, but a succession of small steps in a staircase,⁵³ as shown in Figure 5b. The theory for cyclic voltammetry is based on voltage ramps and not on voltage steps; therefore, it is crucial that the step potential (which is the height of the step) is small enough so the two approaches are nearly equivalent.

The result of a CV is a plot of current, I , measured between the working electrode and the counter electrode, versus applied potential, E , measured between the working electrode and the reference electrode. Such plot is known as voltammogram. Figure 6 shows the voltammogram of a reversible reaction with only one electron transfer. When the potential sweep goes from positive to negative values, the reduction process is taking place and the peak obtained is called cathodic. On the contrary, when the sweep goes from negative to positive values, the oxidation is occurring and the obtained peak is called anodic. For a reversible reaction, the ratio between the maximum current (height) of the cathodic peak, I_{cp} , and the height of the anodic peak, I_{ap} , should be 1.⁵⁴

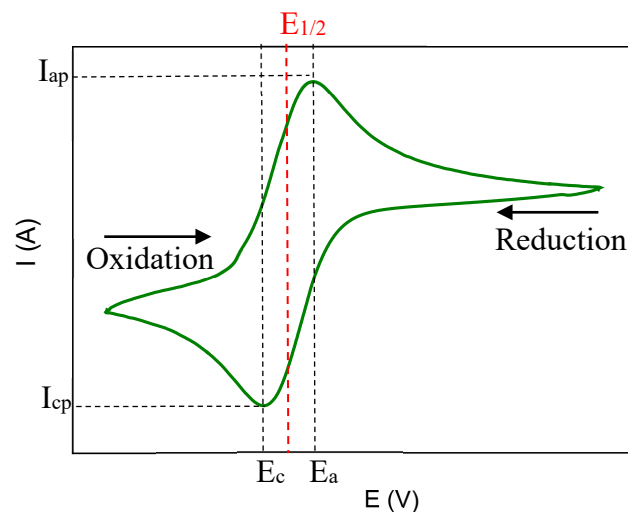


Figure 6. Typical voltammogram of a reversible reaction. I_{cp} and E_c correspond to the maximum current and the potential of the cathodic peak. I_{ap} and E_a are the maximum current and the potential of the anodic peak. $E_{1/2}$ is the half-wave potential.

The half-wave potential, $E_{1/2}$, is defined in Eq. [12], where E_a and E_c are the potential of the anodic and cathodic peaks, respectively (see Figure 6). Eq. [12] can be used in combination to the Nernst equation (Eq. [13], where E is the potential of the electrochemical cell in V, $E^{\circ'}$ is the potential in V of the reaction at a temperature T in K, R is the universal gas constant in $\text{J mol}^{-1} \text{K}^{-1}$, n the number of transferred electrons, $[\text{Ox}]$ is the molar concentration of the oxidized species and $[\text{Red}]$ the molar concentration of the reduced species) to determine directly the potential $E^{\circ'}$ of the redox reaction at the working temperature. This is possible because for $E_{1/2}$, $[\text{Red}] = [\text{Ox}]$ at the electrode surface, and, therefore, $E_{1/2} = E^{\circ'}$. In the same way, with a known $E^{\circ'}$ it would be possible to determine the number of electrons transferred in an electrochemical reaction.

$$E_{1/2} = \frac{E_a + E_c}{2} \quad [12]$$

$$E = E^{\circ'} + \frac{RT}{nF} \ln \frac{[\text{Ox}]}{[\text{Red}]} \quad [13]$$

Unfortunately, in most of the cases the plots obtained from CV are not similar to Figure 6, as factors like multiple electron transfer or irreversibility of the reaction hinder the data treatment. Therefore, voltammograms like the ones depicted in Figure 7 are more common. For such reactions, CV is a useful preliminary essay to determine the potential window at which the experiment should be carried out and to identify sorption phenomena like the one shown in

Figure 7b, where the loop showed in the insert of the voltammogram indicates the deposition of the analyte on the electrode.⁵⁶ However, in these cases the use of CV for the determination of the reaction potential or the number of electrons transferred is not feasible and other methods like the rotating disk electrode must be used.

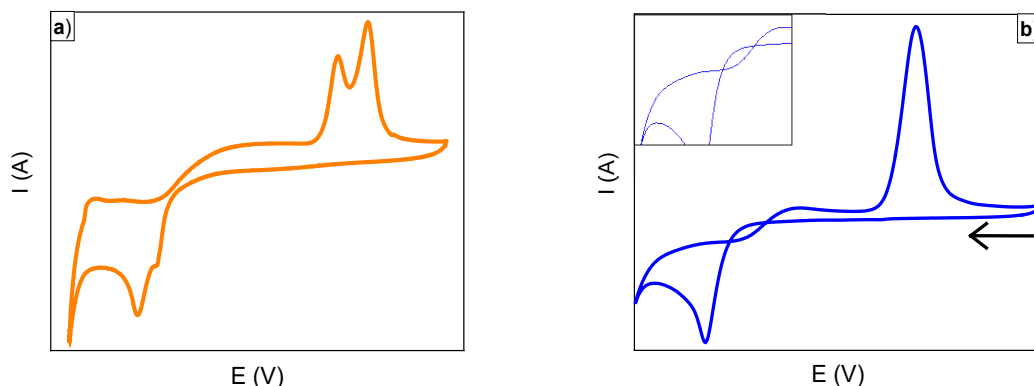


Figure 7. Cyclic voltammograms of complex systems. a) Cyclic voltammogram of a multielectron transfer. b) Cyclic voltammogram of an analyte being deposited on the working electrode.

b) The Randles-Sevcik equation and the Levich equation

According to the IUPAC, the diffusion layer (DL) is “the region in the vicinity of an electrode where the concentrations are different from their value in the bulk solution.”⁵⁷ From Figure 8 it can be inferred that the definition of the thickness of the diffusion layer, δ , is arbitrary because the concentration of the analyte on the surface, c^* , approaches asymptotically to the concentration in the bulk solution, c .

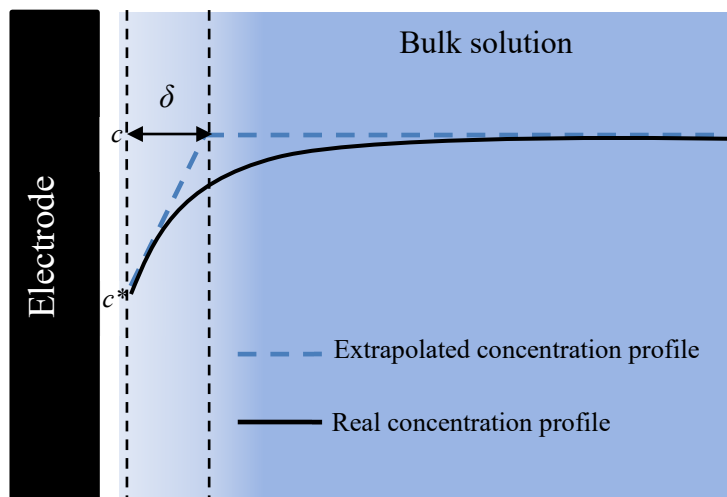


Figure 8. Schematic representation of the diffusion layer. c is the concentration of the analyte in the bulk solution; c^* is the concentration in the diffusion layer. Modified from reference ⁵⁷.

In general, the thickness of the diffusion layer depends on the diffusion coefficient of the analyte in the solvent. More specifically for voltammetric measurements, it depends on the scan rate of the experiment: the slower the scan rate, the thicker the diffusion layer, which affects directly the peak current, I_p . The relationship between the scan rate and the peak current is described by the Randles-Sevcik equation, Eq. [14] that at 25 °C becomes Eq. [15].

$$I_p = 0.4463nFAc \left(\frac{nFvD}{RT} \right)^{1/2} \quad [14]$$

$$I_p = 2.69 \cdot 10^5 n^{3/2} A c D^{1/2} v^{1/2} \quad [15]$$

where n is the number of electrons transferred, F the Faraday constant in $C \text{ mol}^{-1}$, A the area of the electrode in cm^2 , c the analyte concentration in mol cm^{-3} , D the diffusion coefficient in $\text{cm}^2 \text{ s}^{-1}$, T the temperature in K and v the scan rate in V s^{-1} . For a Randles-Sevcik analysis, several cyclic voltammograms of the same analyte solution are performed at different scan rates, as shown in Figure 9a. The I_p is then plotted against $v^{1/2}$, known as a Randles-Sevcik plot (Figure 9b), and from the slope of such plot D or n can be determined. However, for this work with technetium, both n and D are unknown and, therefore, another equation is required to solve the system.

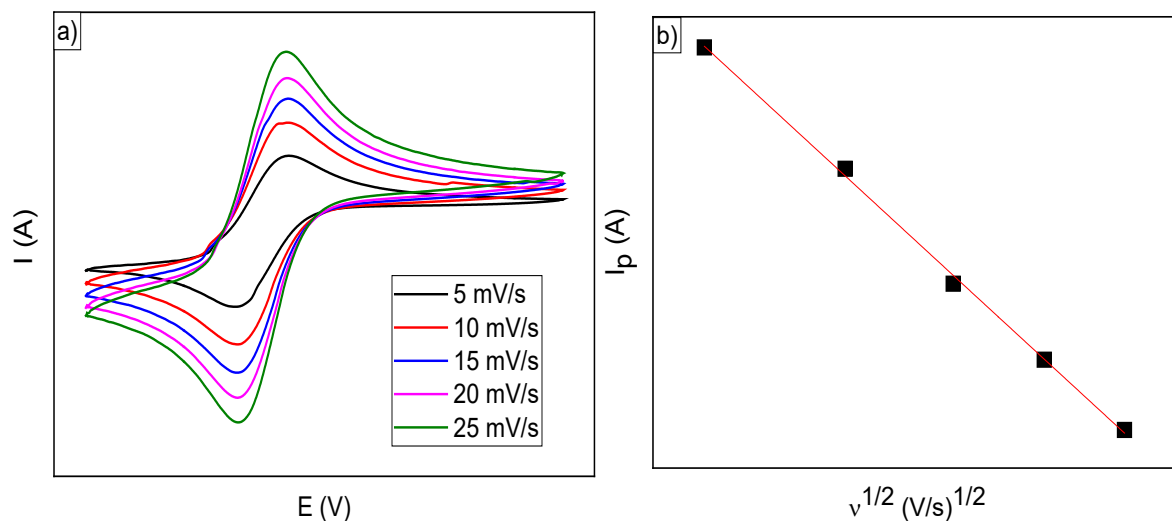


Figure 9. Randles-Sevcik analysis. a) Cyclic voltammograms at different scan rates. b) Randles-Sevcik plot.

During a cyclic voltammetry, the mass transport of the analyte is controlled only by diffusion because it is a stationary process, i.e. no convection is taking place as no agitation should be performed during the experiment. There is also an inexhaustible supply of fresh analyte due to

the fact that the volume on the diffusion layer is negligible compared to the volume of the bulk solution. In this case, if the redox reaction is prolonged in time, the thickness of the DL will increase indefinitely, which will result in non-steady-state current density, meaning that the current density changes with time.

The rotating disk electrode (RDE) is an instrumental design feature to stir the solution due to its rotation. This drags some of the solution to the spinning disk while the centrifugal force removes it away from the center of the electrode, as shown in Figure 10. This results in a constant laminar flow of the solution across and towards the electrode. Such flow fixes the thickness of the diffusion layer leading to a steady-state current density that, contrary to the cyclic voltammetry, is not limited by the diffusion of the analyte in the solution. In this scenario, while the thickness of the diffusion layer will be controlled by the solution flow, i.e. convection, the transport rate of the analyte will be controlled by its diffusion through the DL.

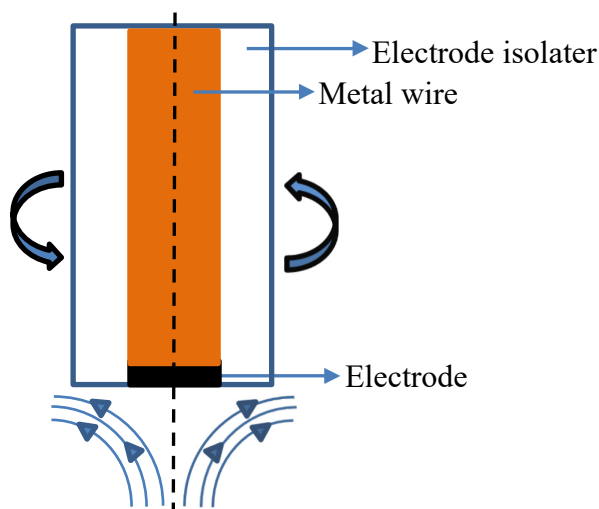


Figure 10. Schematic representation of the rotating disk electrode and the flux of the solution.

The solution flow can be controlled by the electrode rotation and the behavior of the current in a RDE experiment can be modelled by Eq. [16], which is the Levich equation, where n is the number of electrons transferred, F the Faraday constant in C mol^{-1} , A the area of the electrode in cm^2 , ν the kinematic viscosity in $\text{cm}^2 \text{s}^{-1}$, D the diffusion coefficient in $\text{cm}^2 \text{s}^{-1}$, c the analyte concentration in mol cm^{-3} and ω the angular velocity of the RDE in rad s^{-1} .

$$I_L = (0.620)nFA\nu^{-1/6}D^{2/3}c\omega^{1/2} \quad [16]$$

The peak current obtained in a CV will become a plateau-like region when using an RDE. This plateau is the limiting current, I_L , depicted in Figure 11a, and when it is plotted vs $\omega^{1/2}$ (Levich

plot, Figure 11b) it can be used to determine D or n, like with the Randles-Sevcik equation (Eq. [15]).

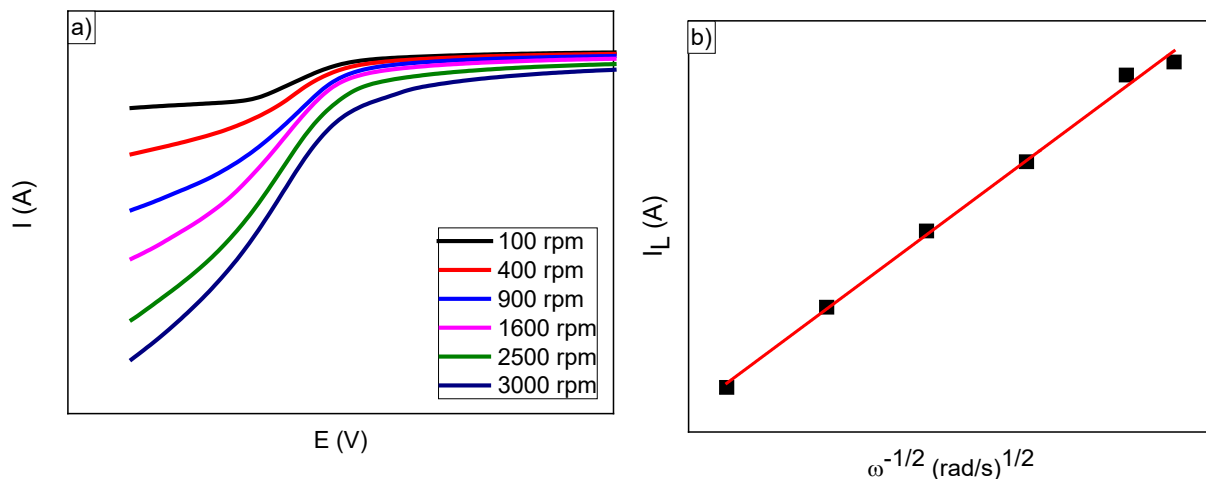


Figure 11. Levich analysis. a) Potential sweeps at different angular velocities. b) Levich plot.

In order to determine the reduction mechanism for technetium in this work, both equations have been combined as shown below.

Being X the slope of the Levich plot and Y the slope of the Randles-Sevcik plot, two equations (Eq. [17] and [18]) are given for two unknown variables (D and n):

$$X = 0.620FA\nu^{-1/6}CD^{2/3}n \quad [17]$$

$$Y = 2.69 \cdot 10^5 ACn^{3/2}D^{1/2} \quad [18]$$

After solving the equation system, the Eq. [19] and [20] are derived for D and n respectively:

$$D = \left(\frac{\alpha E}{X} \right)^2 \quad [19]$$

$$n = \frac{Y}{\alpha D^{3/2}} \quad [20]$$

where $\alpha = 0.620FA\nu^{-1/6}C$, $\beta = 2.69 \cdot 10^5 AC$ and $E = (Y/\beta)^{3/2}$.

c) Chronoamperometry coupled with ultraviolet–visible spectroscopy (CA/UV-vis)

In chronoamperometry, the current generated after an applied potential step is measured as a function of time. This technique is also known as potentiostatic coulometry and, in summary, is a controlled-potential bulk electrolysis. Figure 12 shows the typical plot obtained, called chronoamperogram.

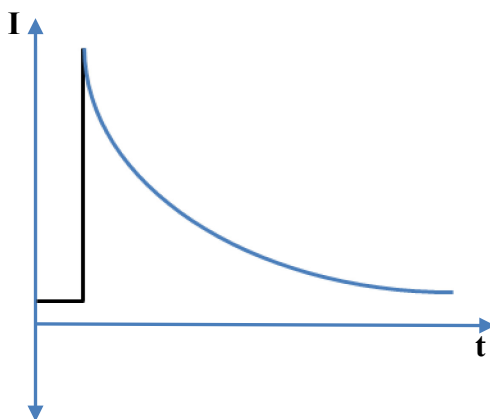


Figure 12. Chronoamperogram.

Like in voltammetry, chronoamperometry produces two types of currents: the capacitive current, which decays exponentially with time, and the faradaic current that is a result of the electron transfer and decays with time as described by the Cottrell equation (Eq. [21]).

$$I = \frac{nFAc\sqrt{D}}{\sqrt{\pi t}} \quad [21]$$

where I is the current (A), n the number of electrons involved, F the Faraday constant (C mol^{-1}), A the area of the electrode (cm^2), c the initial concentration of the electroactive analyte (mol cm^{-3}), D is the diffusion coefficient of the analyte ($\text{cm}^2 \text{s}^{-1}$) and t the time (s).

As the capacitive currents are not involved in the redox process, in order to use the Cottrell equation, only the second part of the chronoamperogram, colored in blue in Figure 12, must be used in the data analysis, which can yield the number of electrons involved in the redox process.

If the diffusion coefficient of the analyte in the solvent is known, the information of the number of electrons can be used to characterize the reaction products. However, this information will

be obtained by means of the RDE and, for this reason, the chronoamperometry will mainly be used in this work for the controlled-potential bulk electrolysis after determining the potential of intermediary oxidation states appearing within CV. The electrolysis will be monitored by UV-vis aiming at the identification of the oxidation state of technetium.

As its name indicates, ultraviolet–visible spectroscopy works in the ultraviolet and the adjacent visible spectral wavelength regions (190 – 750 nm). Its working principle is based on the fact that molecules can absorb energy of this region of the electromagnetic spectrum to excite electrons from their basal state to higher anti-bonding molecular orbitals. Such electrons might be non-bonding, called n-electrons, or bonding, σ and π -electrons. The measure of how radiation is attenuated when it passes through the sample is called absorbance, A , and it depends on the sample concentration as described by the Beer-Lambert law, Eq. [22], where c is the sample concentration, d the path length and ϵ the extinction coefficient of the analyte.

$$A = c d \epsilon \quad [22]$$

Different molecules absorb radiation of different wavelengths. The absorption spectrum shows a number of absorption bands corresponding to functional groups within the molecule. Even though UV-vis spectroscopy cannot elucidate alone the structure of a compound, some compounds of technetium intermediary oxidation states have characteristic UV-vis bands, as mentioned before, which could be used for their identification.

1.2. Reduction of Tc(VII) in NaClO₄

The results presented in this section are part of the paper “Exploring the reduction mechanism of ⁹⁹Tc(VII) in NaClO₄: A spectro-electrochemical approach” in preparation for Inorganic Chemistry.

1.2.1. Cyclic voltammetry

The cyclic voltammograms of the 0.5 mM Tc solutions in 2M NaClO₄ and of the pure background solution at five different pH values are shown in Figure 13. As it was mentioned before, NaClO₄ was selected as background electrolyte because it does not form complexes with technetium.³⁵ The voltammograms of NaClO₄ clearly indicate no electrochemical changes in the potential window used for this study (Figure 13b). Therefore, the electrochemical behavior of Tc solutions depicted in the CVs of Figure 13a can be attributed only to technetium in water.

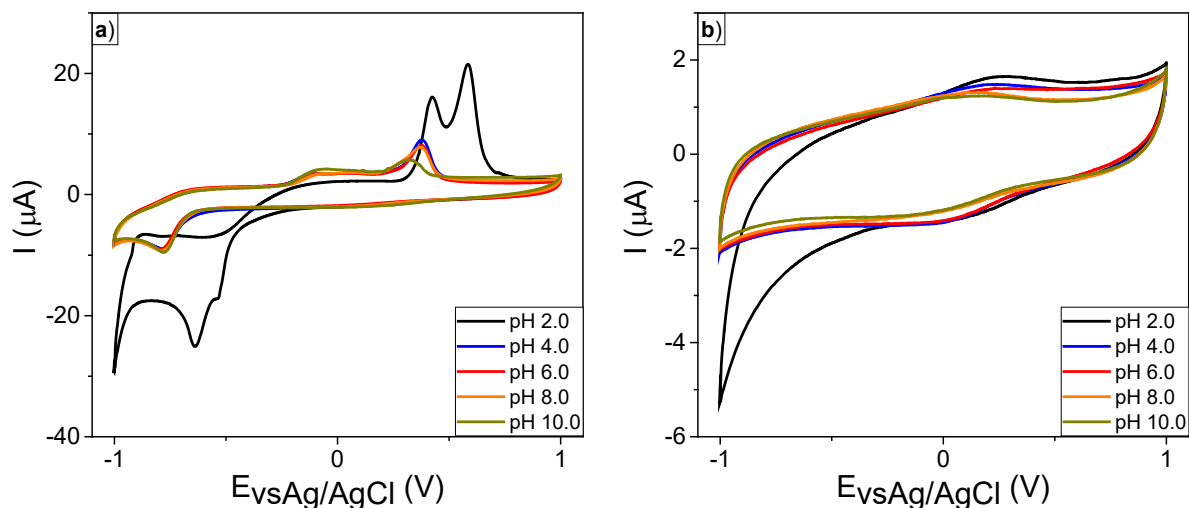


Figure 13. Cyclic voltammograms of a) 0.5 mM Tc solutions in 2M NaClO₄ at different pH values and b) Cyclic voltammograms of 2 M NaClO₄ solutions at different pH values. Scan rate: 10 mV s⁻¹.

For the technetium solutions considerable changes in voltammograms at different pH values are observed. At pH 2.0, the CV suggests the brief formation of an intermediary oxidation state at -534 mV during the reduction. This behavior would be in good agreement with the Latimer diagram of technetium under acidic conditions⁵⁸ (Figure 3) according to which the reduction from Tc(VII) to Tc(IV) would have Tc(VI) as intermediary. Nevertheless, several authors suggest that Tc(VI) would be too unstable in water and it would rapidly disproportionate to

Tc(VII) and Tc(V),^{20,37,38} which increases probability that the oxidation state of the intermediary shown in Figure 13a is Tc(V). A second cathodic peak (CP) is formed around -620 mV and may correspond to the formation of Tc(IV). At $\text{pH} \geq 4$, Figure 13a shows that the reduction of Tc(VII) is direct since only one CP around -780 mV is obtained during the CV. This peak is tentatively assigned to the formation of Tc(IV) and it is shifted with respect to the second cathodic peak at pH 2.0 due to the change on the reduction mechanism. As it was already discussed in section 1.1.1, under alkaline conditions the conflicting reports on the mechanism hindered the construction of a proper Latimer diagram for technetium.²⁰ It is not even clear if the reduction takes place with intermediaries or in one single step: On one hand, some authors^{38,39} propose the reduction from Tc(VII) to Tc(III) passing through Tc(IV), while others suggest that the final product would be Tc(IV) with Tc(V) as an intermediary step.^{36,41,42} On the other hand, Grassi et al.³⁷ propose the reduction from Tc(VII) to Tc(IV) with the direct transfer of three electrons. However, it must be remarked that all these previous studies used ions like Cl^- as background electrolytes that are well known to form complexes with technetium,³⁵ clearly interfering with its reduction in water. The data presented in Figure 13a is more reliable with respect to the mechanism determination in water as ClO_4^- will not coordinate technetium.

1.2.2. Rotating disk electrode

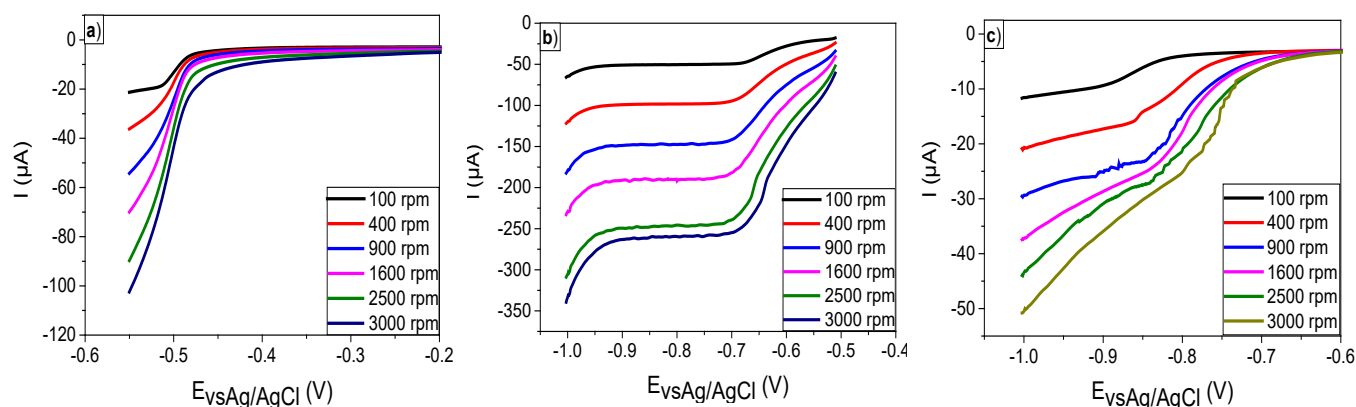


Figure 14. Reduction curves of 0.5 mM Tc solutions in 2M NaClO_4 . a) First cathodic peak at pH 2.0. b) Second cathodic peak at pH 2.0. c) Cathodic peak at pH 10.0. Scan rate: 10 mV s^{-1} .

The CVs depicted in Figure 13a gave an idea of the reduction mechanism of Tc(VII). However, they cannot be used for the determination of the amount of electrons transferred during the process and, in consequence, the rotating disk electrode was employed. Since the behavior of technetium in the perchlorate media at $\text{pH} \geq 4.0$ is almost independent of the pH, the systems at pH 2.0 and pH 10.0 were selected to perform the experiments with the RDE. The reduction

curves of 0.5 mM Tc in 2 M NaClO₄ at pH 2.0 and 10.0 are presented in Figure 14, where the first CP at pH 2.0 makes reference to the intermediary species found around –534 mV in the CV.

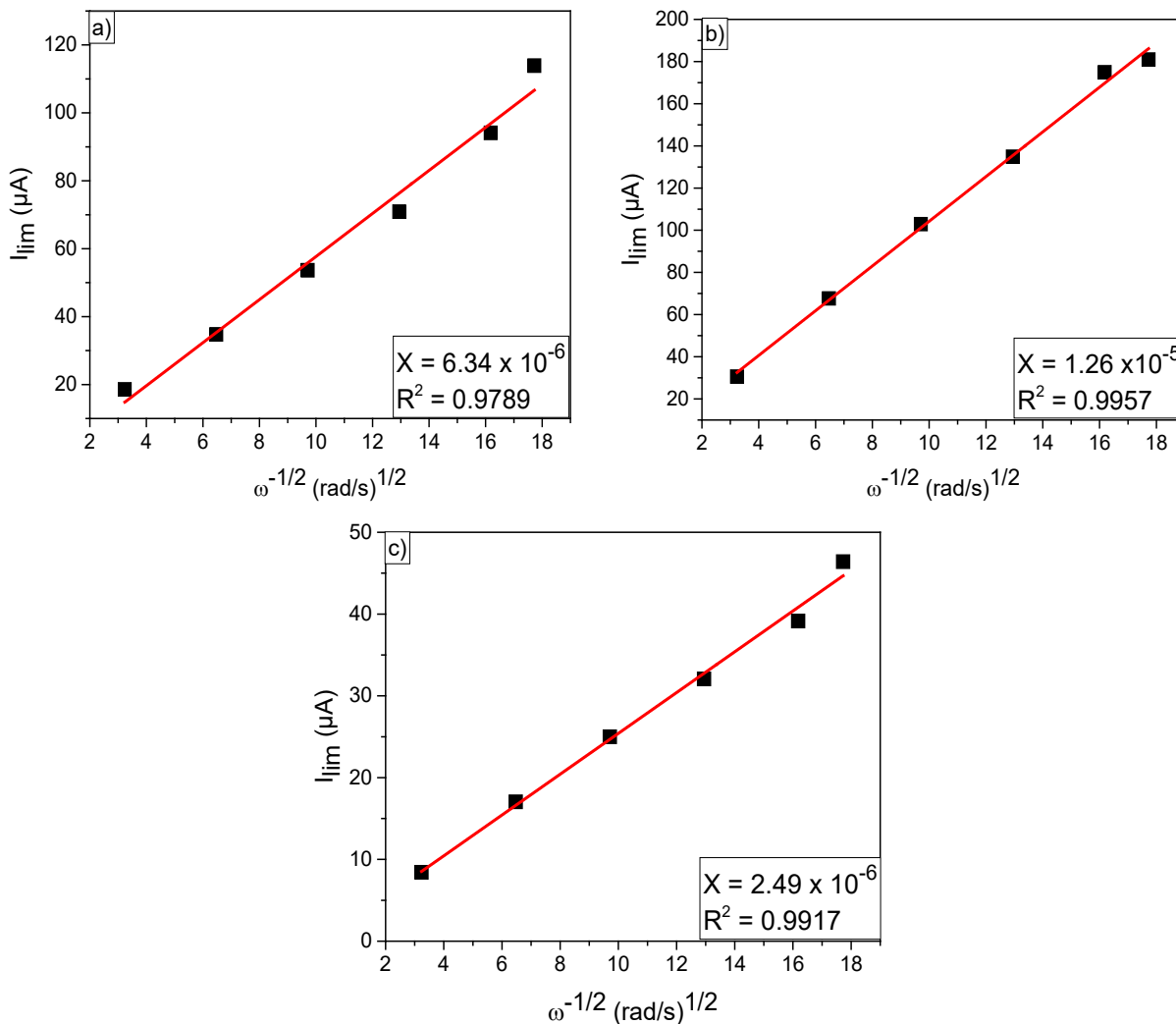


Figure 15. Levich plots of 0.5 mM Tc solutions in 2M NaClO₄. a) First cathodic peak at pH 2.0. b) Second cathodic peak at pH 2.0. c) Cathodic peak at pH 10.0. X is the Levich slope (Eq. [17]).

While the I_{lim} are clearly proportional to the square root of the angular velocity at both pH values (Figure 15), the Randles-Sevcik plots presented in Figure 16 show that the I_p also have a linear correlation with the square root of the scan rate, making the data presented here valid for the mathematical treatment of section 1.1.2b). For solving Eq. [19] and [20] the viscosity of the system was assumed as the kinematic viscosity of 2 M NaClO₄ in water ($8.90 \times 10^{-3} \text{ cm}^2 \text{ s}^{-1}$)⁵⁹ because the concentration of the electrolyte is high enough compared to the concentration of the analyte (0.5 mM Tc) to assume that the viscosity will only be governed by the salt.

At pH 2.0, the diffusion coefficient in 2 M NaClO₄ for the electroactive species responsible of the first cathodic peak was $4.28 \times 10^{-5} \text{ cm}^2 \text{ s}^{-1}$ whereas for the second it was $2.63 \times 10^{-4} \text{ cm}^2 \text{ s}^{-1}$. At pH 10.0, the electroactive species has a diffusion coefficient of $5.75 \times 10^{-6} \text{ cm}^2 \text{ s}^{-1}$ in 2 M NaClO₄. Since the starting species at both pH values is Tc(VII) in the form of TcO₄⁻, it is clear that TcO₄⁻ is the electroactive species of the first CP at both pH 2.0 and pH 10.0. Unfortunately, previous studies on Tc diffusion coefficients are extremely limited and most of them deal with its diffusion in clays like bentonite.⁶⁰ However, for the sake of comparison, it is possible to see in these studies that the diffusion coefficient of pertechnetate decreases as the pH increases, which is also the case in this work in 2 M NaClO₄.

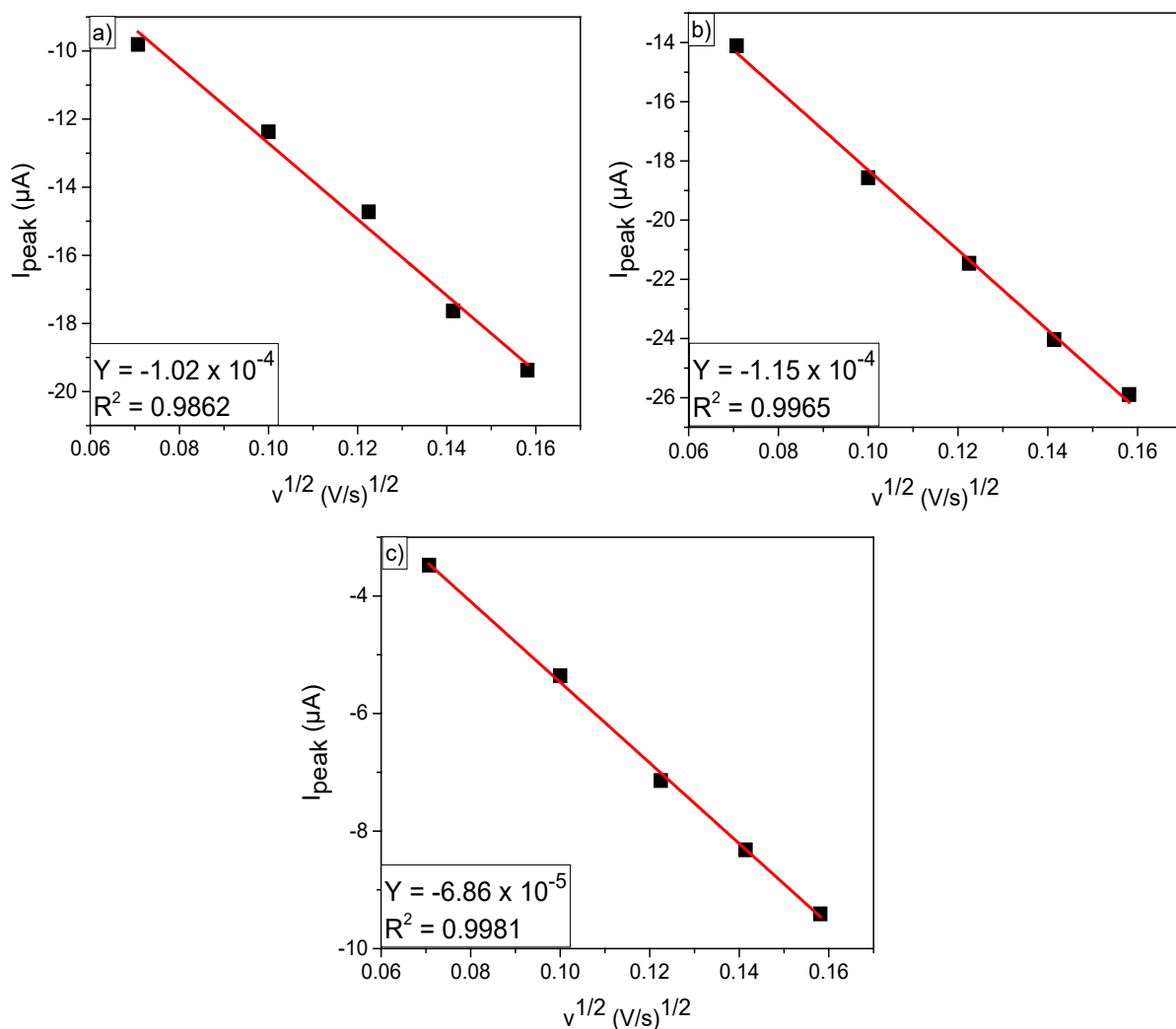


Figure 16. Randles-Sevcik plots of 0.5 mM Tc solutions in 2M NaClO₄. a) First cathodic peak at pH 2.0. b) Second cathodic peak at pH 2.0. c) Cathodic peak at pH 10.0. Y is the Randles-Sevcik slope (Eq. [18]).

Lastly, using the diffusion coefficients, it was found that at pH 2.0 the reduction of Tc(VII) begins with the transfer of 2.1 ± 0.3 electrons yielding Tc(V) as an intermediary oxidation state that afterwards, with the pass of 1.3 ± 0.3 electrons, becomes Tc(IV). At pH 10.0, the reduction of Tc(VII) is direct with the transfer of 3.2 ± 0.3 to produce Tc(IV). The results found for the reduction of Tc(VII) in NaClO₄ with the RDE are summarized in Table 1.

Table 1. Reduction mechanism of Tc(VII) in NaClO₄ at pH 2.0 and 10.0 in their respective cathodic peaks (CP).

CP \ pH	2.0	10.0
1	$\text{Tc(VII)} + 2.1 \pm 0.3 \text{ e}^- \rightarrow \text{Tc(V)}$ $D = 4.28 \times 10^{-5} \text{ cm}^2 \text{ s}^{-1}$	$\text{Tc(VII)} + 3.2 \pm 0.3 \text{ e}^- \rightarrow \text{Tc(IV)}$ $D = 5.75 \times 10^{-6} \text{ cm}^2 \text{ s}^{-1}$
2	$\text{Tc(V)} + 1.3 \pm 0.3 \text{ e}^- \rightarrow \text{Tc(IV)}$ $D = 2.63 \times 10^{-4} \text{ cm}^2 \text{ s}^{-1}$	----

1.2.3. Spectro-electrochemical measurements

Figure 17 shows the UV-vis data collected during chronoamperometry in the spectro-electrochemical cell. At the beginning of the spectro-electrochemical experiment only Tc(VII) is present as the UV-vis spectra presents two signals at 247 and 289 nm that are characteristic of TcO₄⁻.¹⁹ Upon stepwise reducing the potential to -1000 mV, these Tc(VII) features are clearly reduced in intensity and finally disappear at the end of the experiment, i.e. Tc(VII) was fully reduced.

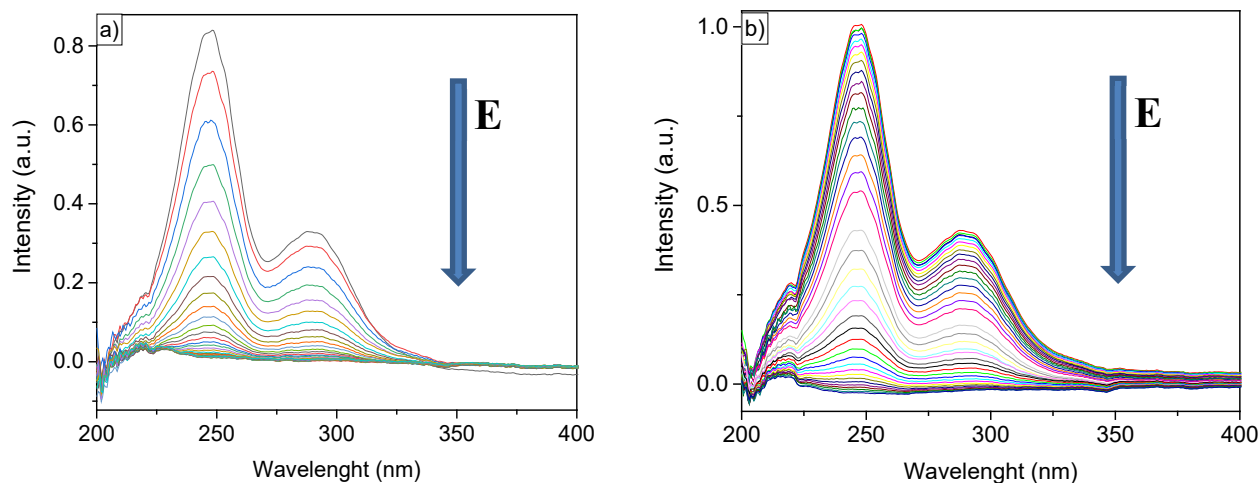


Figure 17. UV-vis spectra of 0.5 mM Tc solutions in 2M NaClO₄ measured during the chronoamperometry. a) pH 2.0. b) pH 10.0.

In contrast to CV, the spectral data at pH 2.0 and pH 10.0 are equal, meaning that at pH 2.0 no changes are detected that could be attributed to the intermediary species. The present data give hints that intermediary and final species are inactive in the UV-vis range or that the reduction from the intermediary species Tc(V) to Tc(IV) is too fast to be detected by the used set-up.

After the total reduction of Tc(VII) at both pH values, a black solid was deposited on the glassy carbon electrode. According to the electrochemical analysis, this solid should be Tc(IV) which explains why no signal of this oxidation state was found by UV-vis. The solid easily detached itself from the electrode as soon as it got dry, meaning that no irreversible sorption of technetium took place on the electrode. For further molecular characterization the solid was studied by Raman microscopy and ^{99}Tc NMR.

1.2.4. Solid analysis

Figure 18 shows the Raman spectra of the solids obtained after the complete reduction of Tc(VII) in 2 M NaClO₄ at pH 2.0 and 10.0.

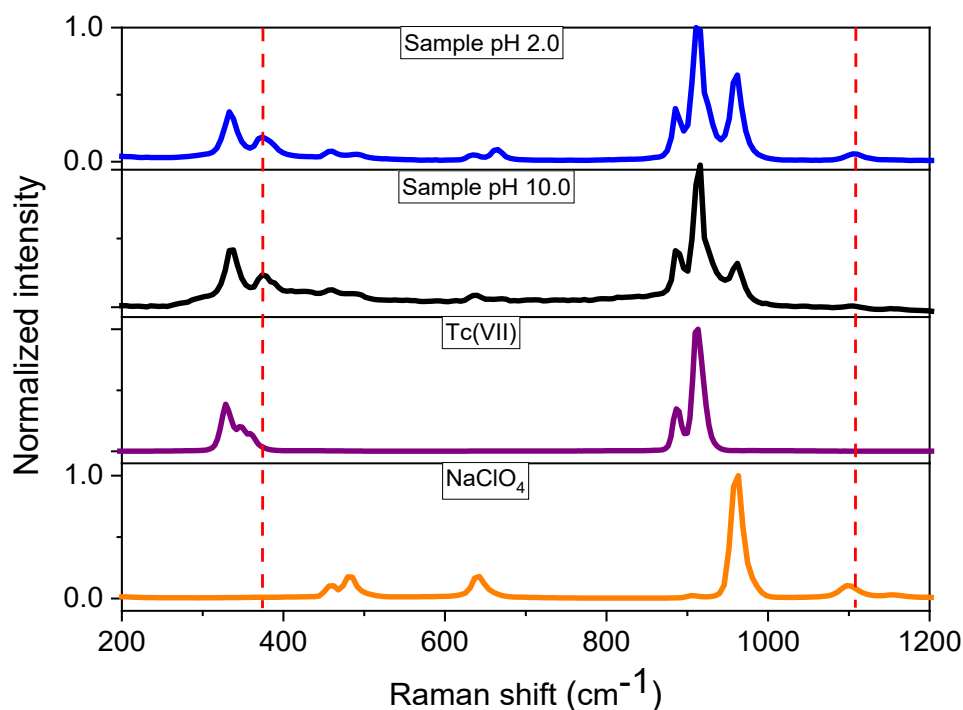


Figure 18. Raman spectra of the black solid obtained after the total reduction of 0.5 mM Tc(VII) in 2M NaClO₄ at pH 2.0 and 10.0 during the spectro-electrochemical essays. The Raman spectra of K₂TcO₄ and NaClO₄ have been added for comparison. The red dotted lines highlight the unidentified bands that correspond only to the black solid.

By comparing the spectra, it is clear that the chemical identity of the solids at both pH values is the same, confirming partially the reduction mechanisms proposed after the measurements with the RDE, since both of them yield Tc(IV) as the final reduction product. The bands at 458, 632, 666 and 960 cm^{-1} present in the samples can be attributed to NaClO_4 that was recrystallized along with the technetium solid after the electrode got dry. The bands at 333, 885 and 913 cm^{-1} could be identified as the TcO_4^- structure and they would correspond to Tc-O vibrations.^{61,62} After the assignment of the bands matching NaClO_4 and TcO_4^- , two unidentified bands at 374 and 1107 cm^{-1} remain, corresponding to Tc(IV) species suggested by the electrochemical analysis. So far, no Raman reference has been published for Tc(IV).

Since the resulting solids have the same chemical identity independent of the initial pH, it was decided to produce a second batch of the solid at pH 2.0 for NMR because at this pH the reduction was faster. Thus, the solid was dissolved in deuterated dimethyl sulfoxide (DMSO) (for more details, see section I in the experimental methods). The obtained ^{99}Tc -NMR spectrum shows a very broad (>10 kHz line width) feature at -1251 ppm. The latter is considered an authentic signal instead of artifacts from, e.g., rolling baseline, as it could be reproduced for varied acquisition parameters. The signals around -866 and -976 ppm in Figure 19 are considered artefacts as they were not reproducible throughout the experiment.

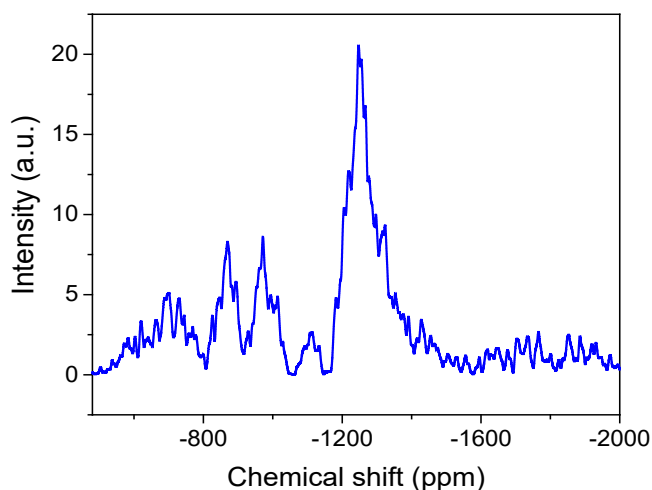


Figure 19. NMR spectrum of the black solid obtained after the total reduction of 0.5 mM Tc(VII) in 2M NaClO_4 at pH 2.0. Chemical shifts are reported relative to 1 mM aqueous NH_4TcO_4 .

The odd oxidation states of technetium (I, III, V and VII) are diamagnetic and, therefore, they have specific chemical shift ranges among which they can be found (see Table 2)^{63,64} The even oxidation states (II, IV and VI) are paramagnetic and, in consequence, their ^{99}Tc NMR signals

appear at different chemical shifts depending on the compound structure. The signal presented in Figure 19 does not appear in the range expected for any of the odd oxidation states and, since Tc(II) and Tc(VI) are too unstable to exist as solid phases with no complexing agent stabilizing them,³⁵ it is safe to conclude that the solid produced after the total reduction of Tc(VII) was Tc(IV), whose Raman spectrum is reported for the first time in this work, and confirms the reaction mechanisms found with the RDE.

*Table 2. Tc chemical shift ranges of the Tc odd oxidation states.*⁶⁴

Tc oxidation state	Tc chemical shift range (ppm)
0	-2477
I	-1460 to -3517
III	-78 to -1229
V	5500 to 806
VII	396 to 0

1.3. Summary

The reduction mechanism of Tc(VII) in 2 M NaClO₄ was studied by combining electrochemical and spectroscopic methods. Since NaClO₄ is inert in the potential window used and it does not form complexes with technetium, the findings presented here show the behavior of technetium in water. The cyclic voltammetries demonstrated that the reduction mechanism depends on the pH showing the formation of an intermediary oxidation state at pH 2.0 whereas at pH ≥ 4.0 the reduction occurred in one step. The combination of the Levich and the Randles-Sevcik analysis showed that at pH 2.0 the reduction of Tc(VII) begins with the transfer of 2.1 ± 0.3 electrons to produce Tc(V) that rapidly gains 1.3 ± 0.3 electrons to finally form Tc(IV). At pH ≥ 4.0 the reduction is direct from Tc(VII) to Tc(IV) after the transfer of 3.2 ± 0.3 electrons. A schematic representation of the reduction mechanisms is presented in Figure 20.

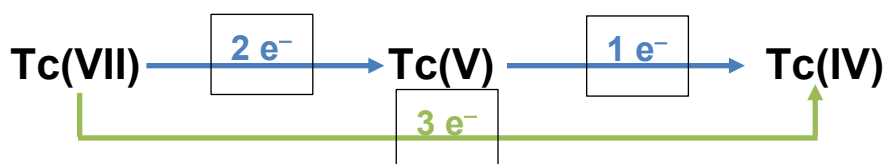


Figure 20. Schematic representation of the Tc(VII) reduction mechanism. Blue arrows correspond to pH 2.0 while the green arrow represents pH ≥ 4.0 .

The spectro-electrochemical analysis was not able to detect the intermediary Tc(V) that should have been formed between -530 and -540 mV at pH 2.0. This might be explained by a fast conversion to Tc(IV) that is more stable, a low extinction coefficient combined with small concentrations of Tc(V) that made it undetectable, or simply because the Tc(V) species formed in the reduction does not absorb light in the UV-vis region. Nevertheless, the reduction at both pH 2.0 and 10.0 was complete since the two characteristic UV-vis bands of Tc(VII) at 247 and 289 nm fully disappeared after the application of the reductive potential. At the end of the spectro-electrochemical experiments a black solid was deposited on the glassy carbon electrode regardless of the initial pH. The Raman spectra of the two solids (one obtained at pH 2.0 and the other at pH 10.0) showed that their chemical identity was the same. Two bands at 374 and 1107 cm^{-1} are tentatively to Tc(IV), since they were not observed in the spectral data of Tc(VII) nor NaClO₄. The ^{99}Tc -NMR spectra showed a chemical shift at -1251 ppm that could only correspond to the even oxidation states of technetium among which the only stable one under the working conditions is Tc(IV). Therefore, the solids obtained after the complete reduction of Tc(VII) consisted in Tc(IV), confirming thus the findings of the Levich and the Randles-Sevcik analysis.

Chapter 2.

Reductive immobilization of technetium by iron sulfide (FeS₂)

Under repository conditions, iron sulfide will be formed as both pyrite (cubic FeS₂) and the metastable marcasite (orthorhombic FeS₂) due to corrosion processes and microbial action.⁶⁵ Moreover, both iron sulfide polymorphs are accessory minerals in crystalline and clay rocks, which are considered potential host rocks for nuclear waste repositories.^{66,67} Bearing this in mind, previous works have studied Tc(VII) removal by pyrite in presence²⁵ and absence of humic substances,^{26,27} finding that it scavenges Tc(VII) from solution by triggering its reduction to Tc(IV). However, several issues have not been addressed in these studies: i) The pH effect on this removal is not clear as the authors have worked in a rather narrow pH range from 4 to 7 even though pyrite possesses an extensive pH stability range from 2 to 10.⁶⁸ ii) The molecular mechanisms involved have not been determined yet, which constitutes a large gap in the knowledge required to design and optimize a sustainable and efficient retardation strategy for Tc contamination. iii) The marcasite (commonly misidentified and confused with pyrite⁶⁸) reactivity has not been addressed, even though under repository conditions it will be formed along pyrite and, most probably, it will affect the Tc redox chemistry. iv) Even though the re-oxidation from Tc(IV) to Tc(VII) is very fast, no studies have been performed to check the extent of Tc re-mobilization from the pyrite surface into water as potential migration medium.

This chapter deals with the reductive immobilization of Tc(VII) by pure pyrite and a synthetic mixture marcasite-pyrite 60:40 in water and in 0.1 M NaCl. It combines batch experiments

performed under a wide variation of important parameters such as pH, contact time and Tc concentration with the application of several advanced spectroscopies, namely Raman microscopy, XPS and XAS, in order to gain a comprehensive molecular level understanding on the interaction between technetium and pyrite and the effect of marcasite in the Tc removal from solution.

2.1. Theoretical background

2.1.1. *Geochemical barriers*

Geochemical barriers have been used historically to prevent or to remediate water pollution. They should be built in zones of the Earth's crust with sharp physical or chemical gradients in order to control contaminant migration.⁶⁹ Depending on whether they let water flow or not, they can be classified as permeable or confining barriers.⁷⁰ Confining barriers are designed to prevent pollutant migration by acting like shields that inhibit water flow so the contaminants could only leave the barrier through diffusion.^{69,70} In contrast, in a permeable barrier additional material is placed in the near field to prevent break-through of a plume of contaminated ground water.⁷¹ Water can flow freely while the contaminant is filtered by the barrier through processes like degradation (chemical or biological processes that transform the pollutants into harmless compounds), precipitation (formation of insoluble compounds of the pollutant that cannot migrate with water) and adsorption (formation of complexes between the barrier material and the pollutant). In general, the materials used for the construction of permeable reactive barriers should possess the ability of changing the pH or redox potential, cause precipitation, have high sorption capacity, and/or release nutrients to promote the biological degradation of the contaminants.⁷²

According to the International Atomic Energy Agency (IAEA), a cumulative volume of $8.3 \times 10^5 \text{ m}^3$ of high-level and $7.3 \times 10^5 \text{ m}^3$ of low and intermediate-level radioactive waste have been produced worldwide until the early 2000s.⁷³ While several measures have been taken to properly discard low and intermediate-level waste and a significant portion of such pollutants is already stored in disposal sites,⁷⁴ the 2020s decade has started with no final repository for high-level radioactive waste in operation. Despite several concepts are considered for the nuclear waste management, such as deep boreholes or deep geological repositories (DGR), all of them consist of storing the nuclear waste underground in geological stable emplacements. However, the internationally most accepted concept is the DGR because its mechanical, chemical and physical properties have been widely studied since the 1960s and it is considered the safest option up to date.¹³ Therefore, the research is focused in the design and construction of mined repositories building multi-barrier systems capable of isolating the waste from the biosphere over long periods of time up to one million years,¹⁴ when the radioactivity of the spent nuclear fuel products has fallen below the natural radioactivity levels of the original uranium ore used to produce the nuclear fuel.

An example of a sophisticated approach specifically designed for crystalline host rock is the KBS-3 concept developed by the Swedish Nuclear Fuel and Waste Management Co as presented in Figure 21. The fuel pellets are assembled in rods and packed into gas-tight canisters made of copper and cast iron. Then the final canisters are enclosed with bentonite clay and they are lastly deposited underground surrounded by the bedrock. In the worst-case scenario, if water trespasses the confining barrier, reaches and corrodes the canisters, the released soluble radionuclides should be retarded by the natural permeable barriers surrounding the repository.

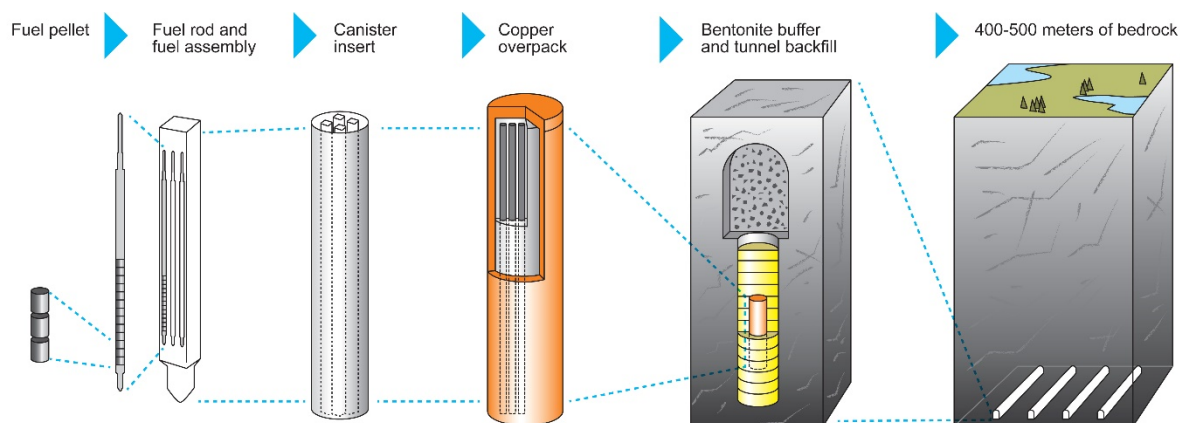


Figure 21. Scheme of the KBS-3 concept (developed by Swedish Nuclear Fuel and Waste Management Co). Taken from reference ⁷⁵.

As several chemical and physical processes can take place at the same time, a proper understanding of the interactions between the barriers and the long-lived radionuclides, as well as the chemical environment expected inside the repository are crucial for the design of such structures. For starting, it is important to bear in mind that a relatively short period under oxygen atmosphere is to be expected due to the oxygen occluded in the closed repository. After such time, the limited amounts of underground oxygen and the combination of reducing minerals like sulfides and ferrous materials with the engineered barriers (containing, for example, steel canisters) should have reached a long-lasting reducing environment.¹⁴ These conditions reduce the migration of most RNs whose immobility is favored when they are in lower oxidation state. That would be the case of technetium, whose interactions with different materials (especially with iron minerals) will be summarized in the next sections.

2.1.2. Technetium geochemistry

As it has already been mentioned, technetium distribution in the environment depends strongly on its speciation and the overall redox conditions. Under aerobic atmosphere, technetium is

found mainly as pertechnetate (TcO_4^-), a highly soluble anion that exhibits low sorption into the constituent minerals of soils and rocks. Such low sorption can be explained due to the fact that the surface charge of most minerals is dependent on the pH. Under acidic conditions it is positive while under alkaline conditions it is negative.^{76,77} The pH at which the surface charge is neutral is called point of zero charge and for most soil and rock forming minerals it is lower than the pH of the groundwater, so the surface charge is negative and it repels anions like pertechnetate, hindering even more its immobilization as TcO_4^- is already inert per se.¹⁵ As a consequence, technetium is transported to (and into) the subsurface almost at the same velocity as groundwater. Although Tc was used as an excellent tracer of oceanic currents,¹¹ this behavior is alarming in case of Tc transport through the biosphere from contaminated areas and for the safety case of repositories for high-level nuclear waste.

For typical agricultural and horticultural soils, the Eh ranges from 100 to 600 mV and the pH is located between 4 and 8.⁷⁸ According to a Pourbaix diagram of technetium in low carbonate, sulfate and halide systems (Figure 22), under pH neutral values, Tc(VII) is reduced between 200 and 100 mV to Tc(IV), whose main form, $\text{TcO}_2 \cdot n\text{H}_2\text{O}$, has a low solubility in water ($\text{Log } K_s = 8.17 \pm 0.05$ ¹⁶) and, in consequence, less mobile than pertechnetate. Under acidic conditions pertechnetate formation is favored between 100 and 600 mV. However, reduced species of technetium have been found under these conditions due to the availability of reducing agents. For example, in wet soils at pH 7 iron(II) formation starts around 150 mV, while sulfate and sulfide formation commences at -50 mV.^{11,78}

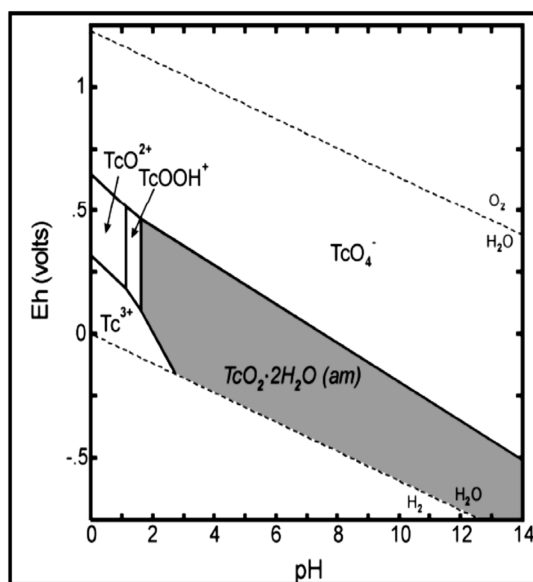


Figure 22. Pourbaix diagram of technetium in low carbonate, sulfate and halide systems. Taken from reference ¹¹.

The presence of reduced technetium species under Eh conditions that should favor pertechnetate formation was also found by several studies of Tc uptake by plants.^{79–81} Due to the reduced mobility of Tc under the optimal conditions for plant growth ($5.5 < \text{pH} < 7.5$ and $100 \text{ mV} < \text{Eh} < 600 \text{ mV}$) that clearly promotes TcO_4^- , the authors suggest technetium biological fixation involving reducing bacteria, or reduction caused by the presence of organic matter.

In contrast, Tc(VII) has been found in scenarios where its reduction is expected. For example, Cui et al.^{82,83} showed that in the presence of relatively high concentrations of Fe(II) in solution, the reduction from Tc(VII) to Tc(IV), thermodynamically feasible under such conditions, exhibits a very low reaction-rate. On the contrary, works on the heterogeneous reduction^{84–88} have found that the kinetics of the reaction increase significantly when the Fe(II) is a part of the structure of a mineral, like FeS_2 for example, and is maximal when the iron is pre-sorbed onto a mineral surface.

In summary, technetium mobility in the environment is governed not only by the Eh of the system, but also by two other factors: i) The availability of reducing agents, especially iron and sulfide and ii) The presence of iron, nitrate and sulfate reducing bacteria and organic matter.

a) Mechanisms involved in technetium removal by mineral phases

Besides precipitation and incorporation, adsorption on mineral surfaces is the main mechanism for the removal of contaminants from aqueous systems. It is defined as any process by which mass transfer of a chemical species from solution to solid surfaces occurs.⁷⁰

The adsorption capacity of a material depends on its surface properties, such as specific surface area, type, presence and concentration of reactive sites and charge. The strength of the interaction between the surface (sorbent) and the dissolved species (sorbate) is determined by the sorption mechanism and the chemical conditions, therefore, adsorption experiments must analyze several variables like contact time, pH, ionic strength, and the mineral and pollutant concentration. The overall redox conditions of the system are also an important parameter for this study since Tc(VII) is not significantly adsorbed on most surfaces while Tc(IV) adsorbs reasonably well onto a variety of materials.

There are two main adsorption mechanisms: i) anionic or cationic exchange (Figure 23) and ii) surface complexation. In the case of pertechnetate interactions with iron sulfide, the ionic exchange is not possible, as the mineral has no exchangeable sites.

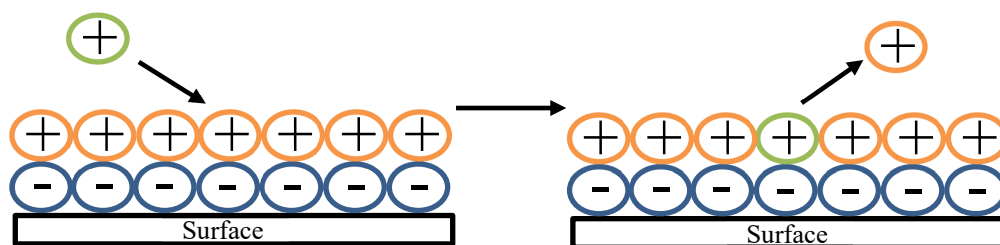


Figure 23. Schematic representation of the cation exchange.

Surface complexation (Figure 24) takes place when the reactive sorption sites interact with the pollutant in the interphase mineral/aqueous phase. The interaction of the mineral and the pollutant is ruled by the charge of the mineral and the aqueous speciation. Thus, the surface complexation depends on the parameters such as pH, Eh, ionic strength, presence of ions and dissolved gas (such as CO₂).⁸⁹ Depending on their nature, surface complexes can be classified as inner- and outer-sphere complexes.

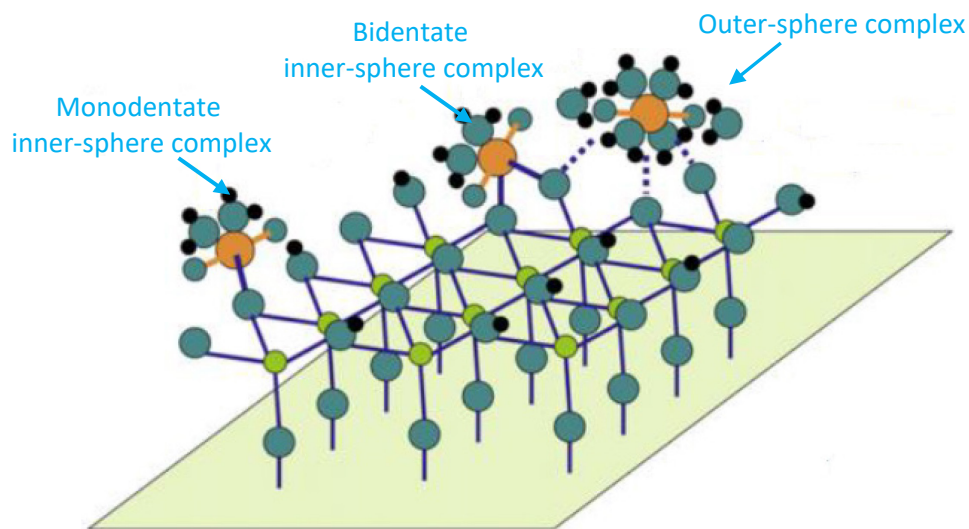


Figure 24. Schematic representation of surface complexation. Modified from reference ⁹⁰.

Inner-sphere complexes occur when chemical reactions take place between the functional surface sites and the pollutant (Figure 24). Such interactions lead in the case of (hydr)oxides to the formation of a metal-oxygen-ligand (M-O-L) complex whose reversibility is low. Due to this irreversibility, the pollutant retention via inner-sphere complexation is less dependent on the ionic strength, which can be used to identify this type of sorption with batch experiments. Outer-sphere complexation (Figure 24) occurs when the pollutant has mostly electrostatic interactions with the mineral surface or when the adsorption involves water molecules or inert ligands, which means that the process is non-specific and depends on the ionic strength.

Therefore, its activation energy is lower compared to inner-sphere sorption and, consequently, the reversibility of the outer-sphere complexation is much higher.

Even though adsorption is considered the main mechanism for pollutants removal at the mineral-water interface, other processes like surface precipitation, incorporation and surface mediated redox reactions are significantly relevant on the technetium uptake by mineral systems.^{91,92} The reduction from Tc(VII) to Tc(IV) generally results in the formation of products like TcO₂ or TcS_x whose solubility is very low compared to that of pertechnetate, leading, therefore, to technetium immobilization. However, it is worth mentioning that the re-oxidation from Tc(IV) to Tc(VII) is very fast and the mere precipitation of Tc(IV) solids is not an ideal remediation method, since the exposure to an aerobic environment would most probably result in Tc(VII) re-mobilization. The same problem arises when technetium is immobilized by the formation of an outer-sphere complex with the surface of the mineral. Because of the weaker nature of the interaction, such sorption complex will not be able to resist re-oxidation,^{93–96} nor overall changes in the chemical conditions, such as pH or ionic strength.

A more sustainable retention mechanism is co-precipitation, a process by which simultaneous precipitation of a solid (or host) with a trace of one or more elements by any mechanism at any rate occurs, as shown in Figure 25.⁹⁷ If the atomic structure of the host and the trace is very different, they will occur together as morphologically distinct solids. This process is known as co-precipitation by inclusion. When there is some structural compatibility, a mixture of the two solids can be produced at the mineral surface by a co-precipitation involving sorption. Co-precipitation is more likely to stabilize technetium under aerobic conditions because the interaction of the mineral with the pollutant is stronger. In the case of inner-sphere complexation, the tracer is “buried” under the host, i.e. it is protected against the oxidation and further mobilization.

Furthermore, if the structural compatibility between the tracer and the host is very high, that is, if the ionic radius of the tracer is within 15 % of that of one of the constituents of the host, the coordination number is similar, and the charge within the crystal lattice remains balanced,⁹⁸ the tracer pollutant becomes a part of the crystal structure of the mineral phase. This can occur with or without co-precipitation and is also known as incorporation or solid solution formation.^{97,98} An alternative way to form such solid solutions is through in-diffusion. The stabilization of technetium by the mineral structure would prevent its re-oxidation.⁹⁹

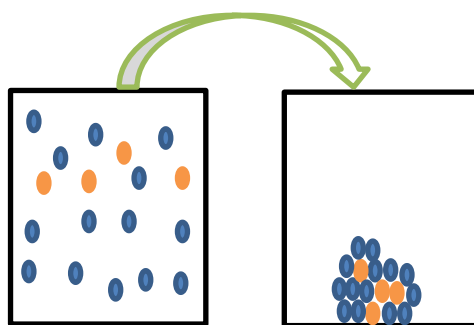


Figure 25. Co-precipitation.

In summary, technetium immobilization by minerals is based on the reduction from Tc(VII) to Tc(IV) followed by adsorption, precipitation or incorporation. In order to avoid re-oxidation (and, therefore, re-mobilization) mechanisms involving strong interaction between Tc and the mineral phase like incorporation, inner-sphere complexation and co-precipitation are the most efficient.

b) Technetium removal by iron minerals

Iron minerals have shown a remarkable ability to immobilize technetium as they trigger its reduction, decreasing its mobility by incorporating, sorbing or precipitating Tc(IV).^{21–24,100} Both, Fe(II) and Fe(III) bearing minerals (sulfides, oxyhydroxides, oxides, carbonates, silicates) are quite abundant in soils, sediments and crystalline rocks. Additionally, they are expected to be present in a nuclear waste repository as corrosion products from the steel canister. In consequence, there is an extensive amount of works using different iron minerals for the reductive immobilization of technetium, that have been summarized in several reviews.^{4,11,34,101,102}

Among this variety of minerals, magnetite (Fe₃O₄) is one of the most widely investigated iron phase because it presents a very high efficiency for Tc(VII) reduction. It has an inverse spinel structure, (Fe(III)_{tetrahedral}Fe(III)_{octahedral}–Fe(II)_{octahedral})₂O₄, that allows the incorporation of Tc(IV) by substituting the Fe(III) in the octahedral site because Fe(III)_{octahedral} in six-fold coordination has a crystal radius (0.785 Å) similar to Tc(IV).¹⁰³ It is worth remembering that among all the retention mechanisms, incorporation of Tc into the mineral structure is the most desirable to prevent Tc re-oxidation and, therefore, re-mobilization.

The laboratory and quantum-mechanical approaches concluded that after the reduction of Tc(VII) by Fe(II), the most favored scenario is Tc(IV) incorporation into magnetite. Other

scenarios involve co-precipitation of TcO_2 like species, as well as the formation of sorption complexes on the surface, depending on the precedence and stability of the magnetite.³⁴

Another interesting iron mineral for Tc removal is goethite ($\alpha\text{-FeO(OH)}$), a very stable mineral phase that can also incorporate Tc(IV) into its lattice for the same reason as magnetite. Quantum-mechanical calculations suggest two mechanisms for such incorporation: the direct substitution of Fe(III) by Tc(IV) into a site next to H^+ to provide charge compensation or an Fe(III) vacancy created by the substitution of three Tc(IV) atoms for four Fe(III) atoms.¹⁰⁴ As with magnetite, experimental works show that after Tc reduction, achieved with the use of reducing agents like FeCl_2 , co-precipitation of Tc with goethite followed. The products of the immobilization go from Tc(IV) incorporated into goethite to Tc(IV)-dimers sorbed onto its surface.³⁴

Hematite ($\alpha\text{-Fe}_2\text{O}_3$) is another ubiquitous iron mineral studied as a prominent candidate for technetium immobilization. In contrast to magnetite and goethite, hematite exhibits a very low capacity for Tc(IV) incorporation as such process is extremely unfavorable according to theoretical calculations.¹⁰⁵ Experimentally, after the reduction from Tc(VII) in the presence of hematite, Tc(IV) species are sorbed on the mineral surface, like on goethite.³⁴

Other examples of Fe minerals with a high ability of immobilizing Tc are ferrihydrite ($\text{Fe}_2\text{O}_3 \times 0.5\text{H}_2\text{O}$), green rust and siderite (FeCO_3),³⁴ and apart from them there are hundreds of works dealing with the potential Tc removal by iron phases. It is clear that the presence of Fe(II) favors the reduction of technetium and Tc(IV) will be precipitated, adsorbed or incorporated into the iron mineral structure.

Fe-bearing minerals have low to no detrimental impact in the environment and they are simple and inexpensive to produce or they are already present as ubiquitous minerals in different environmental systems. For this reason, they are widely investigated and will be probably continue to be relevant candidates for technetium (and other pollutants) remediation.

c) Technetium removal by iron sulfides

Minerals containing iron and sulfides have two types of functional groups on their surfaces: FeOH and FeSH ¹⁰⁶ showing amphoteric behavior and their charge depends on the pH. Below pH 10.0, the sulfide sites dominate over the hydroxyl sites and they will protonate to FeSH_2^+ and Fe_3SH_2^+ , which charges the surface positively¹⁰⁷ and, therefore, the TcO_4^- will be attracted to it and its reduction will be enhanced.

Mackinawite (FeS) removes Tc(VII) up to 98% from ultrapure water. XAS showed that initially Tc(VII) forms a species resembling TcS₂ under anoxic conditions.²³ Afterwards, due to the oxidation of the FeS to goethite, TcO₂ is formed and Tc(IV) can be incorporated into the goethite lattice, which gives the additional advantage that even under aerobic conditions the technetium will remain immobilized.

Bruggeman et al.²⁵ found that pyrite is a good sorbent for Tc(IV). They determined that the solubility of Tc(IV) in water is higher in the presence of humic substances and the addition of FeS₂ increased the K_D value from 933 mL g⁻¹ to 31,622 mL g⁻¹ with increasing concentration of the mineral. Using a Langmuir isotherm model they suggested that the affinity of pyrite for Tc(IV) is high, however there is no proof that adsorption is the only mechanism involved in the Tc-removal by pyrite.

More recently, Huo et al.²⁶ synthesized pyrite nanoparticles to study the Tc(VII) immobilization from ground water and soil. According to their results, at a dosage of 0.28 g L⁻¹, the pyrite nanoparticles were able to rapidly and completely remove 4.88×10⁻⁷ M of Tc(VII) by converting it to insoluble Tc(IV). However, the pH range was limited (from 4 to 7) and they did not provide any conclusions on the chemical structure of the Tc(IV) after its interaction with pyrite.

2.1.3. Technetium detection and quantification in this work

a) Liquid scintillation counting

Liquid scintillation counting (LSC) is a technique used to determine the radioactivity of samples containing α or β particles. When ionizing radiation interacts with the organics present in the scintillation cocktail, many chemical reactions like neutralization, free radical formation and decomposition can occur along with physical processes such as X-ray emission, fluorescence, phosphorescence and energy migration.¹⁰⁸ The products of these interactions are excited molecules that will emit photons. Cascading this effect and shifting subsequently the energy of the re-emitted photons to lower energy (and thus higher wavelengths) finally allows detection by a photon multiplier tube, which will convert them into an electrical pulse recorded as a count. Each molecule can only emit one photon, so the total amount of energy depends directly on the number of excited molecules produced by the ionizing particle.¹⁰⁸

One Becquerel (Bq) is equal to one disintegration per second and can be related to the radionuclide concentration using Eq. [23]:

$$n = \frac{I \cdot t_{1/2}}{N_A \cdot \ln(2)} \quad [23]$$

Where n are the moles and $t_{1/2}$ the half-life of the radionuclide in s, I the intensity in Bq, and N_A Avogadro's number.

b) Scanning electron microscopy

Scanning electron microscopy (SEM) produces images of a sample by scanning the surface with a focused beam of electrons, giving information about the surface topography of the sample with a resolution better than one nanometer.

Image formation is achieved with a scanning principle: the primary electrons are focused into a probe with short diameter that is scanned across the sample. The direction of the beam is changed by electrostatic or magnetic fields. The scan is performed in two perpendicular directions (raster scanning) and it covers a rectangular area of specimen. The image of the sample is formed from the secondary electrons released from each local area.¹⁰⁹

SEM microscopes can be coupled with Energy Dispersive X-ray Spectroscopy (EDX or EDS), an X-ray micro-analytical technique that then also provides information on the chemical composition of a sample for elements with atomic number $Z > 3$

The energy transferred from the electron beam to the sample can expel the atomic electrons from the atom or excite them into an electronic level with higher energy. When this occurs, a positively charged hole is left behind with the ability of attracting other electrons from higher-energy shells. The transition of an electron from a higher-energy shell to fill the hole of the lower-energy shell produces an X-ray with an energy characteristic of the energy difference between the two shells. This energy depends on the atomic number and, therefore, it can be used to identify elements present in the sample, such as Tc, S and Fe.¹¹⁰

c) Raman microscopy

Raman microscopy couples standard optical microscopy with Raman spectroscopy to characterize local components of a heterogeneous sample. In general, a Raman microscope consists of a microscope coupled with an excitation laser, lenses, a monochromator and a detector like a photomultiplier tube or a charge-coupled device to produce the Raman spectra.¹¹¹

The microscope is used to identify regions of interest on the sample surface, that will then be investigated by Raman spectroscopy.

Raman spectroscopy is commonly used in chemistry to identify the components of a sample by providing a structural fingerprint of molecules based on their vibrational modes. A source of monochromatic light (like the laser coupled with a microscope) interacts with the molecules exciting them and resulting in the energy of the laser photons being shifted up or down. The shift in energy gives information about the vibrational modes in the system that can be related to the chemical identity of the sample.¹¹²

d) X-ray photoelectron spectroscopy

X-ray photoelectron spectroscopy (XPS) is a surface characterization technique used to determine the elements present at the sample surface and the nature of their chemical bonds. When a sample is irradiated with X-rays of sufficient energy, electrons in specific ground states are excited. As explained before, the transitions between energy shells have energies characteristic of every element that can uniquely identify the composition of the sample. Moreover, the photo-ejected electrons from core levels have slight shifts depending on the outer-valence configuration of the material examined. This allows XPS to determine the oxidation states of the elements and characterize the chemical bonds between them.¹¹³

The photo-ejected electrons are collected by an electron analyzer that measures their kinetic energy and produces an energy spectrum of intensity (number of photo-ejected electrons as a function of time) versus binding energy (the energy of the electrons before leaving the atom). Each energy peak on the spectrum corresponds to a specific element. The area of the peak is proportional to the number of atoms present, so integrating the peaks will yield the chemical composition of the sample, while the energy of each peak can determine the bond order and the oxidation state.¹¹³

e) X-ray absorption spectroscopy

X-ray absorption spectroscopy covers a variety of techniques used for the determination of the local geometric and/or electronic structure of an element in a sample. It measures the transitions from the core electronic state of the absorbing element to the lowest unoccupied molecular orbital (LUMO, the excited electronic state) and to the continuum. XAS is a non-destructive, specific technique, meaning that no interference from absorption by the sample matrix will be

detected because the absorption at a specific X-ray photon energy is characteristic for each element.¹¹⁴ The increase of the absorption at certain X-ray photon energy is called absorption edge and corresponds to the energy needed for the transition of an electron into the LUMO or to the continuum. The principal quantum numbers $n = 1, 2$, and 3 , correspond to the K-, L-, and M-edges, respectively.

Figure 26¹¹⁴ shows the Mn K-edge spectra along with two commonly used types of XAS spectroscopy: X-ray absorption near-edge structure (XANES) and Extended X-Ray Absorption Fine Structure (EXAFS). XANES provides detailed information about the oxidation state of the metal atoms while EXAFS yields the coordination number, type, and distance to ligands and neighboring atoms from the absorbing element.¹¹⁴

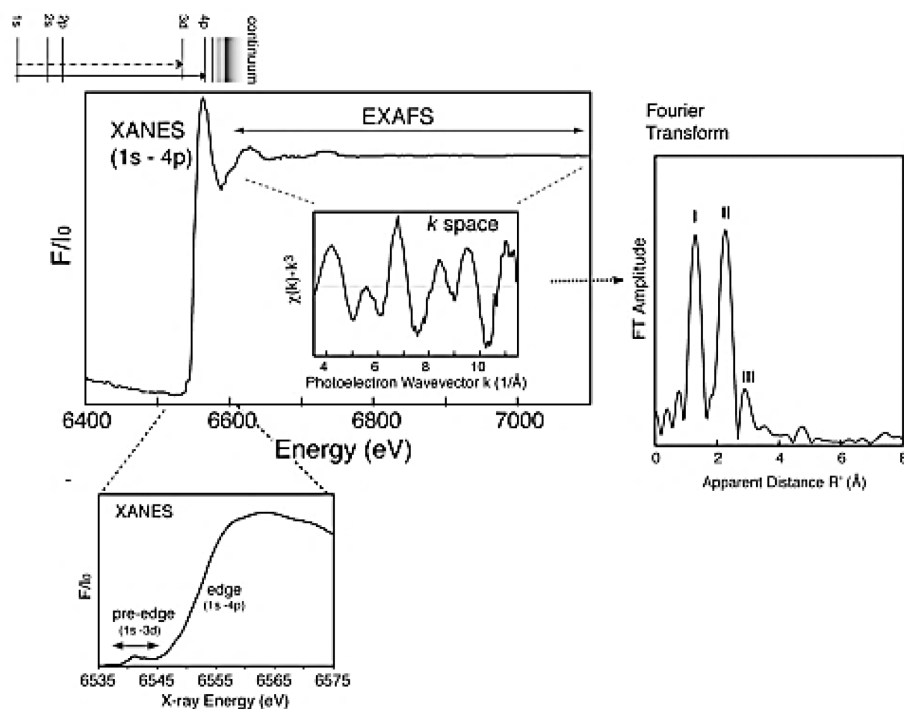


Figure 26. Mn K-edge spectra and the regions of the spectra related to XANES and EXAFS. Taken from reference ¹¹⁴

2.2. Technetium immobilization by pure pyrite

Most of the results presented in this section can be found in Rodríguez et al., Environ. Sci. Technol. 54 (2020) 2678 (DOI: 10.1021/acs.est.9b05341).

2.2.1. Pyrite characterization

Figure 27 shows the characterization experiments of the pyrite. The X-ray diffraction pattern (XRD) in Figure 27a compares the sample with the references of pure pyrite (R050190) and pure marcasite (R060882) provided by the RRUFFTM database.¹¹⁵ The diffractogram of the sample matches to nearly 100% with the pyrite reference, making clear that there is no detectable marcasite contamination in the solid and, therefore, the solid was identified as pure pyrite with an acceptable crystallinity degree, inferred from the sharpness of the peaks.

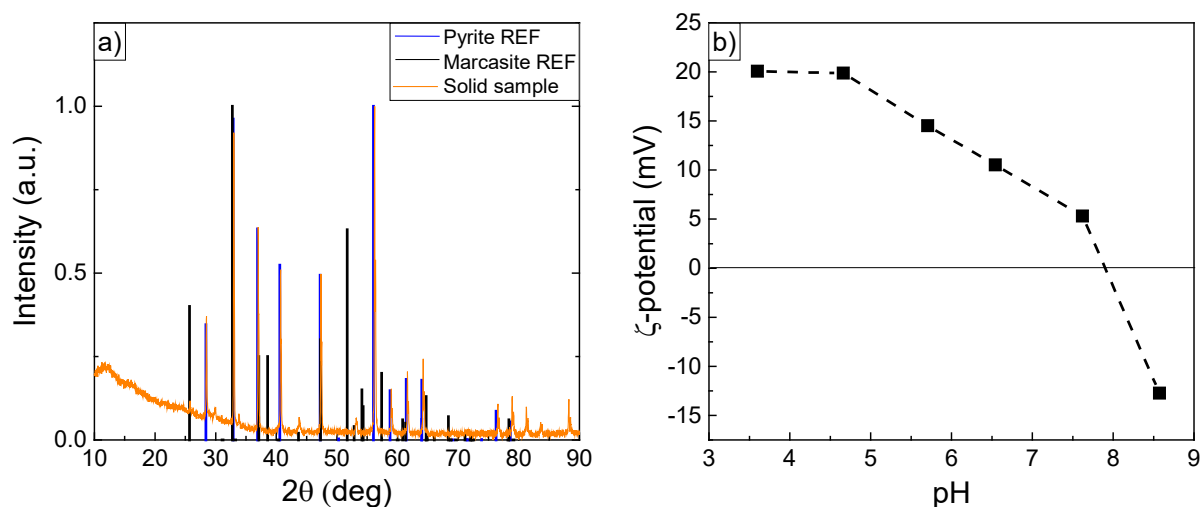


Figure 27. Pyrite characterization experiments. a) Powder XRD b) ζ -potential measurements. The references were taken from the RRUFFTM database.¹¹⁵

The isoelectric point (pH_{IEP}) of the pyrite was determined as 7.9 by ζ -potential measurements shown in Figure 27b. The pH_{IEP} of pyrite highly depends on its origin (whether it is natural or synthetic) and the pre-treatment used.¹¹⁶ The value obtained here is in good agreement with that reported by Bonnissel et al.¹¹⁷ that studied the surface composition by XPS, ruling out the presence of sulfurs or polysulfides that could lead to lower pH_{IEP} values due to negative charges on the surface. According to Bonnissel, the pH_{IEP} of 7.9 indicates that the pyrite surface was initially oxidized (meaning it presented Fe(III) moieties before the Tc addition). However, no initial acid washing was performed because natural pyrite surface shows Fe(III) moieties as

well.¹¹⁸ Lastly, the Brunauer–Emmett–Teller (BET) surface area of pyrite was determined as $2.0 \text{ m}^2 \text{ g}^{-1}$, which is very low and suggests that physical sorption will not play a significant role in the Tc uptake.

2.2.2. Technetium removal from solution: Batch experiments

In this section, the Tc(VII) removal by pure synthetic pyrite studied with batch experiments will be presented. The initial technetium concentration for the kinetics and pH effect experiments was $5 \times 10^{-6} \text{ M}$ and the average final concentration of technetium was around $5 \times 10^{-8} \text{ M}$. It is worth mentioning that even though technetium can be found in the atmosphere and in several marine and terrestrial environments, at concentrations rarely exceeding $1 \times 10^{-9} \text{ M}$,^{10,119} which are very low compared with the initial concentration used in this study. Nevertheless, the isotherms in Figure 28 show that the lower the Tc concentration, the higher its relative removal by pyrite, meaning that the results presented in this section are valid in more realistic scenarios.

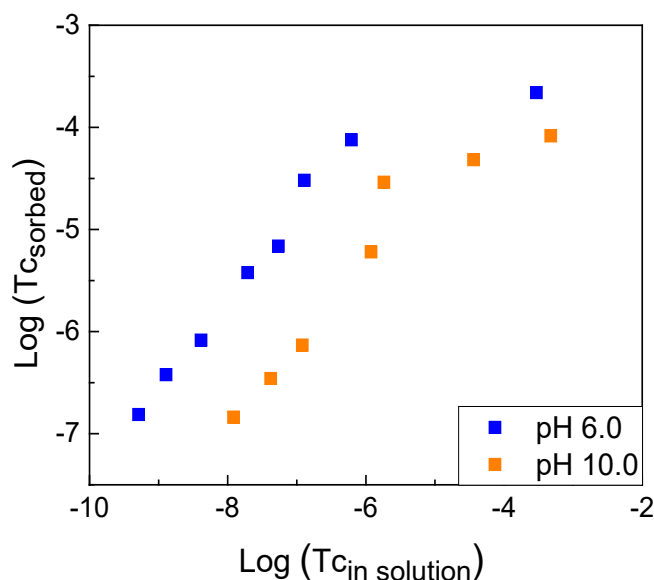


Figure 28. Isotherms of the Tc immobilization by pyrite at pH 6.0 and 10.0.

The pH effect on the Tc retention by pyrite is shown in Figure 29a, where it can be seen that at $\text{pH} > 5.5$ 97 – 100% Tc removal from solution is reached after 1 day. At $\text{pH} < 5.5$, complete Tc retention was achieved only after 35 days, i.e. the reaction kinetics are significantly lower under acidic conditions. Figure 29b shows the Eh – pH diagram of the system Tc + pyrite in water after 14 days in contact. It can be seen that most of these values lie in the stability region of Tc(IV), suggesting that the Tc(VII)/Tc(IV) reduction is directly related to the Tc immobilization by pyrite.

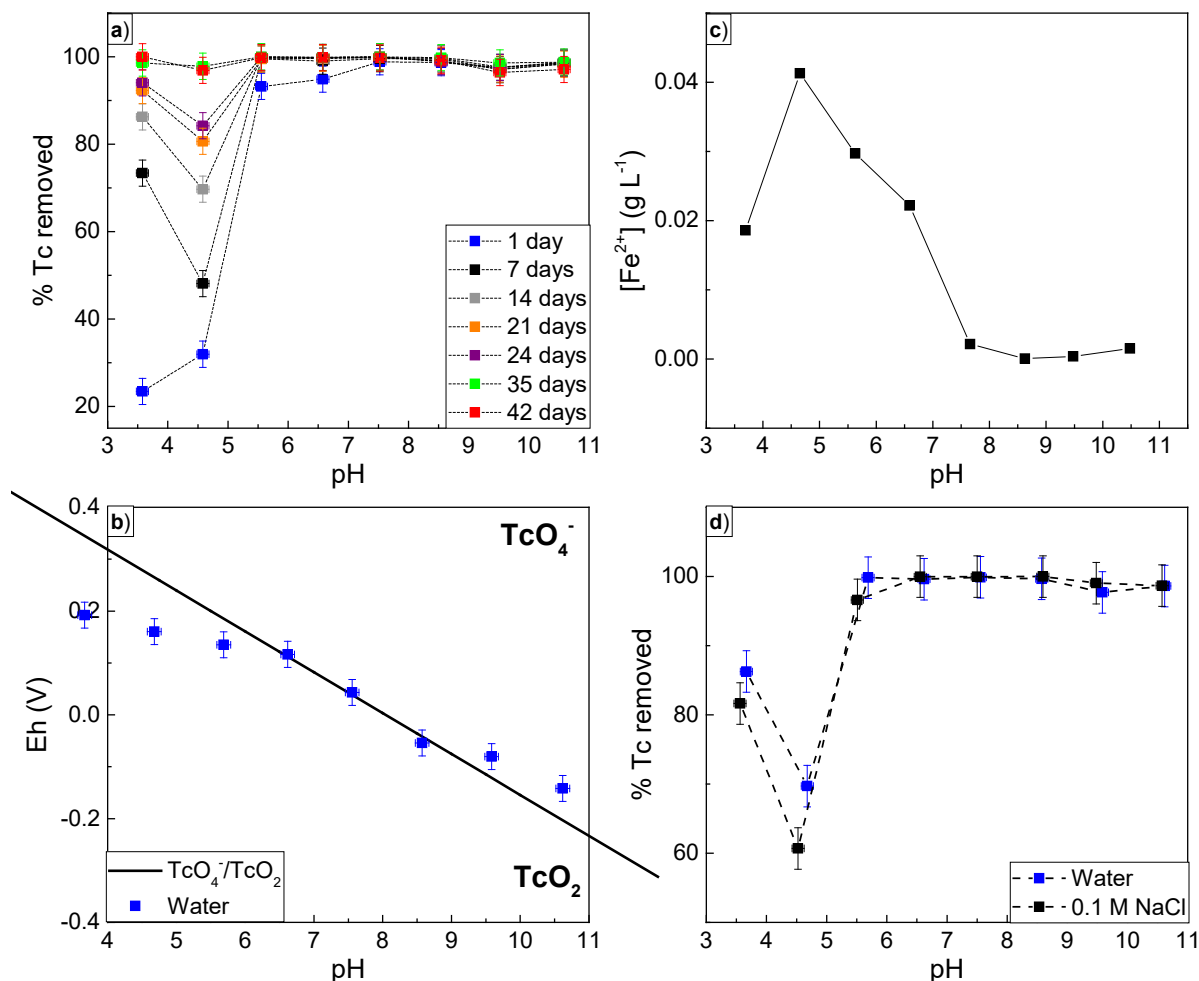


Figure 29. a) pH effect on the Tc(VII) uptake by pyrite for 42 days. b). Eh – pH diagram of the system Tc + pyrite in water after 14 days of contact and calculated equilibrium line between TcO_4^- and TcO_2 . c) Pyrite solubility measured as Fe concentration as a function of pH. d). Effect of 0.1 M NaCl on the Tc(VII) uptake by pyrite after 14 days in contact.

When the contact time is shorter than 35 days, the amount of technetium retained by pyrite is lower at pH 4.5 than at any other pH value, which was attributed to pyrite dissolution. To test this, several suspensions of pyrite in water were prepared at different pH values and the iron concentration in solution was determined by ICP-MS, as shown in Figure 29c. It was found that the highest concentration of Fe in solution was reached at pH 4.5, becoming drastically lower as the pH rises. The result is in good agreement with the work of Bonnissel,¹¹⁷ who concluded that when the pH is higher than 4, Fe(III)(hydr)oxides are formed on the pyrite surface, preventing its dissolution. It has been found that the homogeneous reduction of technetium by Fe^{2+} is not favorable due to its very slow kinetics.⁸³ In contrast, when the Fe^{2+} is part of a mineral structure, like in the case of pyrite, or when it is pre-adsorbed on another mineral phase like

alumina,⁸⁷ the reduction rate increases drastically.^{26,83,86,120} Such kinetic considerations combined with the pyrite dissolution results account for the low removal of Tc by pyrite at pH 4.5.

Figure 29d shows the effect of 0.1 M NaCl on the Tc uptake by pyrite after 14 days in contact. In the presence of NaCl, the Tc removal at pH < 6.5 slightly decreases, which suggests the formation of an outer-sphere sorption complex as the removal appears to depend on the ionic strength. However, at pH \geq 6.5 the percentage of Tc scavenged by pyrite is nearly the same in water and in aqueous NaCl, ruling out the outer-sphere sorption. The decrease of Tc retention by pyrite under acidic pH values in the presence of NaCl could be explained by the increase of TcO₂ solubility with rising ionic strength,^{121,122} as it is possible that a small amount of this insoluble oxide has been formed after Tc reduction.

The re-oxidation of two samples at pH 6.0 and 10.0 is presented in Figure 30. Using the pyrite oxidation rates reported by Williamson et al.,¹²³ it was calculated that the 0.065 g of pyrite used for these experiments should have been completely oxidized only after 50 days. However, as it was mentioned before (section 2.2.1), the pyrite presented some Fe(III) moieties in the surface and, therefore, it was expected that the oxygen interacted more favorably with the Tc(IV) than with the mineral.

According to Figure 30a, the technetium concentration in solution after the exposure to ambient atmosphere remained lower than 1 μ M at both pH values during the 60 days of the experiment. Figure 30b presents the percentage of Tc remaining in solution (%Tc_{sol}) calculated on the basis that the initial Tc concentration (5 μ M) is 100% of the Tc that might be re-mobilized if re-oxidation occurred in contact with O₂, so the Tc in solution (determined with LSC) is a percentage of this initial Tc concentration at each time. %Tc_{sol} can be used to observe slight differences among the two pH values. The maximum %Tc_{sol} at pH 10.0 (11%) is found after seven days of exposure to ambient atmosphere, subsequently it decreases and remains constant under 5% for the rest of the experiment. For pH 6.0, the %Tc_{sol} remains below 7% for the first 40 days and then the maximum %Tc_{sol} (13.5%) is reached at the end of the experiment.

It can be concluded that at pH 10.0 some re-oxidation of Tc(IV) takes place after seven days under ambient atmosphere. This small amount of Tc(VII) is reduced again by pyrite, whose surface remains active even after the formation of a layer of iron(III)(hydr)oxides, meaning it is not passivated against further oxidation.^{117,124} A previous study with Tc(IV) incorporated into magnetite¹²⁵ showed that after 60 days in contact with water containing dissolved O₂, around

10% of technetium was re-oxidized and released from the pure magnetite structure, contrary to the results presented here where the magnetite is formed on the pyrite surface at pH 10.0. Therefore, the role of pyrite in the immobilization is not only to provide the Fe²⁺ for the reduction but also to sustain a dynamic surface that will maintain the Tc as Tc(IV).

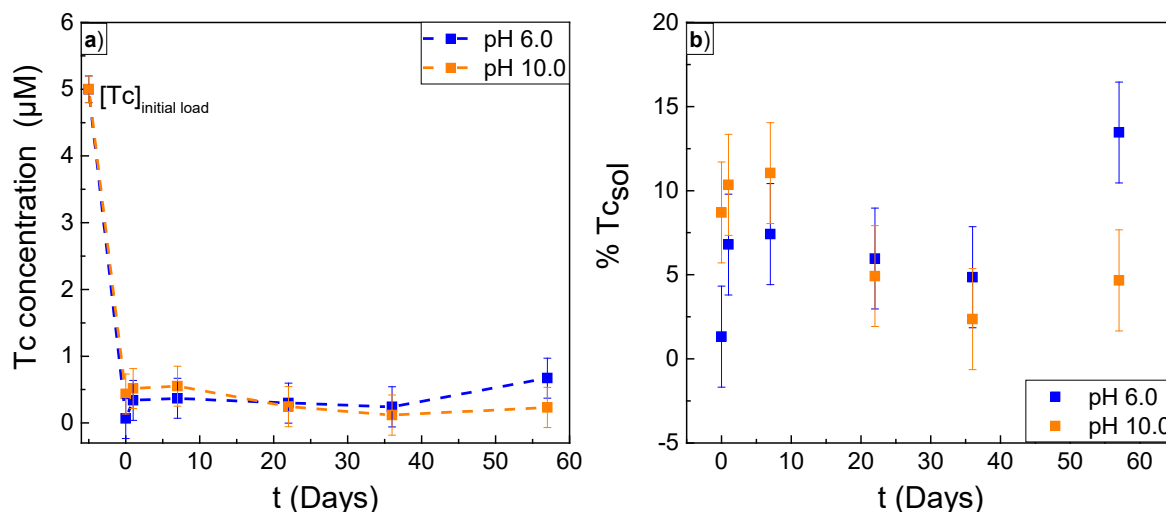


Figure 30. Re-oxidation experiments at pH 6.0 and 10.0 for 2 months. a) Tc concentration in solution b) Percentage of technetium remaining in solution Dashed lines are shown to guide the eye.

A similar behavior might be occurring at pH 6.0; however, the increase of %Tc_{sol} after 57 days under ambient atmosphere is significantly higher at pH 6.0 than at pH 10.0 and it even suggests that at pH 6.0 the immobilizing effect of pyrite is lost. Nevertheless, it is important to take into account that both Figure 30a and Figure 30b do not show a clear trend of the amount of Tc remaining in solution with respect to time. Moreover, it is possible that a further reduction of the newly produced Tc(VII) could take place again as it happened at pH 10.0 after seven days. Therefore, it is not possible to predict if the %Tc_{sol} will increase or decrease and studies at significantly longer time scales are needed.

2.2.3. Morphology of pyrite studied by SEM and Raman microscopy

The changes on the morphology of pyrite after the interaction with technetium were studied by SEM and the micrographs are presented in Figure 31. The surface of the pure mineral at pH 6.0 and 10.0 is very similar although at pH 10.0 a higher amount of small particles (highlighted with the red squares in Figure 31a and Figure 31d) is present. Such small particles could be the Fe(III) initial moieties that have been already mentioned before (section 2.2.1).

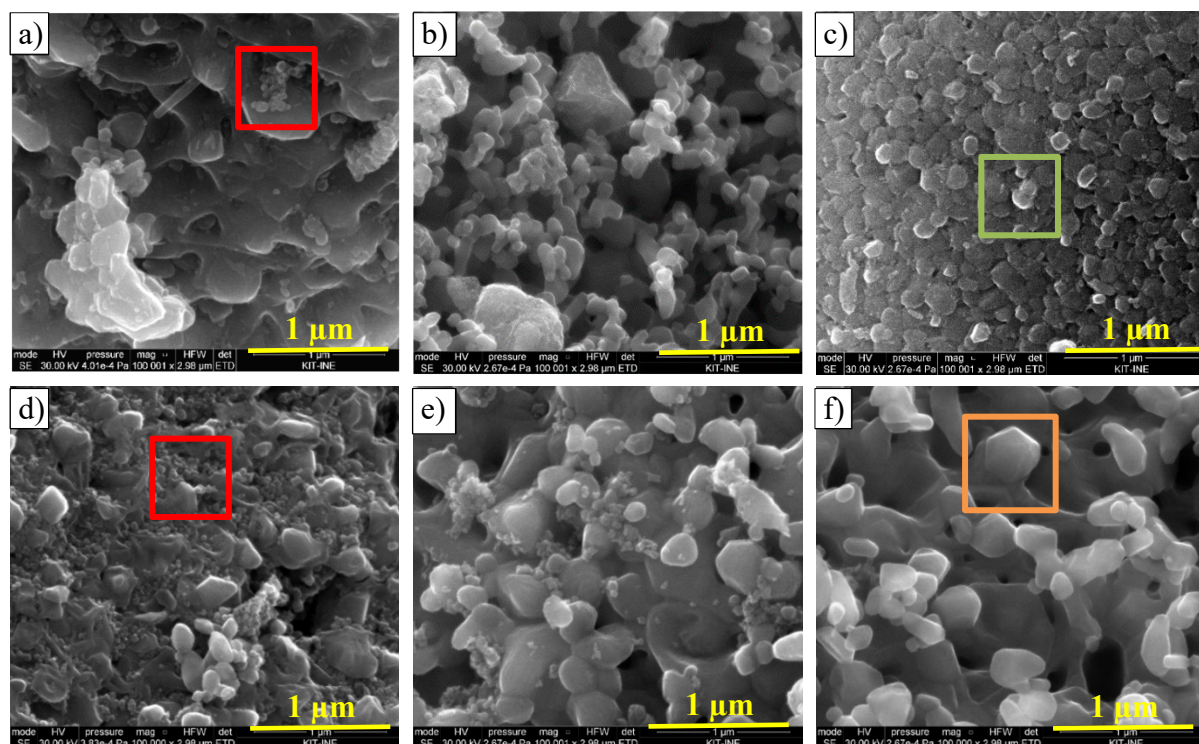


Figure 31. SEM micrographs of pyrite in water. a) at pH 6.0 b) containing 600 ppm Tc load at pH 6.0. c) containing 1000 ppm Tc load at pH 6.0. d) at pH 10.0. e) containing 600 ppm Tc load at pH 10.0. f) containing Tc 1000 ppm Tc load at pH 10.0. Highlighted in red: a) and d): small particles suggesting new iron minerals formation. c) Possible hematite highlighted in green. f) Possible magnetite highlighted in orange. Contact time with Tc: 1 month.

A very drastic change on the mineral can be detected after the interaction with technetium. The pyrite surface becomes smoother: the highlighted small particles disappear the higher the concentration of technetium becomes, which is a result of the redox reaction. On Figure 31c and Figure 31f (pyrite + 1000 ppm Tc), a clear difference between the surface at pH 6.0 and pH 10.0 can be observed, suggesting that the new iron phases formed on the surface after the interaction with Tc at each pH differ. A visual comparison with the micrographs reported by Taitel-Goldman¹²⁶ for hematite formed by recrystallization of large cubic pyrite crystals and synthesized magnetite at 70°C, pH 9.4 and a solution of 4 M NaCl, suggested that those minerals were formed on the pyrite surface at pH 6.0 and pH 10.0 respectively. No EDX analysis of the samples is presented because technetium could not be detected due to its low concentration.

In order to identify the new minerals, Raman microscopy was performed on the Tc-loaded solids at pH 6.0 and 10.0. The identification of hematite at pH 6.0 was possible after comparing the Raman spectra of the sample with the hematite reference R050300 of the RRUFFTM database,¹¹⁵

shown in Figure 32. At pH 10.0, no mineral apart from pyrite was found. A reason might be, that Raman microscopy consists in targeting several regions of the sample obtaining one spectrum per region aiming to find a different species throughout a heterogeneous sample. Therefore, it is necessary to repeat the measurement several times until the new mineral (produced in a low concentration since pyrite was present in excess with respect to technetium) is found. For pH 10.0, as it will be seen in the next section, magnetite was easily identified by EXAFS as a reaction product and, therefore, it was not necessary to invest so much time in the Raman experiment.

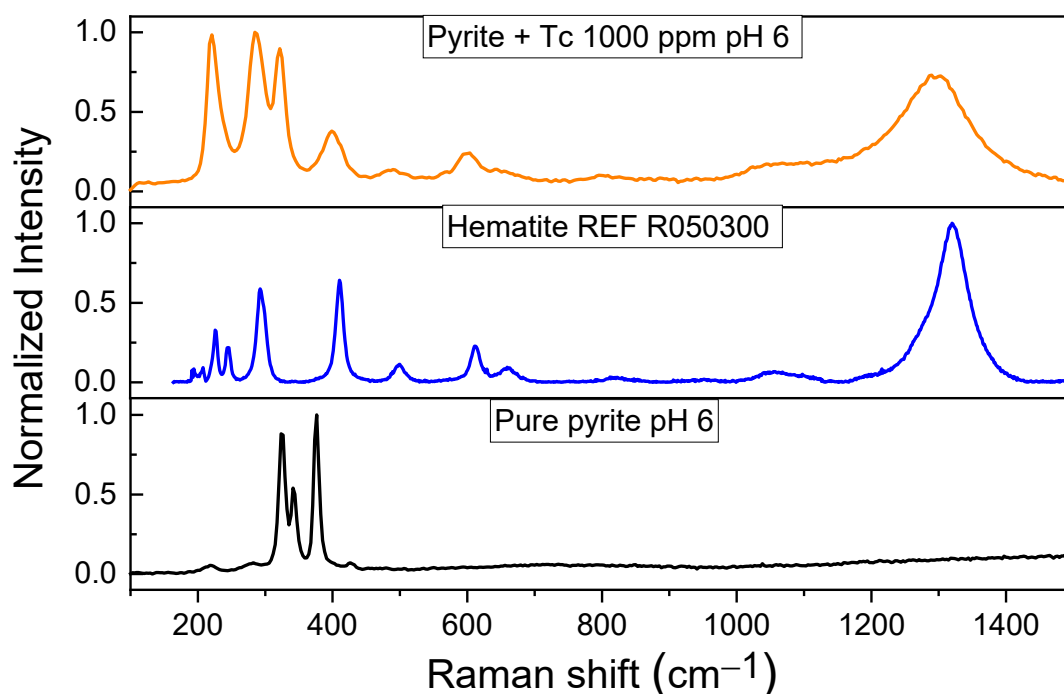


Figure 32. Raman spectra of pyrite before and after contact with Tc (1000 ppm Tc) at pH 6.0 compared with the hematite reference R050300 of the RRUFFTM database.¹¹⁵

2.2.4. Spectroscopic determination of the Tc-removal mechanism

X-ray absorption spectroscopy, speciation calculations and X-ray photoelectron spectroscopy were employed to determine the immobilization mechanism of Tc(VII) by pyrite. Figure 33 presents the Tc K-edge XAS spectra of the Tc-loaded pyrite samples (pyrite + 600 and 1000 ppm Tc at pH 6.0 and 10.0). Details on the samples are given in Table 3. The XANES spectra of all samples in Figure 33a are identical and the comparison with the TcO₂·nH₂O reference

spectra indicates that the samples contain Tc(IV). The absence of the pre-edge peak of Tc(VII) in all samples implies that if any Tc(VII) is present it constitutes less than 2% of the sample.

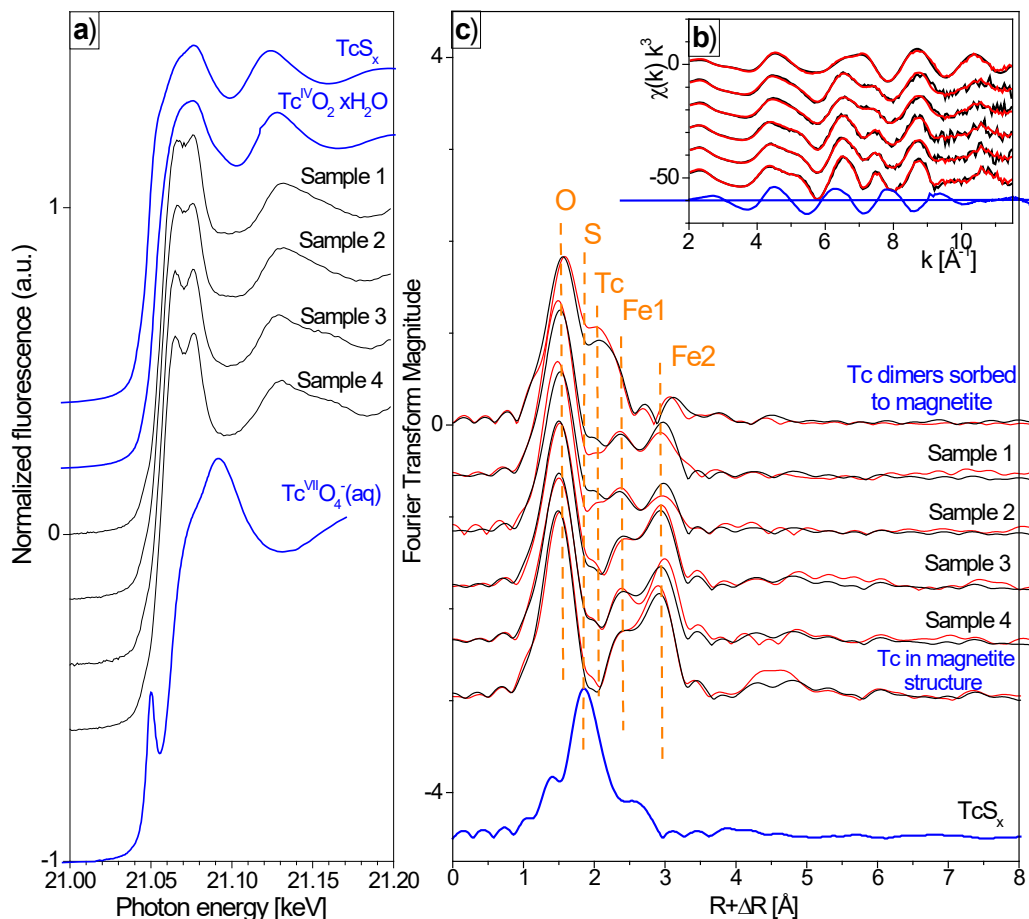


Figure 33. Tc-K edge XAS spectra of Tc sorbed on pyrite. a) XANES. b) EXAFS. c) Fourier Transform Magnitude. The black lines are the experimental data; the red lines in b) and c) are the ITFA reconstruction with two principal components; the blue lines are the reference spectra used for ITFA. The identities of the samples are given in Table 3.

Table 3. Species quantification by iterative transformation target test.

Sample	No	Species 1 (Tc(IV) dimers)	Species 2 (Structural Tc)	Sum
Pyrite + Tc 600 ppm pH 6.0	1	0.86	0.14	1.00
Pyrite + Tc 1000 ppm pH 6.0	2	1.00	0.00	1.00
Pyrite + Tc 600 ppm pH 10.0	3	0.08	0.92	1.00
Pyrite + Tc 1000 ppm pH 10.0	4	0.30	0.70	1.00
Magnetite structure	5	0.00	1.00	1.00

The k^3 -weighted EXAFS spectra and corresponding Fourier transform magnitude (FTM), a pseudo radial distribution function of atoms around Tc centers, are presented in Figure 33b and 31c. The comparison with the reference spectrum of the Tc(IV)S_x proves that technetium is prevalently coordinated to oxygen and not to sulfur. Two additional references were added to the Figure 33c for comparison: one of Tc(IV) dimers sorbed on magnetite,²¹ which is quite similar to the spectra at pH 6.0 (samples 1 and 2), and other of Tc(IV) incorporated into the magnetite structure²¹ that resembles the spectra at pH 10.0 (samples 3 and 4), which can be appreciated in Figure 33b and Figure 33c. According to the principal component analysis performed with the Iterative Transformation Factor Analysis (ITFA) software,¹²⁷ technetium occurs only in two different local structures, i.e. the spectra of the four samples are the result of the linear combination of two principal components (Species 1 and Species 2). An iterative transformation target test was performed with ITFA in order to find the fraction of the two components present in the spectra by setting the fraction of structural Tc equal to 1 (Table 3). It could be concluded that the spectra at pH 6.0 were constituted by the Species 1 similar but not identical to Tc(IV) dimers sorbed on magnetite. The spectra at pH 10.0 corresponded to the Species 2, i.e. structural Tc.

The analysis was repeated adding available reference spectra^{21,128} and it was found that the addition of TcO₂·*n*H₂O, TcS_x or Tc(IV) dimers sorbed on magnetite always resulted in the increase of principal components, meaning that such species are not present in the samples. However, the addition of Tc(IV) incorporated into magnetite by substituting Fe in octahedral sites did not increase the number of components and it provided a good fit for the samples at pH 10.0. The incorporation of Tc(IV) into magnetite, already reported in other works^{21,22}, is possible because Tc⁴⁺ and Fe³⁺ have similar crystal radii (0.785 Å) in six-fold coordination¹⁰³ while Fe²⁺ provides a good charge compensation.^{102,129} Therefore, the Tc(VII) removal by pyrite at pH 10.0 is a result of its reduction to Tc(IV) and subsequent incorporation into magnetite.

For structural identification of Species 1, a shell fitting of the spectrum was performed. The first step was the fit with one Tc-O and two Tc-Fe, as it was suggested by the appearance of the FTM (Figure 33c). Such fit was not able to properly reconstruct the experimental spectra of samples 1 and 2 and, therefore, an additional Tc-Tc shell was added. As a result, a reliable match of the spectrum of Species 1 was obtained and the structural parameters of this fit (Table 4) suggested again the sorption of Tc(IV) dimers on an iron oxide. The first Tc-Fe distance of the sorption complex corresponding to Species 1 is 0.05 Å shorter than that of a Tc sorption complex formed with magnetite while the second Tc-Fe distance is 0.03 Å longer, confirming that the Tc(IV) dimers are not sorbed on magnetite. According to the SEM and Raman results presented in

section 2.3.3, the iron oxide on which the Tc(IV) dimers are sorbed is hematite, that has already been probed to form surface complexes with Tc(IV) dimers.^{84,130,131}

Table 4. EXAFS-derived structural parameters for Tc in the pyrite samples.

Sample	Path	CN [†]	R(Å)	$\sigma^2(\text{\AA}^2)$	$\Delta E^0(\text{eV})$	%R [‡]
Species 1 (sorbed Tc(IV) dimers)	Tc-O	5.8	2.00	0.0046	2.9	8.6
	Tc-Tc	1.3	2.55	0.0100		
	Tc-Fe ₁	1.9	3.07	0.0098 ^c		
	Tc-Fe ₂	2.7	3.55	0.0098 ^c		
Species 2	Tc-O	6 ^f	2.01	0.0043	3.0	6.1
(Structural Tc(IV))	Tc-Fe ₁	6 ^f	3.08	0.0113		
Yalçintaş ²¹	Tc-Fe ₂	6 ^f	3.49	0.0093		

[†]CN (Coordination number), [‡]R (Residual)

Fit errors: CN: $\pm 25\%$; R: 0.01 Å, σ^2 : 0.002 Å², f: fixed, c: constrained

The XPS spectra of the samples at pH 6.0 and 10.0 are presented in Figure 34. There is no visible change of the S 2p spectra (Figure 34a) due to the addition of 1000 ppm of technetium. In contrast, the Fe 2p spectra (Figure 34b) show the formation of Fe(III) at both pH 6.0 and 10.0, confirming the observation of the FTM that the redox active element is iron and not sulfur, i.e. the technetium is coordinated with Fe and not with S. The Fe(III) increases with increasing pH and Tc load (not shown).

It can be seen in the O 1s spectra (Figure 34c) that the $[\text{O}^{2-}]/[\text{OH}^-]$ ratio depends on the pH of the sample, as $[\text{OH}^-]$ is more abundant at pH 6.0 while $[\text{O}^{2-}]$ is favored at pH 10.0. Previous works^{117,132,133} have reported that an increase in pH results in the formation of Fe(III)(hydr)oxides that cover the pyrite surface without passivating it against further oxidation. Such a Fe(III) layer could promote the existence of O-H groups on the surface that would most probably be involved in the inner-sphere complexation occurring at pH 6.0 between Tc(IV) dimers and hematite, supporting the findings of EXAFS and Raman spectroscopy.

The Tc 3d spectra (Figure 34d) show a very interesting difference between the samples at pH 6.0 and 10.0: the peak around 254 eV is only found at pH 10.0 and it indicates the presence of TcS_x species. The concentration of such species is too low to be detected by XAS. However, XPS showed that its concentration increases with increasing Tc load and its formation could be more relevant the higher the pH gets. Indeed, works with mackinawite²¹ and microorganisms¹³⁴

have found the formation of polysulfide species that prevent Tc migration due to their low solubilities. Therefore, it is very relevant to study the removal of Tc by other sulfur minerals like galena or chalcopyrite, as well as the FeS₂ polymorph, marcasite, since they could also be alternatives for Tc remediation.

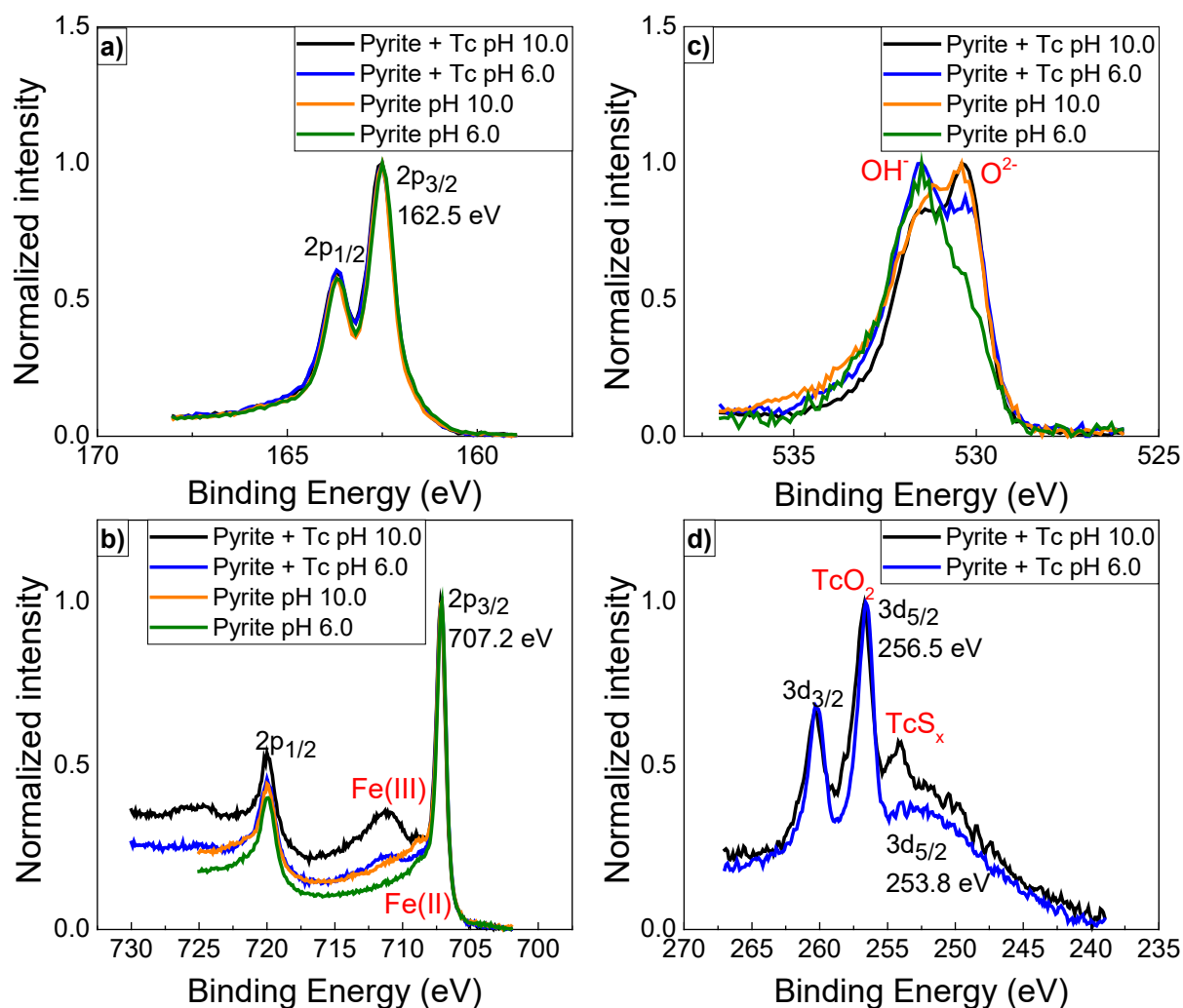


Figure 34. XPS spectra of pyrite before and after the reaction with Tc(VII) ([Tc] = 1000 ppm) at pH 6.0 and pH 10.0. a) S 2p. b) Fe 2p. c) O 1s. d) Tc 3d. Tc 3d elemental lines are superposed by the broad loss line of S 2s.

Lastly, the iron speciation under the experimental conditions ([Tc(VII)] = 5 μ M, [Fe²⁺]_{total} = 20 μ M) is presented in Figure 35. The model predicts the formation of hematite at pH < 7.5 and magnetite at pH > 7.5 after the oxidation of Fe(II) due to the reduction of Tc(VII), which explains the different removal mechanisms depending on the pH. In conclusion, the removal of Tc(VII) by pyrite starts with its reduction to Tc(IV) promoted by the structural Fe(II)

and it is followed by either the inner-sphere complexation of Tc(IV) dimers on hematite at pH 6.0, or the Tc(IV) incorporation into magnetite by replacing Fe(III) in octahedral position at pH 10.0.

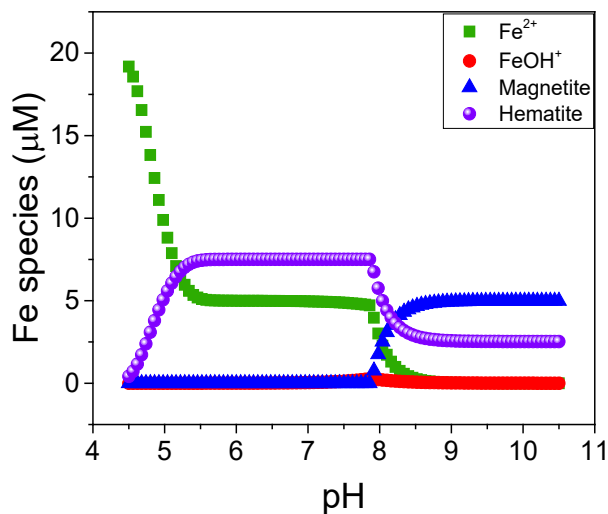


Figure 35. Iron speciation as a function of pH. Calculations have been performed considering the initial presence of 20 μM Fe^{2+} and 5 μM TcO_4^- . The latest Fe^{135} and Tc^{35} thermodynamic databases have been used.

2.3. Tc immobilization by a mixture marcasite-pyrite

Most of the results presented in this section can be found in Rodríguez et al., Chemosphere. 281 (2021) 130904 (DOI: 10.1016/j.chemosphere.2021.130904).

2.3.1. Solid characterization

The synthesis described in section II of the experimental methods yielded a black matt powder whose characterization is shown in Figure 36. The diffractogram (Figure 36a) identified the solid as a mixture of marcasite (orthorhombic FeS₂) and pyrite (cubic FeS₂) by comparing the sample with the references R060882 and R050190 available in the RRUFFTM database.¹¹⁵ The data analysis software yielded a mineral distribution of 60% marcasite and 40% pyrite based on the intensity of the peaks. Such proportion was very adequate to the aim of these experiments because the changes of the technetium removal by this mixture with respect to pure pyrite (section 2.2) can be attributed to the high proportion of marcasite present.

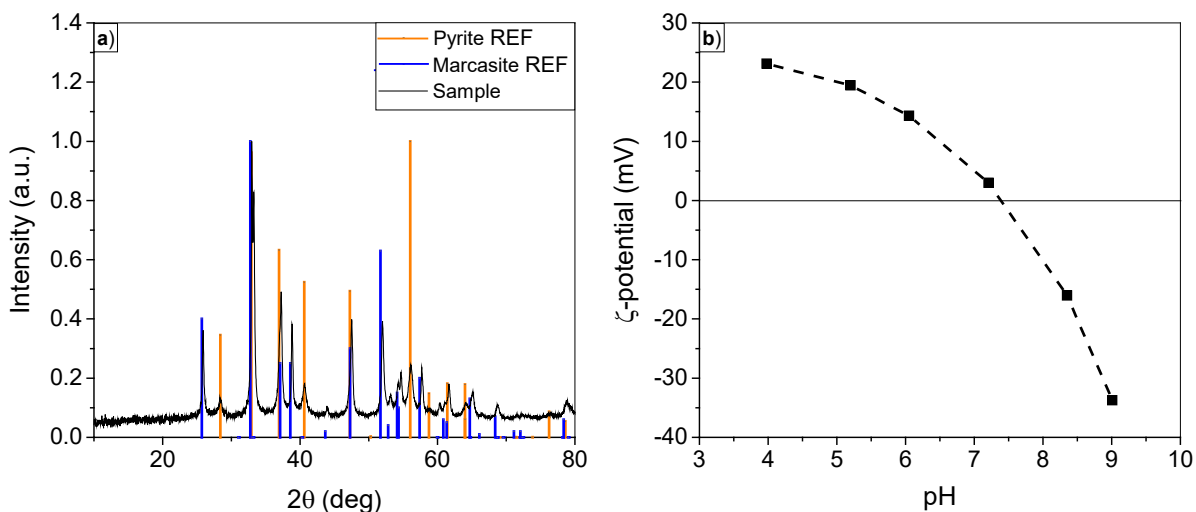


Figure 36. Synthetic FeS₂ characterization. a) Powder XRD. b) ζ-potential measurements for the determination of the isoelectric point.

The ζ-potential measurements (Figure 36b) determined the pH_{IEP} at 7.4. This indicates that the surface of this synthetic FeS₂ was partially oxidized, presenting some Fe(III) moieties.^{117,136} As for pure pyrite (section 2.2.1) no acid pretreatment was used because in natural iron sulfide surfaces the presence of Fe(III) is common.¹¹⁸ Another similarity between this synthetic FeS₂ and the pure pyrite is a low BET surface area of 5.3 m² g⁻¹, which makes physical sorption less feasible as a removal mechanism for technetium.

2.3.2. Tc-removal by the synthetic FeS₂: Batch experiments

The batch experiments of the removal of Tc(VII) by the synthetic FeS₂ are presented in Figure 37. The isotherm (Figure 37a) shows that the lower the concentration of technetium, the better its removal by the synthetic FeS₂, which validates these results for more environmental scenarios, like with pure pyrite (section 2.2.2). The slope of the isotherm is 0.5, suggesting the sorption of Tc on one site type only. Such a value indicates a low affinity between the mineral and Tc¹³⁷ or the precipitation of Tc(IV), most likely as TcO₂.²⁸

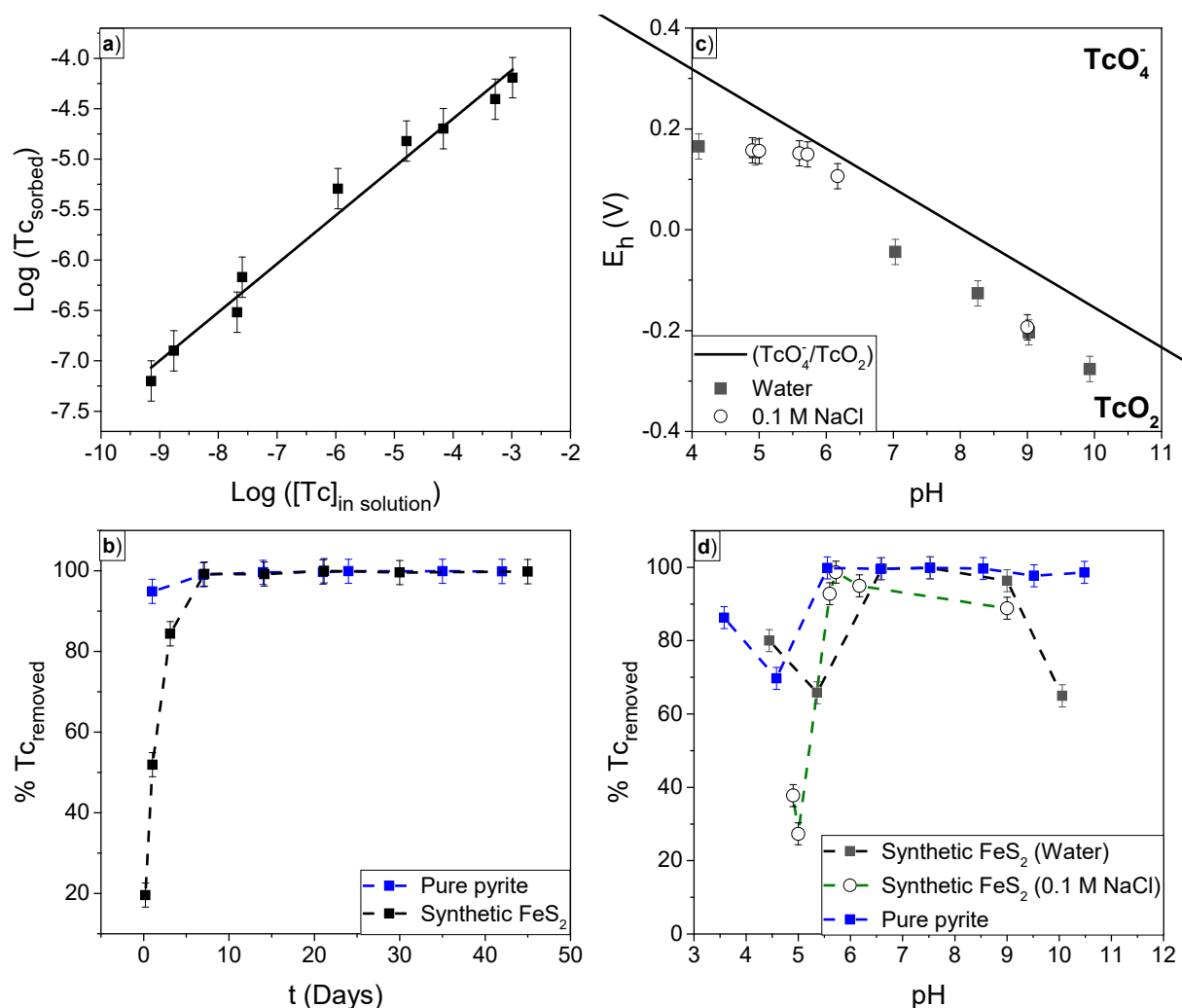


Figure 37. Batch experiments of Tc(VII) removal by synthetic FeS₂. a) Isotherm at pH 6.5 after 14 days of contact b) Scavenging kinetics at pH 6.5. c) Pourbaix diagram of Tc in the presence of synthetic FeS₂ in water and 0.1 M NaCl d) pH effect on water and 0.1 M NaCl after 14 days. Tc removal by pure pyrite is shown for comparison (blue dots). Dashed lines in b and d are shown to guide the eye.

Figure 37b presents the kinetics of the Tc removal at pH 6.5 by both synthetic FeS₂ and pure pyrite. The Tc retention by the synthetic FeS₂ becomes complete after seven days of contact and after 45 days still no re-mobilization of the radionuclei was observed. When compared with pure pyrite, it is clear that the presence of marcasite makes the overall process slower since pyrite needs only one day for removing 95% of Tc from solution.

The Pourbaix diagram (Figure 37c) confirms the reduction from Tc(VII) to Tc(IV) at all the working pH values in both water and 0.1 M NaCl. The pH edge experiments are presented in Figure 37d where a complete retention of Tc is reached at $6.0 < \text{pH} \leq 9.0$. Alike pure pyrite, the Tc removal under acidic conditions by the synthetic FeS₂ is less efficient and this can also be attributed to a higher solubility of FeS₂¹³⁸ that makes the Tc reduction less favorable, as it was explained in section 2.2.2. More surprising is the low retention of Tc by the synthetic FeS₂ at pH 10.0 (65% compared with 99% for pyrite at pH 10.0). This result could be an indication of the formation of TcS_x compounds that could passivate the surface preventing further Tc reduction.¹⁰¹ However, the chemical identity of the reaction products cannot be determined by batch experiments alone and the only hint on the removal mechanism by synthetic FeS₂ is given by the addition of 0.1 M NaCl to the system (Figure 37d). As a result, in the range of $6.0 < \text{pH} \leq 9.0$ no significant change in the retention is observed which rules out outer-sphere complexation.⁷⁷ The decreased Tc scavenging at $\text{pH} < 6.0$ can be attributed to either the formation of an outer-sphere complex or by the increase of the solubility of the Tc(IV) new species due to an increase in the ionic strength.^{121,122}

2.3.3. Spectroscopic analysis of the Tc-loaded solids

The Raman spectra of the synthetic FeS₂ loaded with Tc is presented in Figure 38. At pH 6.0 the formation of hematite as the FeS₂ oxidation product was confirmed by comparison with the reference R050300 of the RRUFF database.¹¹⁵ This result is very similar to the one obtained for pure pyrite (section 2.2.3) and points to the formation of an inner-sphere complex between Tc(IV) dimers and the hematite surface. Like in the batch experiments, the difference between the synthetic FeS₂ and the pure pyrite is very significant at pH 10.0. Unlike with pyrite, the Raman spectra show a band at 993 cm⁻¹ which indicates the presence of Fe(II)-sulfate-hydrate minerals like rozenite (FeSO₄×4H₂O), shown in Figure 38 for comparison. The formation of sulfates indicates that the reduction of Tc(VII) at this pH is not triggered by the oxidation of Fe²⁺, but of S²⁻. This is also supported by the high spectral similarity between the synthetic FeS₂ and the Tc-loaded synthetic FeS₂. It is noteworthy to mention that the band at 478 cm⁻¹ present

in the synthetic FeS_2 before and after the interaction with Tc can be attributed to the Fe(III) moieties mentioned in section 2.3.1.¹³⁹

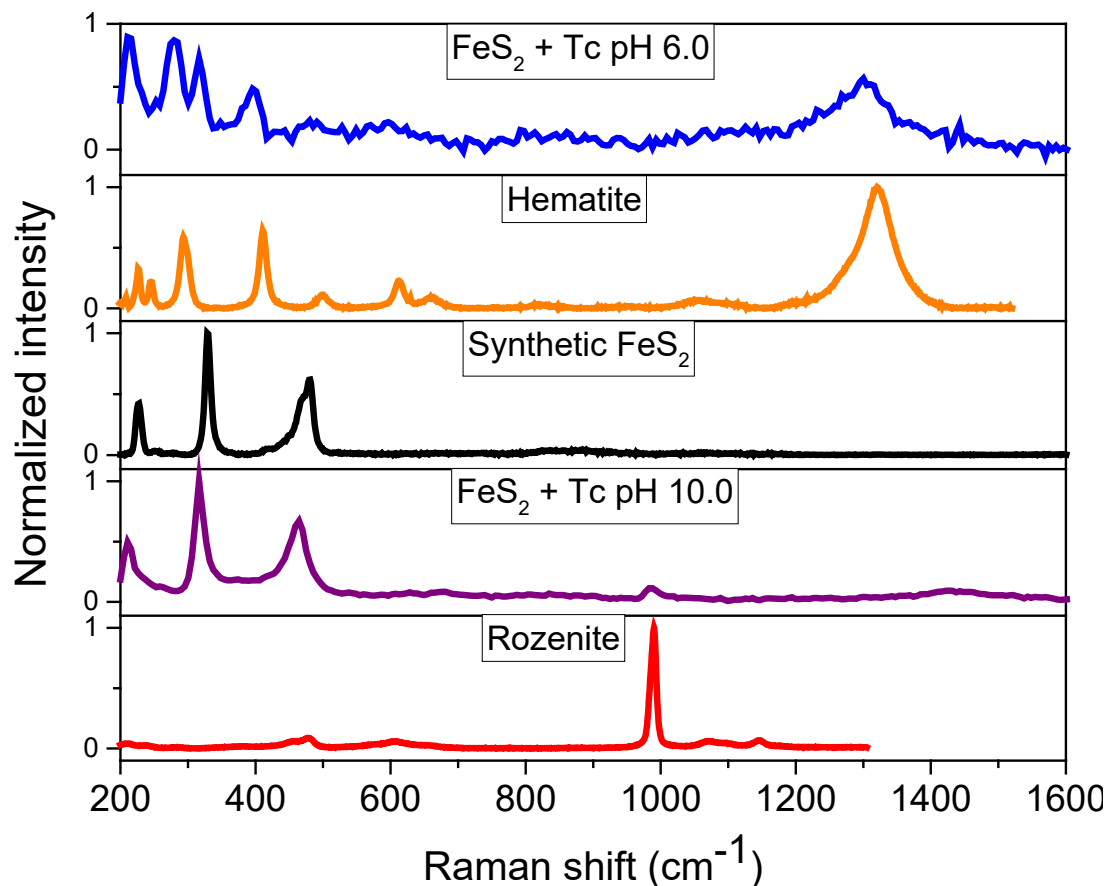


Figure 38. Raman spectra of the solids obtained after 15 days of interaction of the synthetic FeS_2 with Tc(VII) at pH 6.0 and pH 10.0. The spectra of pure FeS_2 and reference spectra of hematite (reference R050300) and rozenite ($\text{FeSO}_4 \times 4\text{H}_2\text{O}$, reference R070187) are shown for comparison.¹¹⁵

The Fe 2p, S 2p, O 1s, and Tc 3d XPS spectra are shown in Figure 39. The Fe 2p spectra (Figure 39a) illustrates that the formation of Fe(III) occurs only at pH 6.0 in a very small proportion when compared with pure pyrite (section 2.2.4, Figure 34). At pH 10.0 no Fe(III) is observed, which combined with the Raman spectra confirms that at this pH value the redox active species of the synthetic FeS_2 is S^{2-} and not Fe^{2+} . However, no formation of sulfate is detected in the S 2p spectra (Figure 39b) while the Fe 2p_{3/2} and S 2p_{3/2} binding energies can be unequivocally assigned to FeS_2 . This would be a consequence of the low concentration of sulfate present in the sample as it is the product of the incomplete reduction of 5 μM Tc, which is below the XPS detection limit. In contrast, Raman microscopy allows the identification of species that are located only in specific spots of the sample, as it would be the case of sulfate since it is a product

of the heteroreduction of technetium. Additionally, the low intensity of the band at 993 cm⁻¹ is a confirmation of the low concentration of sulfate in the sample.

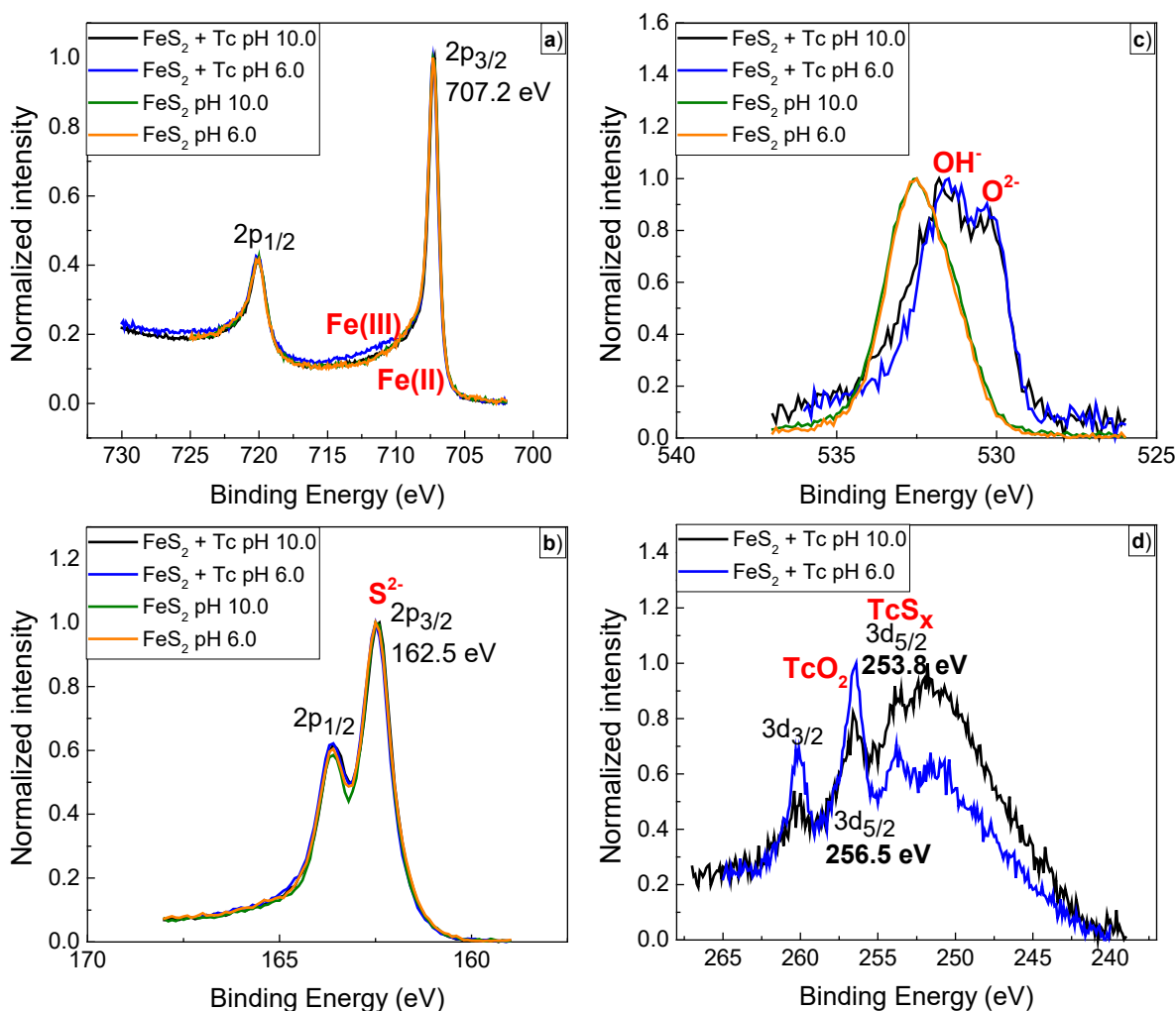


Figure 39. XPS spectra of the synthetic FeS₂ mixture before and after the reaction with Tc(VII) ([Tc] = 1000 ppm) at pH 6.0 and pH 10.0. a) Fe 2p. b) S 2p. c) O 1s. d) Tc 3d. Tc 3d elemental lines are superposed by the broad loss line of S 2s.

The signal at 532.3 eV in the O 1s spectra of the pure synthetic FeS₂ (Figure 39c) can be assigned to adsorbed water.¹⁴⁰ This signal disappears after the interaction with Tc at both pH values, where the formation of similar proportions of OH⁻ and O²⁻ can be observed. It is also possible to confirm the presence of TcO₂ in both samples using the peak at 256.5 eV in the Tc 3d spectra (Figure 39d). This Tc 3d_{5/2} signal is more intense at pH 6.0, indicating that the formation of technetium oxide is favored at this pH value. Another Tc 3d_{5/2} peak was found at 253.8 eV at both pH values, although the peak intensity is higher at pH 10.0. This peak can be related to the

formation of TcS_x compounds that were not detected in the S 2p spectra due to their low concentration, like in the case of sulfate.

Speciation diagrams for Tc(VII) reduction in the presence of Fe^{2+} and/or S^{2-} are presented in Figure 40. A quantitative reduction from Tc(VII) to TcO_2 is predicted throughout the working pH range (pH 4.5 – 10.5). When the reduction is promoted only by Fe^{2+} (Figure 40a) the main species of Fe(II) in solution are Fe^{2+} at pH < 7.0 and Fe(OH)^+ and Fe(OH)_2 at pH > 7.0, whereas the main species of Fe(III) are hematite at pH < 6.5 and magnetite at pH > 6.5. In case the reduction is promoted only by S^{2-} (Figure 40b) HS^- is the main S(-II) species in the entire pH range and the sulfur oxidation products are elemental sulfur $\text{S}_{(\text{cr})}$ at pH < 5.0 and SO_4^{2-} at pH > 5.0.

When the Tc(VII) reduction is triggered by both Fe^{2+} and S^{2-} (Figure 40c) the formation of solid pyrite and mackinawite as well as the presence of aqueous Fe^{2+} , FeOH^+ and HS^- is favored while Fe(III) and oxidized sulfur species are present in low concentrations. This is a consequence of the excess of Fe^{2+} and S^{2-} with respect to Tc(VII), as they have concentrations 20 and 40 times higher than the radionuclei, respectively. Consequently, the amount of iron and sulfur fully oxidized products is smaller in comparison to the formation of the Fe(II) and S(-II) main species found in the speciation. It is noteworthy to mention that the set-up conditions of the calculations might be less realistic. This is because the Tc homoreduction by Fe^{2+} and S^{2-} was assumed, which was clearly not the case in these experiments. However, it has been reported that when Fe^{2+} and SO_4^{2-} are together in solution at pH > 7.0, the formation of FeSO_4 is favored.¹⁴¹ Even though the speciation patterns presented here need to be carefully evaluated, they support the findings of the Raman spectra.

In conclusion, the removal of Tc by the synthetic FeS_2 starts with the reduction from Tc(VII) to Tc(IV) promoted by Fe^{2+} at pH 6.0 and, surprisingly by S^{2-} at pH 10.0. The reactions products would be hematite at pH 6.0 and Fe(II)SO_4 and TcS_x at pH 10.0.

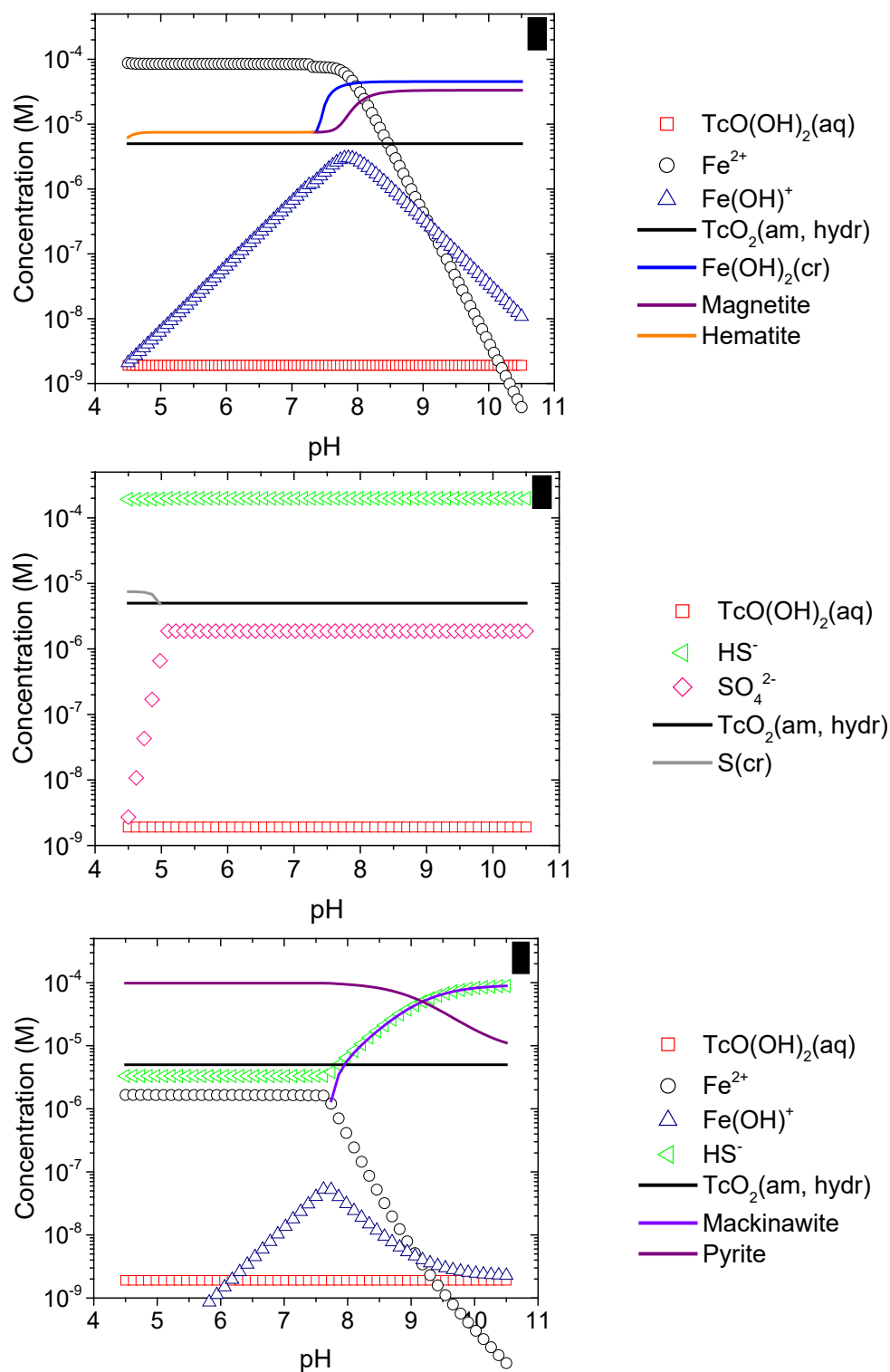


Figure 40. Calculated speciations as a function of pH. Tc(VII) reduction in the presence of a) Fe^{2+} b) S^{2-} and c) both Fe^{2+} and S^{2-} . Calculations have been performed considering the initial presence of $20 \mu\text{M Fe}^{2+}$ and $5 \mu\text{M TcO}_4^-$. The latest Fe^{135} and Tc^{35} thermodynamic databases have been used.

2.3.4. Re-oxidation essays

Figure 41 shows the batch experiments of the re-oxidation essays. Like in the case of pure pyrite (section 2.2.2), the oxygen concentration needed to oxidize the mineral was rapidly reached due to the stirring of the samples under ambient atmosphere and the subsequent openings of the tubes for pH adjustment and sampling. Figure 41 shows that the initial Tc concentration at pH 10.0 was 1.13 μM and it decreased after the exposure to ambient atmosphere to 0.48 μM . This is a result of the high reactivity of marcasite rapidly forming H_2SO_4 , when exposed to oxidizing conditions.¹⁴² It explains why the pH values always turned acidic when the samples were exposed to ambient atmosphere (for more details, see section II in the experimental methods). The production of H_2SO_4 reduces the remaining Tc(VII) in solution at $\text{pH}_{\text{initial}}$ 10.0 and can be also the reason why the Tc concentration remained lower than 1 μM for 50 days in both samples.

Similar to pure pyrite, in the last point of the experiments (64 days) the re-oxidation apparently begins and is faster in the sample with $\text{pH}_{\text{initial}}$ 6.0. This indicates a stronger interaction of the Tc(IV)-species with the mineral at pH 10.0 and suggests the formation of an inner-sphere complex at pH 6.0 and co-precipitation or incorporation at pH 10.0. It is also important to bear in mind the higher proportion of TcO_2 at pH 6.0 indicated by XPS (section 2.3.3) that also explains a faster re-oxidation of technetium at this initial pH value.

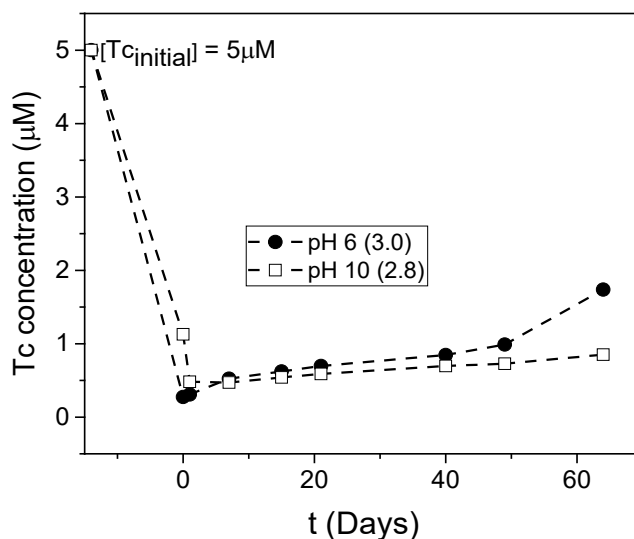


Figure 41. Tc concentration in suspension for 64 days in ambient atmosphere at different pH values ($\text{pH}_{\text{initial}} = 6.0$ and 10.0; pH after exposure to ambient atmosphere was 3.0 and 2.8, respectively).

Dashed lines are shown to guide the eye.

The Raman spectra of the Tc-loaded synthetic FeS₂ after 50 days under ambient atmosphere are presented in Figure 42a. Both samples have the same chemical identity, i.e. a mixture of the initial synthetic FeS₂ and solid elemental sulfur. This was also confirmed by XRD (Figure 42b) and the speciation calculations (Figure 40b) supporting the formation of S_(cr) at low pH values. It can be derived that the initial pH of the sample does not play a role for the speciation after the exposure to ambient O₂, which is most probably related to the production of H₂SO₄. These results suggest that the re-oxidation of Tc, and thus its re-mobilization, could only start after all the marcasite present has been consumed, which would limit the technetium distribution within the repository near and far field.

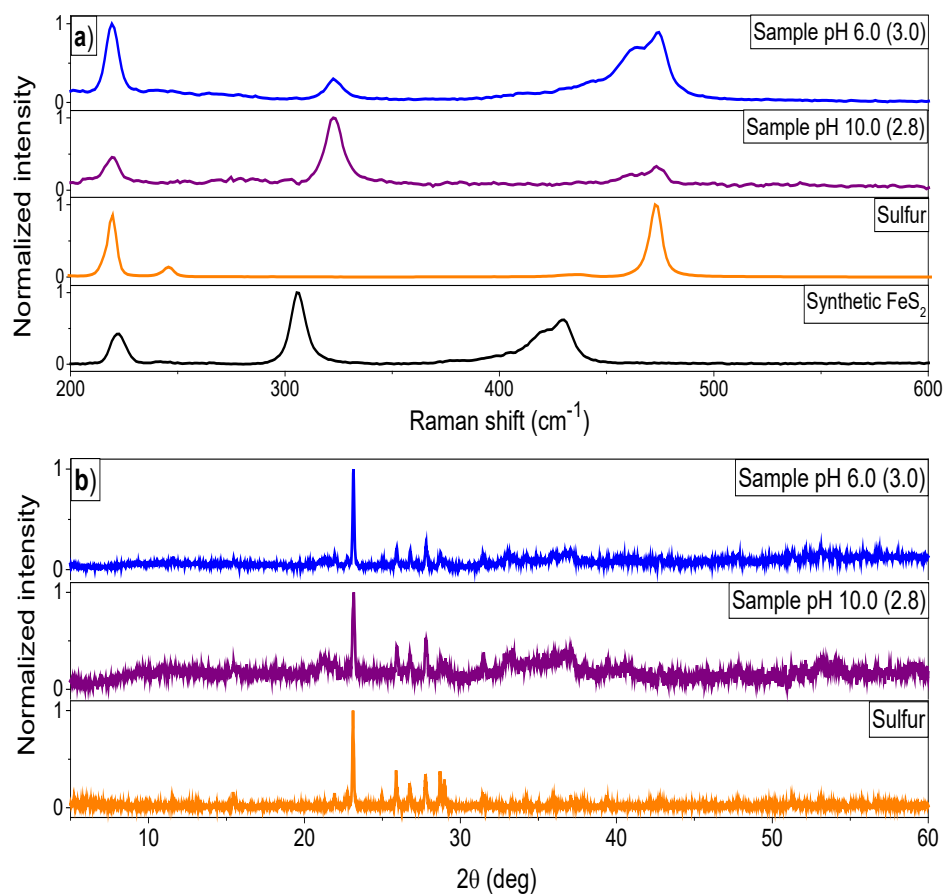


Figure 42. a) From top to bottom: Raman spectra of the solids at $pH_{initial}$ 6.0 and 10.0 after 50 days of exposition to ambient atmosphere. The Raman spectra of sulfur (reference R040135) and of the synthetic FeS₂ mixture are shown as reference.¹¹⁵ b) From top to bottom: XRD of the solids at $pH_{initial}$ 6 and 10 after 50 days of exposition to ambient atmosphere. The XRD sulfur (reference R040135) is shown as reference.¹¹⁵

2.4. Summary

The $^{99}\text{Tc(VII)}$ retention by pure pyrite and by a mixture marcasite-pyrite 60:40 (synthetic FeS_2) was studied in a broad pH range by combining batch sorption experiments and several spectroscopic techniques, as well as diffraction, microscopy and speciation modelling. Even though the Tc initial concentration used in this work (5 μM) is several orders of magnitude higher than the usual Tc concentration in the environment ($1 \times 10^{-9} \text{ M}^{10,119}$), the isotherms of both systems showed that the lower the Tc concentration, the higher its removal, making the results presented here valid for more realistic environmental scenarios.

It was found that at all pH values Tc(VII) was reduced to Tc(IV) after the interaction with the minerals. The Tc removal by both solids presents slow kinetics at acidic pH values as a consequence of the increase of the solubility of FeS_2 at $\text{pH} < 5.0$, which makes the Tc(VII) reduction less efficient. At $\text{pH} \geq 5.5$ pyrite was able to remove almost 100% of technetium from solution within one day. The presence of marcasite makes the process slower and less efficient, since the synthetic FeS_2 needed seven days to quantitatively scavenge Tc from solution at $6.0 < \text{pH} < 9.0$. At pH 10.0 only 64% of technetium was retained after 14 days.

The combination of XAS, XPS and Raman microscopy identified two different mechanisms for the Tc removal by pyrite depending on the pH, which was supported by the speciation of iron under the working conditions that predicted the formation of hematite at $\text{pH} < 7.5$ and magnetite at $\text{pH} > 7.5$ on the pyrite surface. Thus, at pH 6.0 the inner-sphere complexation between Tc(IV)-dimers and hematite was observed, while at pH 10.0 the incorporation of Tc(IV) into magnetite by replacing an Fe(III) in octahedral position was found.

In the presence of marcasite the formation of hematite at pH 6.0 was also observed by Raman microscopy, which suggests that the removal mechanism is the same as in the case of pure pyrite. However, at pH 10.0 the surprising formation of a Fe(II)SO_4 -like mineral was observed by Raman microscopy and supported by the speciation calculations. This implies that, contrary to what was expected from pure pyrite, at this pH value the species responsible for the Tc(VII) reduction is S^{2-} and not Fe^{2+} . The change of the predominant redox active element at pH 10.0 would be responsible for the slower and less effective Tc uptake and can be explained by a higher reactivity of marcasite that results in the formation of H_2SO_4 after its oxidation. The formation of sulfate after the reduction of Tc(VII) has never been reported before, which reflects the poor understanding available so far on the interaction between sulfur and technetium,

highlighting the importance of more works in this matter. Despite the differences between the Tc interaction with pure pyrite and the synthetic FeS₂ at pH 10.0, there is a common point for the two solids: the formation of TcS_x compounds found by XPS, which is in good agreement with previous studies of the Tc retention by mackinawite²¹ and in the presence of microorganisms.¹⁰¹ The role of these TcS_x compounds in the overall retention mechanism is not clear because they could either passivate the mineral against further reduction, precipitate or simply be transient phases in the total redox process.

A schematic representation of the Tc(VII) removal by FeS₂ is given in Figure 43.

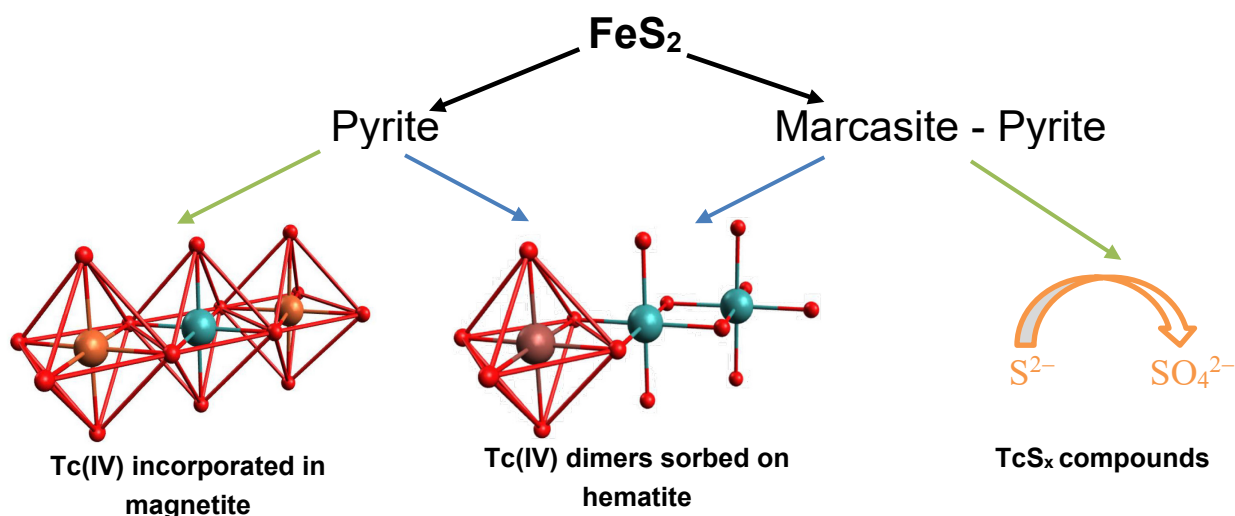


Figure 43. Schematic representation of the reductive immobilization of Tc(VII) by FeS₂. Blue arrows represent pH 6.0; green arrows represent pH 10.0.

The re-oxidation essays showed that both solids are able to keep Tc as Tc(IV) for at least two months. Interestingly, in the case of marcasite the production of H₂SO₄ was independent of the initial pH of the samples and it promoted the reduction of the Tc(VII) still present in solution. The higher stability of pyrite kept the surface available for the reduction of any re-oxidized Tc(VII) moiety. Studies on a longer time scale (probably months) should be carried out to determine at which point the minerals lose the ability to inhibit Tc(IV) re-oxidation. Nevertheless, the fast kinetics of the Tc removal by pyrite and the relatively long time along which it retains technetium under aerobic conditions make it a good candidate for remediation of contaminated waters, as it will be able to uptake technetium (and possible other pollutants) in the same way that activated charcoal does with organic impurities. This could also be considered even in the presence of marcasite, although it would require more time to reach Tc full removal.

Concluding remarks, environmental significance and perspectives

A comprehensive study on the mechanisms for the surface-mediated reduction of Tc(VII) has been performed. As a first approach, spectro-electrochemical methods were employed to determine that in a non-complexing medium, i.e. 2 M NaClO₄, the reduction follows two different mechanisms depending on the pH: at pH 2.0, Tc(VII) gains 2.1 ± 0.3 electrons to produce Tc(V) that rapidly reduces to Tc(IV) with the transfer of 1.3 ± 0.3 electrons. At pH ≥ 4.0 a direct transfer of 3.2 ± 0.3 electrons yields Tc(IV). For the first time, the reduction mechanism of Tc(VII) in non-complexing media has been approved by using spectro-electrochemical methods, closing finally a knowledge gap in the understanding of basic technetium aqueous chemistry. Furthermore, this study provided not only an accurate determination of the electrons transferred in the system depending on the pH but also the Raman features found at 374 and 1107 cm⁻¹ assigned to Tc(IV) will probably be of great use for the identification of Tc(IV)O₂ in more applied fields, which, until now, was only possible by more expensive spectroscopies like XAS or XPS.

As a second approach, a combination of batch experiments and spectroscopic methods was used to study the interactions of technetium with pyrite and marcasite. Both iron sulfides promote the reduction from Tc(VII) to Tc(IV). The overall process is faster and more efficient in pure pyrite, that quantitatively removes Tc from solution by forming an inner-sphere complex between Tc(IV) dimers and surficial hematite at pH 6.0 or incorporating it into surficial magnetite structure at pH 10.0. The presence of marcasite makes the process slower but complete at pH 6.0, where the formation of hematite suggests that the removal mechanism is the same as with

pure pyrite, and incomplete at pH 10.0, where the surprising formation of Fe(II) sulfate minerals was found, which has never been observed before. Hence, while for pyrite at pH 6.0 and 10.0 and in the presence of marcasite at pH 6.0 the redox active species was Fe^{2+} as expected, at pH 10.0, due to the fast oxidation of marcasite, the redox active species is S^{2-} . Moreover, the interaction with both iron sulfides delays the re-oxidation of Tc(IV) for at least two months of exposition to ambient atmosphere. Additionally, this work has proven that even in the “do nothing” option, natural attenuation of the technetium mobility is to be expected in the near and far field of nuclear waste repositories like Yucca Mountain in the USA, Onkalo in Finland or the Forsmark site in Sweden, where pyrite and probably marcasite are abundant,^{32,143,144} or in repositories that use materials like bentonite as host-rock and backfill material, where iron sulfide will be found as accessory material.³³

The results presented here have closed several gaps in our general knowledge of the Tc(VII) reduction in water. This is crucial for real engineered and natural environments with high radioecological interest: the interaction of technetium with ubiquitous materials like iron sulfide, that is found in a variety of geological formations like sedimentary deposits, hydrothermal veins and metamorphic rocks. This also applies for several proposed nuclear waste repositories, either due to the soil composition or due to its presence as accessory mineral in host rocks or backfill materials or even corrosion products encountered in the near field. Regardless of the amount of results, it is very common that every study ends up generating new research questions. It is the case also with this work, which has given new perspectives for further studies that will be described below:

For starting, the formation of Tc(V) in aqueous solution did not play any role on the technetium retention by FeS_2 . However, in the US-Hanford site several reports of non-pertechnetate species with exotic oxidation stated like Tc(I) and Tc(II) have been issued since 2004.^{145–149} Such species are stabilized by carbonyl and nitrosyl ligands and it is possible that the Tc(V) unstable in water can be also stabilized by other inorganic or organic ligands present in e.g. the minerals or humic substances. In this sense, the spectro-electrochemical methodology applied for the basic system 0.5 mM Tc in 2 M NaClO_4 can also be applied in the presence of complexing ligands like NO_3^- , HCO_3^- , or glycolate that are more relevant from the environmental point of view. This approach would be useful to understand the mechanistic implication of the complexation on the reduction but can also be used to determine formation constants of relevant Tc-complexes.

The surprising formation of iron sulfate minerals after the reduction of Tc(VII) in the presence of marcasite, as well as the finding of TcS_x by XPS in both mineral systems stress the importance of sulfur in the Tc(VII) reduction and open the door to further studies on the interaction between Tc and S in other sulfur minerals like galena (PbS) or chalcopyrite (CuFeS_2). Furthermore, the clear impact of marcasite on the retention of technetium by pyrite highlights the role of polymorphism on the scavenging ability of minerals and, in consequence, further studies comparing Tc-removal by other polymorphs, like hematite ($\alpha\text{-Fe}_2\text{O}_3$) and maghemite ($\gamma\text{-Fe}_2\text{O}_3$) should be performed.

Experimental methods

Radiation safety. ^{99}Tc is a β -particle emitter with a long half-life (2.14×10^5 years) and must be handled only in a dedicated radiochemistry laboratory with specific radiation safety measurements in place.

I. Spectro-electrochemical experiments

Sample preparation

$\text{K}^{99}\text{TcO}_4$ was provided by the Institute of Radiopharmaceutical Cancer Research from Helmholtz-Zentrum Dresden-Rossendorf. $\text{NaClO}_4 \cdot \text{H}_2\text{O}$ (purity $\geq 98\%$, PanReac AppliChem ITW Reagents). All solutions were prepared with Milli-Q water (resistivity of $18.2 \text{ M}\Omega \cdot \text{cm}$, Water Purified®). In general, 7 mL of 0.5 mM Tc solutions were prepared in 2 M NaClO_4 at different pH values. The pH was adjusted by adding small amounts (less than 10 μL) of HClO_4 or NaOH , so changes in ionic strength or viscosity were negligible.

Cyclic voltammetry and RDE

The cyclic voltammetry and the experiments with the RDE were performed with the 884 Professional VA instrument from Metrohm using a three-electrode set-up of the same brand. The working electrode was a glassy carbon disk with $2.0 \pm 0.1 \text{ mm}$ of diameter used in stationary mode for CV and in hydrodynamic mode for RDE. The electroactive area of the electrode was determined as $0.035 \pm 0.001 \text{ cm}^2$ with a Randles-Sevcik analysis of 10 mM $\text{K}_3\text{Fe}(\text{CN})_6$ in 1.0 M KNO_3 . ^{150}Pt was used as counter electrode and Ag/AgCl (3M KCl) as reference electrode. This device was used under normal atmosphere at 25°C . The solutions were always purged with N_2 for 20 minutes before any measurement.

Spectro-electrochemical cell

Figure 44 presents the diagram of the in-house-build spectro-electrochemical cell. The orange-colored line represents the glovebox (GS Glovebox-System GS050912; $< 1 \text{ ppm O}_2$) used to ensure inert atmosphere. The experiments were performed at 21°C , which is the glovebox temperature. The cell holder was printed with a 3D printer (3DWOX 1, Sindoh). The three-electrodes cell (dimensions: wide $20 \times$ depth $10 \times$ height 30 mm) was made of quartz with a path length of 0.5 cm. The electrodes used were a glassy carbon rod (ALS Japan) as working electrode, Ag/AgCl as reference electrode (ALS Japan) and Pt as counter electrode (ALS Japan). The electrodes were connected to a potentiostat (PGSTAT 101, Metrohm) located outside the

glovebox. Both the lamp (AvaLight-DH-S-BAL, Avantes) and the spectrometer (AvaSpec-ULS2048 StarLine, Avantes) were located outside the glovebox and they were connected to the cell holder via fiber optics.

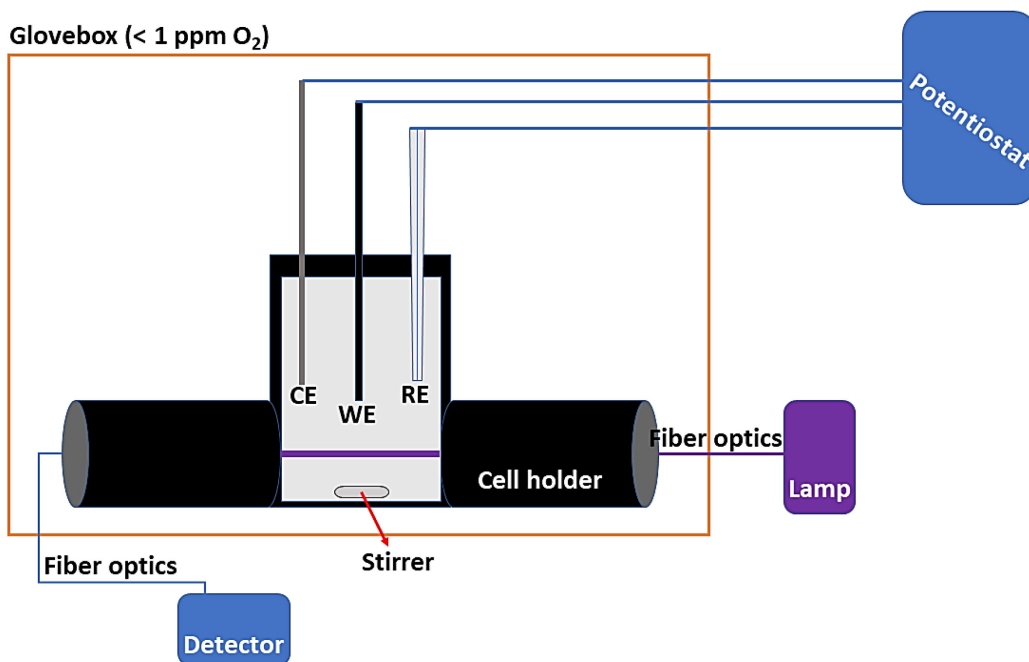


Figure 44. Schematic representation of the in-house-build spectro-electrochemical cell.

In general, the Tc solution was placed in the quartz cell and agitated throughout the entire experiment with a 0.5 cm magnetic stirrer. A potential staircase of 10 mV steps was applied while UV-vis spectra were continuously recorded in the range from 200 to 1100 nm with an integration time of 10 ms. For pH 2.0 the potential staircase started at -490 mV, while for pH 10.0 it started at -620 mV; for both pH values the potential staircase ended at -1000 mV. Each potential was applied for 4 minutes, in parallel one spectrum was recorded every 30 seconds, yielding 8 spectra per potential value that were afterwards averaged to reduce the noise.

Solid analysis

After the reduction of Tc(VII) in the spectro-electrochemical cell, a black solid was deposited on the working electrode. The solid detached immediately when the electrode was taken out of the solution to dry. It was collected and placed on a cell containing two CaF₂ Raman quality windows⁸⁷ and after the solid got dried under N₂ atmosphere, the cell was sealed to avoid the contact with oxygen during the experiment. The Raman spectra were measured outside the

glovebox with a Raman microscope (Aramis, Horiba) using a He – Ne Laser with a 10-fold objective with a D 0.3 filter, a pin-hole of 500 μm and a slit of 600 μm .

A second batch of the solid was produced and it was dissolved in deuterated dimethyl sulfoxide (DMSO- d_6 , 99.8% D, Deutero GmbH Germany) and, inside a glovebox, transferred into a gas-tight 5 mm NMR sample tube equipped with a low-pressure PTFE valve. The sample was heated up to 60 °C in order to improve solubility. ^{99}Tc -NMR spectra were obtained on a 14.1 T Agilent DD2-600 NMR system operating at a corresponding ^{99}Tc resonance frequency of 134.8 MHz, using a 5 mm oneNMRTM probe. Owing to the large chemical shift range (6000 ppm \approx 800 kHz), sufficient excitation was assured by sweep-range partitioning. The depicted spectrum is the sum of 600,000 accumulations obtained after a 15 μs $\pi/2$ single-pulse excitation, an acquisition time of 150 ms and a relaxation delay of 500 ms. Chemical shifts are reported relative to 1 mM aqueous NH_4TcO_4 .

II. Tc scavenging experiments

General notes.

- a) The majority of the preparations were performed under N_2 atmosphere inside a glovebox (GS Glovebox-System GS050912; < 1 ppm O_2) at 21°C. Unless indicated otherwise, experiments were performed under inert atmosphere.
- b) The Milli-Q water (resistivity of 18.2 $\text{M}\Omega\cdot\text{cm}$, Water Purified[®]) used for the experiments was boiled for two hours for degassing, sealed and cooled down to room temperature before its use inside the glovebox.
- c) The pH was adjusted by adding either NaOH or HCl. A pH meter pH3110 from WTW was used with a pH electrode from SI Analytics Blue Line (calibration with pH buffers 4.006, 6.865 and 9.180). For both solids the pH was adjusted at least twice a week through the duration of the experiments. The amounts of acid or base added were never higher than 10 μL in order to ensure that the variation on Tc concentration and ionic strength was small enough to be neglected as the total volume of the sample was 32 mL.
- d) The Eh was measured with no agitation during 30 minutes. An Eh electrode from Mettler Toledo calibrated with a redox buffer solution (220 mV / pH 7) was used.

Solids and synthesis

The pure synthetic pyrite was purchased from Alfa Aesar (REF: 12842). The mixture marcasite-pyrite 60:40 (hereafter referred to simply as synthetic FeS_2) was synthesized following the procedure described by Huo et al.:²⁶ First, 200 mL of 0.1 M FeCl_3 (Merck, purity $\geq 99\%$) and

200 mL of 0.2 M NaHS (Acros Organics, purity $\geq 99\%$) were prepared and purged with N₂ for 30 minutes. Then, the solutions were mixed in a round flask of 500 mL and left under N₂ atmosphere for other 30 minutes. Finally, the mixture was sealed and aged for 24 hours in a stove at 60°C. The black powder obtained was separated by ultracentrifugation and dried by lyophilization.

The Brunauer-Emmett-Teller (BET) specific surface area of both solids was determined by isotherm experiments with N₂ at 77 K (Multipoint Beckman Coulter surface analyzer SA 3100).

Solid characterization

a) X-Ray powder diffraction (XRD)

Both solids were analyzed by XRD (MiniFlex 600 powder XRD, by Rigaku) using Cu K α ($\lambda = 1.54184$ Å) as X-ray source, that has an X-ray generation of 40 kV / 15 mA (600 W). The spectrum was recorded in a scan continuous mode. The sample preparation was carried out inside a N₂ glovebox (GS Glovebox-System GS050912; < 1 ppm O₂), where the solid was homogenized with an agate mortar and then mounted on an airtight sample holder (Rigaku) to ensure the inert conditions during the measurement. The data analysis software used was PDXL: integrated x-ray powder diffraction software, Version 2.8.1.1, Rigaku.

b) Scanning electron microscopy (SEM)

The micrographs of both solids were obtained by using a FEI Quanta 650 FEG environmental scanning electron microscope. Both the sample preparation and the SEM were carried under anoxic atmosphere. SEM-ED spectra of selected areas were acquired by use of a Thermo Scientific UltraDry, i.e. Peltier cooled, silicon drift X-ray detector and the NORAN System7 microanalysis system, software version 3.3

c) ζ -potential measurements

0.05 g L⁻¹ solid suspensions were prepared in 0.1 M NaCl between pH 3.0 and pH 10.0 inside the glovebox and the aliquots of the suspensions were transferred into disposable cuvettes (DTS1070, Malvern). The cuvettes were taken outside of the glovebox, where the ζ -potential measurements were rapidly performed (Zetasizer Nano Series Nano-ZS, Malvern Instruments) at 25 °C. Five different scans of 30 seconds were carried out for every sample. The presented values are calculated as an average of the five independent measurements.

d) Pyrite solubility

Eight suspensions of pyrite in water (1.3 g L^{-1}) were prepared in the pH range from 3.5 to 10.5. The samples were equilibrated under horizontal shaking for 3 weeks adjusted the pH as it was mentioned in section 2.2.6. Afterwards, they were centrifuged ($600 \times g$ for one hour) and an aliquot of 1 mL from the supernatants was acidified with 10 μL of concentrated HNO_3 . The Fe^{2+} concentration was measured by inductively coupled plasma mass spectroscopy, ICP-MS (NexION 350x, Perkin Elmer).

Batch experiments

Table 5 summarizes the conditions of the batch experiments. A general procedure started with the preparation of a suspension of $1.3 \pm 0.2 \text{ g L}^{-1}$ of the mineral (pyrite or synthetic FeS_2) in water or in 0.1 M NaCl (NaCl(s) from Merck, purity $\geq 99\%$) depending on the experiment. The required volume of a $\text{K}^{99}\text{TcO}_4$ stock solution ($9.22 \times 10^{-3} \text{ M}$) was added and the pH was adjusted to the required value.

Table 5. General conditions of the batch experiments carried out with the pyrite and the synthetic FeS_2 at $1.3 \pm 0.2 \text{ g L}^{-1}$.

Experiment	Kinetics	pH effect	Isotherm
$[\text{Tc(VII)}]_0 \text{ (M)}$	5.0×10^{-6}	5.0×10^{-6}	$2 \times 10^{-7} - 2 \times 10^{-3}$
pH	3.5 - 10.5	3.5 - 10.5	6.0 and 10.0
Contact time (days)	1 - 42	1 - 42	14

Subsequently, the suspensions were agitated for hours or days on a horizontal shaker. After the distinct contact time, pH and Eh were measured. The mineral phase was separated from the suspension by ultracentrifugation ($2.4 \times 10^5 \times g$ for 1 hour). 0.25 mL of supernatant were mixed with 5 mL of scintillation cocktail (Ultima GoldTM, Perkin Elmer) and placed in the liquid scintillation counter (1414 LSC Winspectral α/β Wallac, Perkin Elmer; detection limit: 25 cpm; measuring time: 10 minutes) to determine the remaining Tc concentration in solution. Using Eq. [24] the cpm of the sample are converted to Bq mL^{-1} .

$$(\text{Bq mL}^{-1})_{\text{Sample}} = \frac{\text{cpm}}{60 \text{ s} * 0.25 \text{ mL}} \quad [24]$$

The percentage of technetium removed is given by Eq. [25].

$$\%Tc_{\text{removed}} = \frac{((\text{Bq mL}^{-1})_{\text{Initial}} - (\text{Bq mL}^{-1})_{\text{Sample}}) * 100}{(\text{Bq mL}^{-1})_{\text{Initial}}} \quad [25]$$

For the construction of the isotherms, the activity of the sample was converted from Bq mL⁻¹ to mol L⁻¹ to obtain the amount of Tc in solution, Tc_{sol}. Tc_{sorbed} was found with Eq. [26].

$$Tc_{sorbed} = \frac{Tc_{initial} - Tc_{sol}}{Solid\ concentration} \quad [26]$$

Where Tc_{initial} is 5×10⁻⁶ mol L⁻¹ and the solid (pyrite or synthetic FeS₂) concentration is 1.3 g L⁻¹.

Re-oxidation essays

Suspensions of the minerals (1.3 ± 0.2 g L⁻¹) were prepared and the necessary amount of the K⁹⁹TcO₄ stock solution used in the batch experiments was added to reach 5.0×10⁻⁶ M Tc. The pH values were adjusted to 6.0 or 10.0 depending on the sample and the final volume was 35 mL stored in 50 mL polypropylene tubes. They were kept under constant agitation for 5 days for pyrite and 14 days for the synthetic FeS₂, after which the complete removal of Tc from solution was confirmed by LSC as described before. Afterwards, the tubes were opened outside the glovebox under ambient atmosphere for one hour with constant agitation. Then they were closed and left on a horizontal shaker for 60 days outside the glovebox, during which the pH was adjusted twice a week as in the batch experiments for pyrite. In the case of the synthetic FeS₂, despite the initial pH (6.0 or 10.0), the pH became acidic after few hours, due to the production of H₂SO₄ after the marcasite oxidation. The pH was adjusted every day for two weeks but the desired values were never sustained. Therefore, it was decided not to adjust the pH any further and leave it at the stable value reached after the exposure to ambient atmosphere (pH = 3.0 instead of 6.0 and 2.8 instead of 10.0). The suspensions were regularly sampled by taking 5 mL aliquots to quantify the Tc concentration in the supernatant by LSC as described before.

Sample preparation for spectroscopy

0.140 g of the mineral were mixed with 50 mL of water and the necessary amount of the K⁹⁹TcO₄ stock solution used in the batch experiments was added to obtain ≈ 1000 and 600 ppm of Tc load in the final solid. The pH was adjusted to 6.0 and 10.0 and the samples were left under constant agitation for one month along which the pH was adjusted twice a week, like in the batch experiments. Afterwards, the solid was separated by ultracentrifugation (2.4×10⁵ × g for 1 hour) and distributed for separate analysis SEM, XPS, XAS (XANES and EXAFS) and Raman microscopy for pyrite and XPS and Raman microscopy for the synthetic FeS₂. Two blanks of mineral suspensions in water (1.3 g L⁻¹) were prepared at pH 6.0 and 10.0, left in horizontal

agitating for one month, adjusting the pH occasionally. They were measured at the same conditions as the Tc-containing samples.

XPS

The wet paste was re-dissolved in approximately 1 mL of water inside polypropylene vials that were closed and introduced in a sealed container inside the glovebox and transported to the Karlsruhe Institute of Technology, KIT, for the measurements. In general, one drop of suspension was dried on an indium foil. This was mounted onto a sample holder and moved into the XPS system PHI 5000 VersaProbe II (ULVAC-PHI Inc.) using a transfer vessel without air contact. The XPS system is equipped with a scanning microprobe X-ray source (monochromatic Al K α (1486.7 eV) X-rays). An X-ray source power of 32 W was used to record the survey scans of the conductive samples and to pass energy of the analyzer of 187.85 eV. Narrow scans of the elemental lines were recorded at 23.5 eV pass energy, which yields an energy resolution of 0.67 eV FWHM at the Ag 3d $_{5/2}$ elemental line of pure silver.

The calibration of the binding energy scale of the spectrometer was performed using binding energies of elemental lines of pure metals (monochromatic Al K α : Cu 2p $_{3/2}$ at 932.62 eV, Au 4f $_{7/2}$ at 83.96 eV). The error of binding energies of elemental lines is estimated to be \pm 0.2 eV.

XAS

The sample preparation and data treatment here presented corresponds only to the pure synthetic pyrite loaded with Tc. The synthetic FeS $_2$ was not analyzed by XAS because the presence of both iron sulfides would have complicated the data treatment, i.e. assign the signals to either pyrite or marcasite.

The wet pastes for XAS were mounted on doubled sealed plastic sample holders inside the glovebox. Afterwards, they were taken outside the glovebox, immediately flash-frozen with liquid nitrogen and then stored in a liquid nitrogen container for transportation to the Karlsruhe Institute of Technology (KIT).

Spectra were acquired at the KARA Synchrotron Radiation Source at KIT in fluorescence mode at the Tc-K edge (21044 eV) in steps of 0.5 eV for XANES and 0.05 Å $^{-1}$ steps for EXAFS up to 12.5 Å $^{-1}$. The measurements were performed at 15 K in a He cryostat. The energy of the Si(111) double-crystal monochromator was calibrated using a Mo-foil (K-edge at 20 000 eV). In order to collimate the beam into the monochromator crystal reject higher-order harmonics,

two Rh-coated crystals were used. The spectra were acquired with a 13-element, high-purity, solid-state Ge detector (Canberra) with digital spectrometer (XIA XMAP). Spectral processing included normalization, transformation from energy into k-space, subtraction of a spline background. Shell fits were performed with WinXAS following standard procedures.¹⁵¹ All fits were done in R-space (1 to 3.5 Å) of k^3 -weighted spectra (2.0 to 11.5 Å⁻¹ providing a shell resolution of 0.17 Å) using theoretical backscattering amplitudes and phase shifts calculated with FEFF 8.2¹⁵² on clusters ($R_{\text{max}} = 8$ Å) derived from magnetite¹⁵³ and TcO₂¹⁵⁴ structures. Under such conditions, Tc was placed into the central 6-coordinated Fe position to i. produce Tc-doped magnetite and ii. replace the part of backscattering Tc atoms by Fe for the latter structure to produce a model for Tc-Tc dimers sorption complexes. Debye-Waller factor were restricted to float between 0.002 Å⁻¹ and 0.012 Å⁻¹. Furthermore, spectra were analyzed by the ITFA software package.^{21,127,155} Briefly, three factors are used to determine the number of spectral components: i) the minimum of the Malinowski, which is an indicator value calculated for all principal components, ii) a visual inspection of the principal components to discriminate the ones containing the EXAFS signal by discriminating the background and the noise and iii) the reconstruction of the experimental data by a minimum number of components. Varimax rotation and iterative transformation target test modules are then used to identify the spectral endmembers and to extract their EXAFS spectra.

Raman microscopy

10 µL of the re-suspension from the XPS samples were deposited on a Raman cell containing CaF₂ window.⁸⁷ Once the solid was dried, the cell was sealed and placed in a Raman microscope (Horiba, model Aramis) using a He – Ne Laser with a 10-fold objective with a D 0.3 filter, a pin-hole of 500 µm and a slit of 600 µm.

Speciation calculations

Calculations were performed using the code Chess V2.4.¹⁵⁶ The most recent thermodynamic databases for Fe¹³⁵ and Tc³⁵ were used combined with their recommended S thermodynamic data. In the case of marcasite, it was assumed for the calculations that the Tc(VII) was promoted either by dissolved Fe²⁺ or S²⁻ coming from the complete dissolution of 1.3 g L⁻¹ FeS₂.

Scientific output

Papers

New Insights into $^{99}\text{Tc(VII)}$ Removal by Pyrite: A Spectroscopic Approach

D. M. Rodríguez, N. Mayordomo, A. C. Scheinost, D. Schild, V. Brendler, K. Müller, T. Stumpf.

Environ. Sci. Technol. 54 (2020) 2678 (DOI: 10.1021/acs.est.9b05341)

Reductive Immobilization of $^{99}\text{Tc(VII)}$ by FeS_2 : The Effect of Marcasite

D. M. Rodríguez, N. Mayordomo, D. Schild, S. Shams Aldin Azzam, V. Brendler, K. Müller, T. Stumpf.

Chemosphere. 281 (2021) 130904 (DOI: 10.1016/j.chemosphere.2021.130904)

Exploring the reduction mechanism of $^{99}\text{Tc(VII)}$ in NaClO_4 : A spectro-electrochemical approach

D. M. Rodríguez, N. Mayordomo, A. Parra-Puerto, V. Brendler, K. Müller, T. Stumpf.

(In preparation for Inorganic Chemistry)

Analysis of technetium immobilization and its molecular retention mechanisms by Fe(II)-Al(III)-Cl layered double hydroxide

N. Mayordomo, D. M. Rodríguez, A. Rossberg, H. Foerstendorf, K. Heim, V. Brendler, K. Müller.

Chem. Eng. J. 408 (2021) 127265 (DOI: 10.1016/j.cej.2020.127265)

Technetium retention by gamma alumina nanoparticles and the effect of sorbed Fe^{2+}

N. Mayordomo, D. M. Rodríguez, D. Schild, K. Molodtsov, E.V. Johnstone, R. Hübner, S. Shams Aldin Azzam, V. Brendler, K. Müller

J. Hazard. Mater. 388 (2020) 122066 (DOI: 10.1016/j.jhazmat.2020.122066)

Conferences

Talk (Co-author): Reductive immobilization of $^{99}\text{Tc(VII)}$ by different crystalline phases of iron sulfide (FeS_2)

Tage der Standortauswahl
Freiberg, Germany. 2021

Talk: New studies of the Tc(VII) reduction in aqueous electrolyte media using spectro-electrochemistry

Gesellschaft Deutscher Chemiker (GDCh) Annual Meeting
Dresden, Germany. 2019

Talk (co-author): Tc immobilization by Fe(II)-Al(III)-Cl layered double hydroxide phase

Gesellschaft Deutscher Chemiker (GDCh) Annual Meeting
Dresden, Germany. 2019

Talk (co-author): ^{99}Tc immobilization b aluminum solids containing Fe(II) moieties. The 43rd Symposium on scientific basis for nuclear waste management.

Vienna, Austria. 2019

Poster: Spectro-electrochemical studies of the Tc(VII) reduction in aqueous electrolyte media

17th international conference on the chemistry and migration behavior of actinides and fission products in the geosphere
Kyoto, Japan. 2019

Poster: Reductive immobilization of $^{99}\text{Tc(VII)}$ by different crystalline phases of iron sulfide (FeS_2)

17th international conference on the chemistry and migration behavior of actinides and fission products in the geosphere
Kyoto, Japan. 2019

Talk (co-author): ^{99}Tc retention on Fe(II)-Al(III)-Cl layered double hydroxydes

Goldschmidt 2019 conference
Barcelona, Spain. 2019

Talk: ^{99}Tc retention on pyrite and alumina: the effect of Fe^{2+}

10th International symposium on Tc and Re science and utilization

Moscow, Russia. 2018

Talk (co-author): Environmental fate of fission products: a comprehensive study

Goldschmidt 2018 conference

Boston, USA. 2018

Poster: ^{99}Tc reductive immobilization by Pyrite nanoparticles

18th Radiochemical conference: RadChem 2018

Mariánské Lázně, Czech Republic. 2018

Talk (co-author): Tc immobilization on gamma alumina: a study of the reductant presence and absence

18th Radiochemical conference: RadChem 2018

Mariánské Lázně, Czech Republic. 2018

References

- 1 C. Perrier and E. Segrè, *Nature*, 1947, **159**, 24.
- 2 C. Perrier and E. Segrè, *Nature*, 1937, **140**, 193–194.
- 3 R. Herbert, P. W. Kulke and R. T. H. Shepherd, *Postgrad. Med. J.*, 1965, **41**, 656–662.
- 4 A. H. Meena and Y. Arai, *Environ. Chem. Lett.*, 2017, **15**, 241–263.
- 5 J. P. Icenhower, N. P. Qafoku, J. M. Zachara and W. J. Martin, *Am. J. Sci.*, 2010, **310**, 721–752.
- 6 N. Momoshima, M. Sayad, M. Yamada, M. Takamura and H. Kawamura, *J. Radioanal. Nucl. Chem.*, 2005, **266**, 455–460.
- 7 B. Guérin, S. Tremblay, S. Rodrigue, J. A. Rousseau, V. Dumulon-Perreault, R. Lecomte, J. E. van Lier, A. Zyuzin and E. J. van Lier, *J. Nucl. Med.*, 2010, **51**, 13N-16N.
- 8 S. Jurisson, J. Gawenis and E. R. Landa, *Health Phys.*, 2004, **87**, 423–428.
- 9 Tc cow, <http://www.people.vcu.edu/~mhcrosthwait/clrs461/RadionuclideProduction2.html>, (accessed 10 March 2021).
- 10 E. H. Schulte and P. Scoppa, *Sci. Total Environ.*, 1987, **64**, 163–179.
- 11 J. Icenhower, N. Qafoku, W. Martin and J. M. Zachara, *No. PNNL-18139*, 2008, 1–16.
- 12 International Atomic Energy Agency, *Scientific and Technical Basis for the Geological Disposal of Radioactive Wastes*, Vienna, 2003.
- 13 P. Sellin and O. X. Leupin, *Clays Clay Miner.*, 2014, **61**, 477–498.
- 14 B. Ma, L. Charlet, A. Fernandez-Martinez, M. Kang and B. Madé, *Appl. Geochemistry*, 2019, **100**, 414–431.
- 15 K. H. Lieser and C. Bauscher, *Radiochim. Acta*, 1987, **42**, 205–213.
- 16 T. E. Eriksen, P. Ndalamba, J. Bruno and M. Caceci, *Radiochim. Acta*, 1992, **58–59**, 67–70.
- 17 R. Leggett and A. Giussani, *J. Radiol. Prot.*, 2015, **35**, 297–315.
- 18 Environmental Protection Agency, *National Primary Drinking Water Regulations: Radionuclides*, 2000.
- 19 J. Paquette and W. E. Lawrence, *Can. J. Chem.*, 1985, **63**, 2369–2373.
- 20 S. Chatterjee, G. B. Hall, I. E. Johnson, Y. Du, E. D. Walter, N. M. Washton and T. G. Levitskaia, *Inorg. Chem. Front.*, 2018, **5**, 2081–2091.
- 21 E. Yalçintaş, A. C. Scheinost, X. Gaona and M. Altmaier, *Dalt. Trans.*, 2016, **45**, 17874–17885.
- 22 T. Kobayashi, A. C. Scheinost, D. Fellhauer, X. Gaona and M. Altmaier, *Radiochim. Acta*, 2013, **101**, 323–332.
- 23 F. R. Livens, M. J. Jones, A. J. Hynes, J. M. Charnock, J. F. W. Mosselmans, C. Hennig, H. Steele, D. Collison, D. J. Vaughan, R. A. D. Patrick, W. A. Reed and L. N. Moyes, *J. Environ. Radioact.*, 2004, **74**, 211–219.

- 24 Y. Liu, J. Terry and S. Jurisson, *Radiochim. Acta*, 2008, **96**, 823–833.
- 25 C. Bruggeman, A. Maes and J. Vancluysen, *Phys. Chem. Earth*, 2007, **32**, 573–580.
- 26 L. Huo, W. Xie, T. Qian, X. Guan and D. Zhao, *Chemosphere*, 2017, **174**, 456–465.
- 27 K. H. Lieser and C. H. Bauscher, *Radiochim. Acta*, 1988, **44**, 125–128.
- 28 J. Rard, M. Rand, G. Anderegg and H. Wanner, *Chemical Thermodynamics of Technetium*, OECD Nuclear Energy Agency Data Bank, 1999.
- 29 M. Chotkowski, B. Wrzosek and M. Grdeń, *J. Electroanal. Chem.*, 2018, **814**, 83–90.
- 30 M. Ferrier, J. Roques, F. Poineau, A. P. Sattelberger, J. Unger and A. K. R. Czerwinski, *Eur. J. Inorg. Chem.*, 2014, **3**, 2046–2052.
- 31 F. Poineau, P. F. Weck, K. German, A. Maruk, G. Kirakosyan, W. Lukens, D. B. Rego, A. P. Sattelberger and K. R. Czerwinski, *Dalt. Trans.*, 2010, **39**, 8616–8619.
- 32 S. I. Weiss, L. T. Larson and D. C. Noble, *Pyritic ash-flow tuff, Yucca Mountain, Nevada -- A discussion*, United States, 1994.
- 33 A. Diener, T. Neumann, U. Kramar and D. Schild, *J. Contam. Hydrol.*, 2012, **133**, 30–39.
- 34 C. I. Pearce, R. C. Moore, J. W. Morad, R. M. Asmussen, S. Chatterjee, A. R. Lawter, T. G. Levitskaia, J. J. Neeway, N. P. Qafoku, M. J. Rigali, S. A. Saslow, J. E. Szecsody, P. K. Thallapally, G. Wang and V. L. Freedman, *Sci. Total Environ.*, 2019, **716**, 132849.
- 35 I. Grenthe, X. Gaona, A. V. Plyasunov, L. Rao, W. H. Runde, B. Grambow, R. J. M. Konings, A. L. Smith and E. E. Moore, *Second update on the chemical thermodynamics of uranium, neptunium, plutonium, americium and technetium*, OECD Nuclear Energy Agency Data Bank, Boulogne-Billancourt, France, 2020.
- 36 R. Colton and R. D. Peacock, *Q. Rev. Chem. Soc.*, 1962, **16**, 299–315.
- 37 J. Grassi, J. Devynck and B. Trémillon, *Anal. Chim. Acta*, 1979, **107**, 47–58.
- 38 G. B. S. Salaria, C. L. Rulfs and P. J. Elving, *J. Chem. Soc.*, 1963, 2479–2484.
- 39 G. B. S. Salaria, C. L. Rulfs and P. J. Elving, *Anal. Chem.*, 1963, **35**, 979–982.
- 40 S. I. Zhdanov, A. F. Kuzina and V. I. Spitsyn, *Russ. J. Inorg. Chem.*, 1970, **15**, 803–806.
- 41 L. Astheimer and K. Schwochau, *J. Electroanal. Chem.*, 1964, **8**, 382–389.
- 42 R. Colton, J. Dalziel, W. P. Griffith and G. Wilkinson, *J. Chem. Soc.*, 1960, 71–78.
- 43 M. Chotkowski and A. Czerwiński, *Electrochim. Acta*, 2012, **76**, 165–173.
- 44 M. Chotkowski, M. Grdeń and B. Wrzosek, *J. Electroanal. Chem.*, 2018, **829**, 148–156.
- 45 C. E. Crouthamel, *Anal. Chem.*, 1957, **29**, 1756–1760.
- 46 M. Chotkowski and A. Czerwiński, *Ann. Univ. Mariae Curie-Skłodowska, Sect. AA – Chem.*, 2016, **71**, 141.
- 47 E. Deutsch, W. R. Heineman, R. Hurst, J. C. Sullivan, W. A. Mulac and S. Gordon, *J. Chem. Soc. Chem. Commun.*, 1978, 1038–1040.
- 48 K. Libson, J. C. Sullivan, W. A. Mulac, S. Gordon and E. Deutsch, *Inorg. Chem.*, 1989, **28**, 375–377.
- 49 E. Yalcintas, PhD thesis developed at Karlsruhe Institute of Technology, 2015.
- 50 R. Guillaumont, T. Fanghänel, V. Neck, J. Fuger, D. A. Palmer, I. Grenthe and M. A. Rand, *Update on the chemical thermodynamics of uranium, neptunium, plutonium, americium and technetium*, OECD Nuclear Energy Agency Data Bank, 2003.
- 51 F. Poineau, M. Fattahi, C. Den Auwer, C. Hennig and B. Grambow, *Radiochim. Acta*, 2006, **94**, 283–289.
- 52 C. D. Russell, *Int. J. Appl. Radiat. Isot.*, 1982, **33**, 883–889.
- 53 C. M. A. Brett and A. M. O. Brett, *Electroanalysis*, Oxford University Press, 1998.

- 54 C. M. A. Brett and A. M. O. Brett, *Electrochemistry: principles, methods, and applications*, Oxford University Press, 1993.
- 55 N. Elgrishi, K. J. Rountree, B. D. McCarthy, E. S. Rountree, T. T. Eisenhart and J. L. Dempsey, *J. Chem. Educ.*, 2018, **95**, 197–206.
- 56 M. T. Pise, A. Chatterjee, R. N. Singh, B. P. Kashyap and S. S. V. Tatiparti, *ECS Meet. Abstr.*, 2020, **MA2020-01**, 1189–1189.
- 57 In *IUPAC Compendium of Chemical Terminology*, IUPAC, 2008.
- 58 A. J. Bard, R. Parsons and J. Jordan, *Standard potentials in aqueous solution*, Marcel Dekker, Inc., New York, 1985.
- 59 E. R. Nightingale, *J. Phys. Chem.*, 1959, **63**, 742–743.
- 60 X. Wang and Z. Tao, *J. Radioanal. Nucl. Chem.*, 2004, **260**, 305–309.
- 61 K. Nakamoto, *Infrared and Raman Spectra of Inorganic and Coordination Compounds*, John Wiley & Sons, Inc., Hoboken, NJ, USA, 2008.
- 62 J. Weaver, C. Z. Soderquist, N. M. Washton, A. S. Lipton, P. L. Gassman, W. W. Lukens, A. A. Kruger, N. A. Wall and J. S. McCloy, *Inorg. Chem.*, 2017, **56**, 2533–2544.
- 63 V. A. Mikhalev, *Radiochemistry*, 2005, **47**, 319–333.
- 64 L. A. O’Connell, R. M. Pearlstein, A. Davison, J. R. Thornback, J. F. Kronauge and A. G. Jones, *Inorganica Chim. Acta*, 1989, **161**, 39–43.
- 65 W. M. B. Roberts, A. L. Walker and A. S. Buchanan, *Miner. Depos.*, 1969, **4**, 18–29.
- 66 B. Baeyens, A. Maes and A. Cremers, in *Radioactive Waste Management and the Nuclear Fuel Cycle*, Harwood Academic Publishers, New York, 1985, pp. 391–408.
- 67 E. Gaucher, C. Robelin, J. M. Matray, G. Négrel, Y. Gros, J. F. Heitz, A. Vinsot, H. Rebours, A. Cassagnabère and A. Bouchet, *Phys. Chem. Earth, Parts A/B/C*, 2004, **29**, 55–77.
- 68 D. Rickard, *Sulfidic Sediments and Sedimentary Rocks*, Elsevier B.V, Amsterdam, 2012.
- 69 A. I. Perel’man, *Appl. Geochemistry*, 1986, **1**, 669–680.
- 70 N. Mayordomo Herranz, PhD thesis developed at Universidad de Alcalá, 2017.
- 71 R. M. Powell, D. Schultz and R. Landis, *Permeable Reactive Barrier Technologies for Contaminant Remediation*, Washington, 1998.
- 72 R. Thiruvengkatachari, S. Vigneswaran and R. Naidu, *J. Ind. Eng. Chem.*, 2008, **14**, 145–156.
- 73 Estimation of Global Inventories of Radioactive Waste and Other Radioactive Materials, <https://www.iaea.org/publications/7857/estimation-of-global-inventories-of-radioactive-waste-and-other-radioactive-materials>, (accessed 2 March 2020).
- 74 International Atomic Energy Agency, *Status and Trends in Spent Fuel and Radioactive Waste Management*, Vienna, 2018.
- 75 Basics of the final disposal, http://www.posiva.fi/en/final_disposal/basics_of_the_final_disposal#.X7e4_IiYXIU, (accessed 20 November 2020).
- 76 G. Sposito, *Chemical equilibrium and Kinetics in soils*, Oxford University Press, New York, First., 1994.
- 77 P. C. Hiemenz and R. Rajagopalan, *Principles of Colloid & Surface Chemistry*, Taylor & Francis, New York, 3rd edn., 1997.
- 78 H. Koch-Steindl and G. Pröhl, *Radiat. Environ. Biophys.*, 2001, **40**, 93–104.
- 79 D. J. Ashworth and G. Shaw, *J. Environ. Radioact.*, 2005, **81**, 155–171.
- 80 K. Tagami and S. Uchida, *Chemosphere*, 2005, **60**, 714–717.
- 81 K. Tagami and S. Uchida, *Appl. Radiat. Isot.*, 2004, **61**, 1203–1210.

- 82 D. Cui and T. E. Eriksen, *Environ. Sci. Technol.*, 1996, **30**, 2263–2269.
- 83 D. Cui and T. E. Eriksen, *Environ. Sci. Technol.*, 1996, **30**, 2259–2262.
- 84 T. Peretyazhko, J. M. Zachara, S. M. Heald, B. H. Jeon, R. K. Kukkadapu, C. Liu, D. Moore and C. T. Resch, *Geochim. Cosmochim. Acta*, 2008, **72**, 1521–1539.
- 85 T. S. Peretyazhko, J. M. Zachara, R. K. Kukkadapu, S. M. Heald, I. V. Kutnyakov, C. T. Resch, B. W. Arey, C. M. Wang, L. Kovarik, J. L. Phillips and D. A. Moore, *Geochim. Cosmochim. Acta*, 2012, **92**, 48–66.
- 86 J. M. Zachara, S. M. Heald, B.-H. Jeon, R. K. Kukkadapu, C. Liu, J. P. McKinley, A. C. Dohnalkova and D. A. Moore, *Geochim. Cosmochim. Acta*, 2007, **71**, 2137–2157.
- 87 N. Mayordomo, D. M. Rodríguez, D. Schild, K. Molodtsov, E. V. Johnstone, R. Hübner, S. Shams Aldin Azzam, V. Brendler and K. Müller, *J. Hazard. Mater.*, 2020, **388**, 122066.
- 88 N. Mayordomo, D. M. Rodríguez, A. Rossberg, H. Foerstendorf, K. Heim, V. Brendler and K. Müller, *Chem. Eng. J.*, 2021, **408**, 127265.
- 89 G. E. Brown Jr. and G. Calas, *Geochemical Perspect.*, 2012, **1**, 483–484.
- 90 T. E. Payne, V. Brendler, M. Ochs, B. Baeyens, P. L. Brown, J. A. Davis, C. Ekberg, D. A. Kulik, J. Lutzenkirchen, T. Missana, Y. Tachi, L. R. Van Loon and S. Altmann, *Environ. Model. Softw.*, 2013, **42**, 143–156.
- 91 I. Llorens, M. Fattahi and B. Grambow, *MRS Proc.*, 2006, **985**, 908–985.
- 92 F. B. Walton, J. Paquette, J. P. M. Ross and W. E. Lawrence, *Nucl. Chem. Waste Manag.*, 1986, **6**, 121–126.
- 93 M. S. Lee, W. Um, G. Wang, A. A. Kruger, W. W. Lukens, R. Rousseau and V. A. Glezakou, *Nat. Commun.*, 2016, **7**, 1–6.
- 94 T. A. Marshall, K. Morris, G. T. W. Law, J. F. W. Mosselmans, P. Bots, S. A. Parry and S. Shaw, *Environ. Sci. Technol.*, 2014, **48**, 11853–62.
- 95 K. Morris, F. R. Livens, J. M. Charnock, I. T. Burke, J. M. McBeth, J. D. C. Begg, C. Boothman and J. R. Lloyd, *Appl. Geochemistry*, 2008, **23**, 603–617.
- 96 J. M. McBeth, G. Lear, J. R. Lloyd, F. R. Livens, K. Morris and I. T. Burke, *Geomicrobiol. J.*, 2007, **24**, 189–197.
- 97 W. Chesworth, *Encyclopedia of Soil Science*, Springer, Dordrecht, Dordrecht, 2008.
- 98 Hussain and C. Mustansar, *The Handbook of Environmental Remediation: Classic and Modern Techniques*, CPI Group, Croydon, 2020.
- 99 I. T. Burke, C. Boothman, J. R. Lloyd, F. R. Livens, J. M. Charnock, J. M. McBeth, R. J. G. Mortimer and K. Morris, *Environ. Sci. Technol.*, 2006, **40**, 3529–3535.
- 100 K. Schmeide, A. Rossberg, F. Bok, S. Shams Aldin Azzam, S. Weiss and A. C. Scheinost, *Sci. Total Environ.*, 2021, **770**, 145334.
- 101 C. I. Pearce, J. P. Icenhower, R. M. Asmussen, P. G. Tratnyek, K. M. Rosso, W. W. Lukens and N. P. Qafoku, *ACS Earth Sp. Chem.*, 2018, **2**, 532–547.
- 102 W. W. Lukens, N. Magnani, T. Tylliszczak, C. I. Pearce and D. K. Shuh, *Environ. Sci. Technol.*, 2016, **50**, 13160–13168.
- 103 R. D. Shannon, *Acta Crystallogr. Sect. A*, 1976, **32**, 751–767.
- 104 F. N. Smith, C. D. Taylor, W. Um and A. A. Kruger, *Environ. Sci. Technol.*, 2015, **49**, 13699–13707.
- 105 F. N. Skomurski, K. M. Rosso, K. M. Krupka and B. P. McGrail, *Environ. Sci. Technol.*, 2010, **44**, 5855–5861.
- 106 J. Bebie, M. A. A. Schoonen, M. Fuhrmann and D. R. Strongin, *Geochim. Cosmochim.*

- Acta*, 1998, **62**, 633–642.
- 107 M. Wolthers, L. Charlet, P. R. van Der Linde, D. Rickard and C. H. van Der Weijden, *Geochim. Cosmochim. Acta*, 2005, **69**, 3469–3481.
- 108 D. L. Horrocks, *Applications of Liquid Scintillation Counting*, Academic Press, Inc., New York, 1974.
- 109 R. F. Egerton, *Physical Principles of Electron Microscopy An Introduction to TEM, SEM and AEM*, Springer International Publishing, Second., 2016.
- 110 A. J. Garratt-Reed and D. C. Bell, *Energy-Dispersive X-Ray Analysis in the Electron Microscope*, BIOS Scientific Publishers Limited, Oxford, 2003.
- 111 M. E. Andersen and R. Z. Muggll, *Anal. Chem.*, 1981, **53**, 1772–1777.
- 112 P. J. Larkin, *Infrared and Raman Spectroscopy: Principles and Spectral Interpretation*, Amsterdam, Second., 2018.
- 113 P. van der Heide, *X-Ray Photoelectron Spectroscopy An Introduction to Principles and Practices*, John Wiley & Sons, INC, New Jersey, 2012.
- 114 J. Yano and V. K. Yachandra, *Photosynth. Res.*, 2009, **102**, 241–254.
- 115 B. Lafuente, R. T. Downs, H. Yan and N. Stone, in *Highlights in Mineralogical Crystallography*, De Gruyter, Berlin, 2015, pp. 1–30.
- 116 M. Kosmulski, *Adv. Colloid Interface Sci.*, 2018, **251**, 115–138.
- 117 P. Bonnissel-Gissinger, M. Alnot, J.-J. Ehrhardt and P. Behra, *Environ. Sci. Technol.*, 1998, **32**, 2839–2845.
- 118 G. Hu, K. Dam-Johansen, S. Wedel and J. P. Hansen, *Prog. Energy Combust. Sci.*, 2006, **32**, 295–314.
- 119 K. Shi, X. Hou, P. Roos and W. Wu, *Anal. Chim. Acta*, 2012, **709**, 1–20.
- 120 D. Cui and T. E. Eriksen, *Environ. Sci. Technol.*, 1996, **30**, 2263–2269.
- 121 E. Yalçıntaş, X. Gaona, M. Altmaier, K. Dardenne, R. Polly and H. Geckeis, *Dalt. Trans.*, 2016, **45**, 8916–8936.
- 122 N. J. Hess, Y. X. Xia, D. Rai and S. D. Conradson, *J. Solution Chem.*, 2004, **33**, 199–226.
- 123 M. A. Williamson and J. D. Rimstidt, *Geochim. Cosmochim. Acta*, 1994, **58**, 5443–5454.
- 124 S. Karthe, R. Szargan and E. Suoninen, *Appl. Surf. Sci.*, 1993, **72**, 157–170.
- 125 W. W. Lukens and S. A. Saslow, *Dalt. Trans.*, 2018, **47**, 10229–10239.
- 126 N. Taitel-Goldman, IntechOpen, Rijeka, 2013, p. Ch. 6.
- 127 A. Roßberg, T. Reich and G. Bernhard, *Anal. Bioanal. Chem.*, 2003, **376**, 631–638.
- 128 M. Saeki, Y. Sasaki, A. Nakai, A. Ohashi, D. Banerjee, A. C. Scheinost and H. Foerstendorf, *Inorg. Chem.*, 2012, **51**, 5814–5821.
- 129 C. H. Giles, D. Smith and A. Huitson, *J. Colloid Interface Sci.*, 1974, **47**, 755–765.
- 130 D. P. Jaisi, H. Dong, A. E. Plymale, J. K. Fredrickson, J. M. Zachara, S. Heald and C. Liu, *Chem. Geol.*, 2009, **264**, 127–138.
- 131 T. Peretyazhko, J. M. Zachara, S. M. Heald, R. K. Kukkadapu, C. Liu, A. E. Plymale and C. T. Resch, *Environ. Sci. Technol.*, 2008, **42**, 5499–5506.
- 132 R. Weerasooriya and H. J. Tobschall, *Colloids Surfaces A Physicochem. Eng. Asp.*, 2005, **264**, 68–74.
- 133 E. C. Todd, D. M. Sherman and J. A. Purton, *Geochim. Cosmochim. Acta*, 2003, **67**, 881–893.
- 134 J. H. Lee, J. M. Zachara, J. K. Fredrickson, S. M. Heald, J. P. McKinley, A. E. Plymale, C. T. Resch and D. A. Moore, *Geochim. Cosmochim. Acta*, 2014, **136**, 247–264.
- 135 R. J. Lemire, U. Berner, C. Musikas, D. A. Palmer, P. Taylor and O. Tochiyama,

- Chemical Thermodynamics of Iron. Part 1*, OECD, Paris, France, 2013, vol. 13a.
- 136 D. A. Kitchaev and G. Ceder, *Nat. Commun.*, 2016, **7**, 13799.
- 137 G. Limousin, J.-P. Gaudet, L. Charlet, S. Szenknect, V. Barthès and M. Krimissa, *Appl. Geochemistry*, 2007, **22**, 249–275.
- 138 F. King, *A review of the properties of pyrite and the implications for corrosion of the copper canister Technical Report TR-13-19*, Svensk Kärnbränslehantering AB, Stockholm, 2013.
- 139 M. Hanesch, *Geophys. J. Int.*, 2009, **177**, 941–948.
- 140 S. W. Knipe, J. R. Mycroft, A. R. Pratt, H. W. Nesbitt and G. M. Bancroft, *Geochim. Cosmochim. Acta*, 1995, **59**, 1079–1090.
- 141 B. S. Hemingway, R. R. Seal and I.-M. Chou, *Thermodynamic Data for Modeling Acid Mine Drainage Problems: Compilation and Estimation of Data for Selected Soluble Iron-Sulfate Minerals Open-file Report 02-161*, U.S. Geological Survey, 2002.
- 142 D. Rickard, in *Sulfidic Sediments and Sedimentary Rocks*, Elsevier, 2012, vol. 65, pp. 195–231.
- 143 M. Talikka, *Geological Mapping of the ONKALO Open Cut*, Posiva Oy, Olkiluoto, Finland, 2005.
- 144 M. Löfgren and M. Sidborn, *Mineral. Petrol.*, 2016, **110**, 663–680.
- 145 W. W. Lukens, D. K. Shuh, N. C. Schroeder, K. R. Ashley and L. Alamos, *Sci. Highlight*, 2004, **101**, 3–5.
- 146 I. L. Pegg, *J. Radioanal. Nucl. Chem.*, 2015, **305**, 287–292.
- 147 G. B. Hall, S. D. Chatterjee, T. G. Levitskaia, T. J. Martin, N. A. Wall and E. D. Walter, *Synthesis and Characterization of Tc(I) Carbonyl Nitrosyl Species Relevant to the Hanford Tank Waste: FY 2016 Status Report*, Richland, Washington, 2016.
- 148 T. Levitskaia, A. Andersen, S. Chatterjee, G. B. Hall, E. D. Walter and Was, *Spectroscopic Properties of Tc(I) Tricarbonyl Species Relevant to the Hanford Tank Waste*, Richland, Washington, 2015.
- 149 S. Chatterjee, A. Andersen, Y. Du, M. H. Engelhard, G. B. Hall, T. G. Levitskaia, W. W. Lukens, V. Shutthanandan, E. D. Walter and N. M. Washton, *Characterization of Non-Pertechnetate Species Relevant to the Hanford Tank Waste*, Richland, Washington, 2017.
- 150 Z. O. Ameer and M. M. Husein, *Sep. Sci. Technol.*, 2013, **48**, 681–689.
- 151 T. Ressler, *J. Synchrotron Radiat.*, 1998, **5**, 118–122.
- 152 A. L. Ankudinov and J. J. Rehr, *Phys. Rev. B*, 1997, **56**, R1712–R1716.
- 153 J. P. Wright, J. P. Attfield and P. G. Radaelli, *Phys. Rev. B*, 2002, **66**, 214422.
- 154 E. E. Rodriguez, F. Poineau, A. Llobet, A. P. Sattelberger, J. Bhattacharjee, U. V. Waghmare, T. Hartmann and A. K. Cheetham, *J. Am. Chem. Soc.*, 2007, **129**, 10244–10248.
- 155 A. Rossberg, K. U. Ulrich, S. Weiss, S. Tsushima, T. Hiemstra and A. C. Scheinost, *Environ. Sci. Technol.*, 2009, **43**, 1400–1406.
- 156 J. van der Lee and L. de Wint, *Chess tutorial and Cookbook. Updated for version 3.0*, Ecole des Mines de Paris, Fontainebleau, 1999.

Versicherung

Hiermit versichere ich, dass ich die vorliegende Arbeit ohne unzulässige Hilfe Dritter und ohne Benutzung anderer als der angegebenen Hilfsmittel angefertigt habe. Die aus fremden Quellen direkt oder indirekt übernommenen Gedanken sind als solche kenntlich gemacht. Die Arbeit wurde bisher weder im Inland noch im Ausland in gleicher oder ähnlicher Form einer anderen Prüfungsinstitution vorgelegt und ist auch noch nicht veröffentlicht worden.

Confirmation

I herewith declare that I have produced this thesis without the prohibited assistance of third parties and without making use of aids other than those specified; notions taken over directly or indirectly from other sources have been identified as such. This thesis has not previously been presented in identical or similar form to any other German or foreign examination board.

Dresden, 21.06.2021